SYNTHESIS, CHARACTERIZATION, ANION COMPLEXATION AND ELECTROCHEMISTRY OF CATIONIC LEWIS ACIDS

A Dissertation

by

CHING-WEN CHIU

Submitted to the Office of Graduate Studies of
Texas A&M University
in partial fulfillment of the requirements for the degree of

DOCTOR OF PHILOSOPHY

May 2008

Major Subject: Chemistry

SYNTHESIS, CHARACTERIZATION, ANION COMPLEXATION AND ELECTROCHEMISTRY OF CATIONIC LEWIS ACIDS

A Dissertation

by

CHING-WEN CHIU

Submitted to the Office of Graduate Studies of
Texas A&M University
in partial fulfillment of the requirements for the degree of

DOCTOR OF PHILOSOPHY

Approved by:

Chairs of Committee,	François P. Gabbaï
Committee Members,	David E. Bergbreiter
	Marcetta Y. Darensbourg
	Michael D. Manson
Head of Department,	David H. Russell

May 2008

Major Subject: Chemistry

ABSTRACT

Synthesis, Characterization, Anion Complexation, and Electrochemistry of Cationic Lewis Acids. (May 2008)

Ching-Wen Chiu, B.S., National Chiao-Tung University;

M.S., National Chiao-Tung University

Chair of Advisory Committee: Dr. François P. Gabbaï

Owing to the favored Coulombic attraction between the ammonium group and anion which stabilizes the B-F/B-CN bond against heterolysis, cationic borane [**25**]$^+$ has great affinity toward anions than its neutral analog, and is capable of capturing fluoride or cyanide from water under bi-phasic conditions. By placing the fluorophilic silyl group adjacent to an electrophilic carbocation, a novel fluoride sensor [**45**]$^+$ was obtained. Sensing occurs via a fluoride induced methyl migration from the silicon to adjacent electrophilic methylium center which is unprecedented. As a result of its strong fluoride affinity, [**45**]$^+$ is able to react with KF in aqueous media at pH 7.0.

The electrochemistry study of these cationic Lewis boranes reveals that the cationic character of these boranes serves to decrease their reduction potential and increase the stability of the resulting radicals. In this part of the research, we have prepared a cationic borane [**27**]$^+$, which features two reversible reduction waves at -0.86 and -1.56 (vs. Fc/Fc^+) corresponding to the formation of stable neutral and anionic derivatives. The one-electron reduction of [**27**]$^+$ leads to the formation of a boron containing neutral radical featuring an unusual boron-carbon one-electron π bond.

Further reduction of **27**$^{\bullet}$ results in the formation of the borataalkene derivative [**27**]$^{-}$, which features a formal B=C double bond. The structural changes accompanying the stepwise population of the B-C π-bond are also determined, and this sequential population of B-C π-bonding orbital is also supported by theoretical computations.

In order to understand the impact of the cationic nature of these boranes on their oxidative power, three novel cationic boranes ([**34**]$^{+}$, [**35**]$^{2+}$, and [**36**]$^{3+}$) have been synthesized and their oxidative power were examined via cyclic voltammetry. The CV data of these compounds shows that the reduction potential of these triarylboranes is linearly proportional to the number of the pendant cationic substituents. Substitution of a mesityl group by an Ar^{N+} group leads to an increase of the reduction potential by 260 mV.

ACKNOWLEDGMENTS

First of all, I would like to express my sincere gratitude to my research advisor, Dr. François P. Gabbaï, for his guidance, patience and encouragement. Without his support, I could never have come so far and learned so much. I would also like to thank my committee members, Dr. Bergbreiter, Dr. Darensbourg, and Dr. Manson.

I would also like to acknowledge the members of Dr. Gabbaï's group for their help in the past five years (Dr. Mason R. Haneline, Dr. Thomas J. Taylor, Dr. Charlotte N. Burress, Chirs Dorsey, Todd Hundall, Casey Wade, Youngmin Kim, Dr. Mieock Kim, Dr. Mingxing Qian, and Dr. Min Hyung Lee). Special thanks to Dr. Haudong Wang for his generous advice in everything, and to Dr. Mohand Melaimi for making me able to do theoretical calculations. I must also express my gratefulness to my friends (Li-jung, Judy, Johnny, Xixi, Kin, and Mrs. Han) for helping me through all of the disasters outside the chemistry department. Without them, I would have not been able to come to the lab with any energy.

Finally, I would like to thank my family in Taiwan for their love and support at all levels. To make them proud is one of the most important driving forces in this journey.

TABLE OF CONTENTS

Page

CHAPTER Page

CHAPTER Page

LIST OF FIGURES

Page

Page

Page

Page

Page

Page

Page

Page

Page

Page

Page

Page

Page

Page

Page

LIST OF TABLES

Page

Page

CHAPTER I

INTRODUCTION AND RESEARCH OBJECTIVES

1.1 Definition

Cationic Lewis acids are molecules that feature a Lewis acidic element and carry an overall positive charge. Depending on the distribution of the positive charge, the positive charge can be localized on the Lewis acidic center (A, Figure 1) or on the pendent functionalities (B, Figure 1).

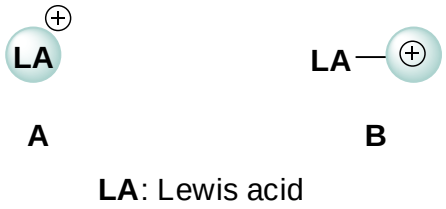

Figure 1: Types of cationic Lewis acids.

1.2 Colorimetric sensing of fluoride anions in aqueous media at neutral pH

1.2.1 Introduction

Fluoride is often added to drinking water because low doses of this anion prevent dental decay in children. According to the Centers for Disease Control and Prevention, 60% of the U.S. population received fluoridated water in 2002.[1] Fluoride is also

---

This dissertation follows the style and format of the *Journal of American Chemical Society*.

found in toothpaste and is sometimes used as an anabolic drug in the treatment of osteoporosis. While the beneficial effects of fluoride are well documented, excessive intake can result in loss of calcium from the tooth matrix, thereby leading to cavity formation and ultimately dental fluorosis. Chronic exposure to high levels of fluoride can cause skeletal fluorosis; an incurable condition resulting from the hardening and calcifying of the bones and joints.[2, 3] Taking into account the adverse effects caused by excessive fluoride intake, a careful monitoring of fluoride concentration in drinking water is necessary. At the academic level, fluoride displays a high hydration enthalpy (ΔH^o = -504 kJ/mol), and its molecular recognition in water at neutral pH constitutes a stimulating intellectual challenge.

The current monitoring technology relies largely on the use of ion selective electrodes.[2, 3] However, access to colorimetric or fluorescence detection methods might be preferred because of lower cost and ease of operation. The colorimetric methods that currently exist for the determination of fluoride are based on the bleaching of colored Al^{3+}, Fe^{3+} or Zr^{4+} complexes bearing organic dyes as ligands.[2, 3] For Zr^{4+}/SPADNS, the presence of fluoride is determined by the decrease in absorbance at 570 nm. Although the method is reliable and relatively cheap, it necessitates acidic media (pH 5) and suffers from interference with anions such as chloride, phosphate and sulfate. Cations such as Al^{3+} and Fe^{3+} which form hexafluoride complexes can also cause interference.[4] As a result, the development of alternative analytical methods appears justified.

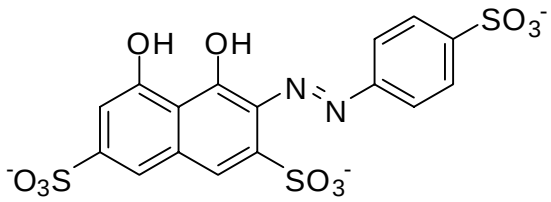

SPADNS

For these reasons, a great deal of effort has been devoted to the design of molecular receptors that selectively sense fluoride. In most cases, the binding sites of the sensors consist of amide, urea, thiourea, guanidinium, and pyrrole functionalities that are capable of hydrogen bonding with the anionic guest.[5-20] Implementation of this strategy has led to the design of very selective fluoride receptors and sensors. *However, as recently noted by Fabbrizzi, fluoride recognition by these derivatives mostly takes place in organic solvents, which greatly limits the scope of their use.*[21] These limitations, which can sometimes be circumvented by immobilization of the receptors,[22] have led a number of researchers to investigate the use of Lewis acidic receptors.

Since boron is intrinsically fluorophilic, a great deal of work has focused on the utilization of Lewis acidic boron compounds for the complexation of fluoride.[23-34] A large part of the recent research has been focused on neutral triarylboranes which readily complex fluoride anions in organic solvents.[35-38] While this property has long been overlooked in the context of anion sensing, the group of Tamao and Yamaguchi showed that such boranes can serve as fluoride sensors with binding constants ranging from 10^5 M^{-1} – 10^6 M^{-1} in organic solvents (Figure 2).[39-42] Since these seminal contributions, a number of other groups have reported related results.[43-48] In triarylborane fluoride

receptors, the boron empty p-orbital mediates conjugation of the aryl substituents and contributes largely to the LUMO of the molecule. This situation is altered in the presence of fluoride, which populates the formerly vacant boron p-orbital upon complexation. Fluoride binding disrupts the frontier orbitals of the organoborane receptor, which is accompanied by drastic changes in the photophysical properties.

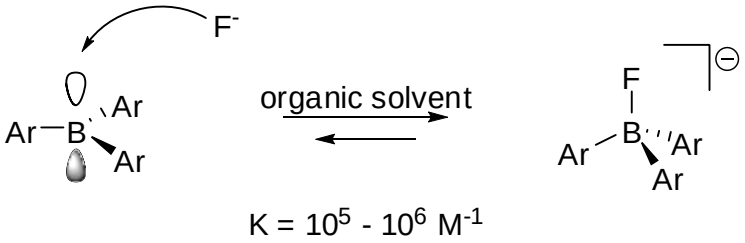

Figure 2: Fluoride complexation of triarylborane.

These changes directly affect the absorption and emission spectra of the receptors that can therefore be used as colorimetric[40] or fluorescent[41, 42] fluoride ion sensors, respectively. Despite the elevated binding constants and advantageous photophysical properties, triarylboranes cannot be used for the molecular recognition of fluoride in water, which induces a dissociation of the resulting anionic triarylfluoroborate complexes.[40]

In order to increase the binding constant of borane based receptors, several groups, including ours, have explored the use of bidentate boranes that chelate fluoride.[43, 49-58] Our efforts in this area have focused on the design of naphthalene based derivatives such as **1** and **2**. Although the fluoride binding constants of such receptors exceed those of

monofunctional analogs by 3 or 4 orders of magnitude, their use in protic environments remains problematic. For example, chelating diboranes such as **1** will undergo a slow hydrolysis in the presence of water or methanol.[43] The heteronuclear B/Hg derivative **2** captures fluoride in 90/10 (vol.) THF/water [52] but not in pure water.

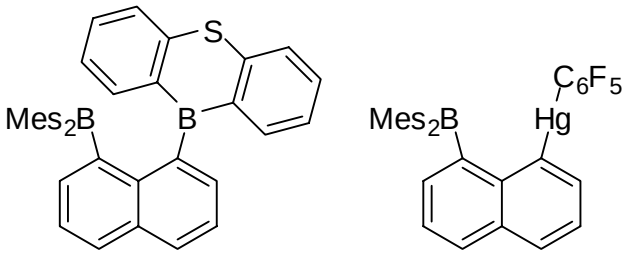

1 2

In an effort to overcome these challenges, we would now like to consider cationic Lewis acids whose dative interaction with the fluoride anion will be strengthened by Coulombic attractions (Figure 3). Such ideas, which have already been applied to the design of various hosts for anions,[59-67] are only emerging in the case of main group Lewis acidic receptors.[68, 69]

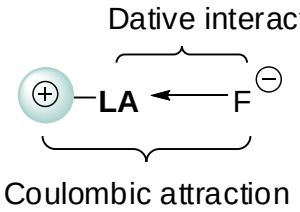

Figure 3: The favored interaction between cationic Lewis acids and fluoride anions.

1.2.2 Objectives

Aim 1: Synthesis of cationic monofunctional boranes and silanes

In order to prepare triarylboranes whose fluoride complexes are stable in water, we propose to synthesize a series of cationic boranes whose fluoride affinity should be increased by favorable Coulombic host-guest attractions. To this end, we plan to synthesize triarylboranes with ammonium or acridinium functionalities bound to one of the aromatic substituents (Figure 4). We also propose to test the applicability of the aforementioned concept to other Lewis acids by synthesizing ammonium or acridinium silanes, which will also be used as fluoride receptors (Figure 4).

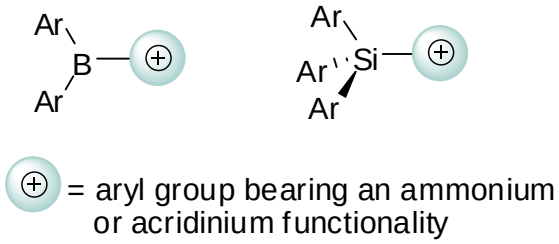

Figure 4: Representations of cationic boranes and silanes (Ar = aryl group).

Aim 2: Evaluation of the anion binding and photophysical properties

In order to guide our synthetic effort toward appropriate targets, the stability and anion binding properties of the cationic boranes and silanes will be studied (Figure 5). These studies should allow us to identify the parameters that dictate anion binding selectivity and water compatibility. We will also investigate the photophysical response given by the boranes and silanes upon fluoride complexation. These studies

should help us identify those systems that can be used as colorimetric or fluorescent sensors.

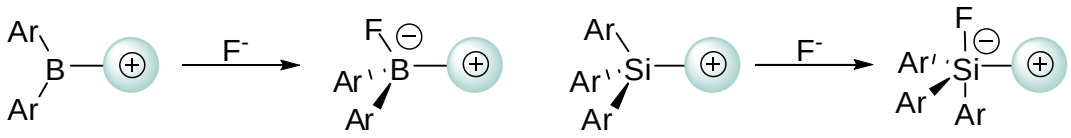

Figure 5: Expected interaction of the cationic boranes and silanes with fluoride.

1.3 Boron centered radicals, one electron π-bonding, and one electron σ-bonding

1.3.1 Introduction

Owing to their isoelectronic relationship to neutral methyl radicals, the chemistry of stable boron-centered radical anions $[Ar_3B]^{\bullet-}$ (**A**, Ar = aryl, Figure 6) has been intensively investigated. These compounds are usually prepared by chemical or electrochemical reduction of neutral tris(aryl)boranes.[70] Although delocalization of the radical over the aryl rings accounts for the stability of such systems,[71-81] both X-ray and EPR studies show that, in some instances, the unpaired electron can be mainly localized at boron.[82] The reduction chemistry of organoboranes has been extended to diboranes of type **B** and **C**, which can be reduced by one electron to produce derivatives featuring a one-electron π–[83-86] or σ–bond,[49, 87, 88] respectively. While the structural characterization of complexes of types **A** and **B** has been achieved, the identity of radicals of type **C** has only been inferred from EPR spectroscopy and DFT calculations.

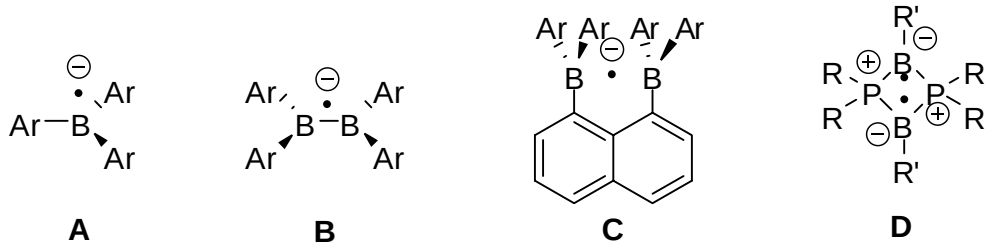

Figure 6: Boron radicals.

A common feature uniting radicals **A**-**C** (Figure 6) is their highly reducing nature. Because of this property, such radicals are very reactive, which complicates their isolation and structural characterization. Taking into account the fundamental knowledge that could be gained from structurally characterizing boron centered radicals, we would like to explore strategies that allow for their stabilization. Development of such strategies is also likely to increase the scope of applications in which such radicals could be used. If sufficiently stable, it is conceivable that such radicals may become useful building blocks for the design of conducting materials.[89-91]

In the context of this research, it is important to consider the recent results obtained by the group of Bertrand, which reported on singlet diradicals of type **D** (R and R' = alkyl or aryl, Figure 6).[92-95] Such compounds can formally be described as resulting from the two-electron reduction of hypothetical bis(phosphonium) precursors. Turning this hypothesis into a design principle, we propose to investigate the synthesis of cationic boranes and explore their reduction chemistry. We expect that the cationic character of these boranes will serve to decrease their reduction potential and increase the stability of the resulting radicals.

The oxidative properties of triarylborane are of interest as well. Tris(pentafluoro)phenylborane is a prototypical example of an electron-deficient borane which has been extensively used as an anion abstractor for the activation of olefin polymerization catalysts.[96-98] Such boranes, which have a Lewis acidity comparable to that of BCl_3, present a number of advantages: they are easy to handle and chemically resistant to protic environments. As a result, fluorinated boranes are being increasingly used as Lewis acid catalysts in organic synthesis.[98] Because of their electron deficiency, these boranes are also emerging as a new class of organic oxidants.[77, 99] This is especially well illustrated by the recent work of Norton and Jäkle, who have shown that the reduction potential of tris(pentafluoro)phenylborane in THF is close to -1.17 V (vs. Fc/Fc^+).[78] This potential is much more positive than that recorded for Mes_3B (-2.73 V vs. Fc/Fc^+), and thus provides a measure of the drastic effect caused by the pentafluorophenyl group.

Beyond the use of fluorinated substituents, we are not aware of any efforts aimed at further increasing the electron deficiency of triarylboranes. In this research, we propose to determine if the introduction of cationic centers can be used to obtain triarylboranes whose oxidative power parallels or perhaps exceeds that of fluorinated boranes.

1.3.2 Objectives

Aim 1: Synthesis of cationic boranes

In the first part of this project, we propose to synthesize, characterize and study monofunctional cationic boranes featuring ammonium and acridinium (Figure 7). These studies are motivated, at least in part, by the fundamental challenges associated with the synthesis and isolation of highly electrophilic species.

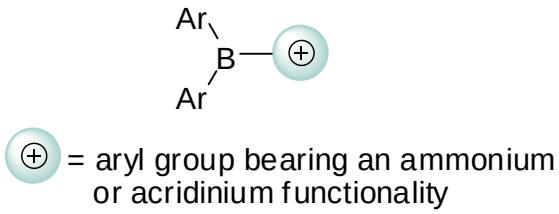

Figure 7: Representation of the cationic boranes proposed in this project. Ar = aryl group.

Aim 2: Reduction of the cationic boranes – Formation of radicals and unusual bonding situations

Once isolated, the formation of radicals by reduction of the cationic boranes will be studied (Figure 8). These experiments should allow us to determine if the cationic character of the boranes serves to decrease their reduction potential and increase the stability of the resulting radicals. These experiments may also provide access to derivatives featuring unusual bonding motifs. In particular, we hope to isolate radicals featuring one-electron carbon-boron π-bonds.

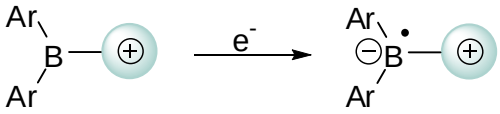

Figure 8: Reduction of the cationic boranes.

Aim 3: Synthesis of polycationic boranes as strong organic oxidants

In the last part of this project, we propose to investigate how the cationic nature of the boranes impacts their oxidative power. In this context we propose to investigate the synthesis of mono-, di- and tri-cationic boranes (Figure 9) and compare their redox properties. The significance of this objective lies in the possible discovery of new organic oxidants, an area in which the use of organoboranes is only emerging.

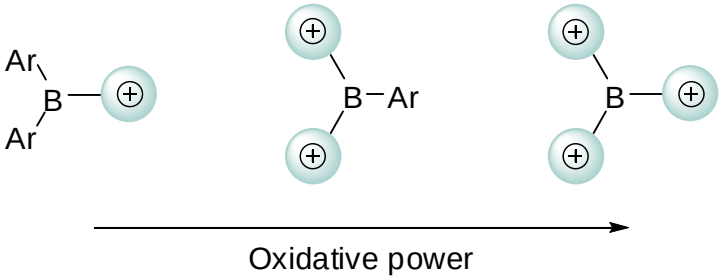

Figure 9: Representation of polycationic boranes placed on an oxidative power scale.

CHAPTER II

BACKGROUND

2.1 Fluoride complexation of triarylboranes

In triarylborane, the empty p orbital of the boron center effectively conjugates with the π-system of the aryl ligands. As the results, triarylboranes have received great attention in a number of optical electronic applications, and have also been used in the context of anion sensing. Upon fluoride complexation, the population of the boron p_π orbital disrupts the π conjugation between the boron atom and the aromatic chromophores leading to drastic changes in the photophysical properties of the molecule as shown in Figure 10. These changes can be easily observed in the absorption spectrum or emission spectrum of a given borane. Therefore, the fluoride binding event can be examined by monitoring changes in the optical properties of triarylboranes upon the addition of anions. The ultimate goal for this research area is to detect fluoride anions in water at neutral pH for obvious practical reasons.

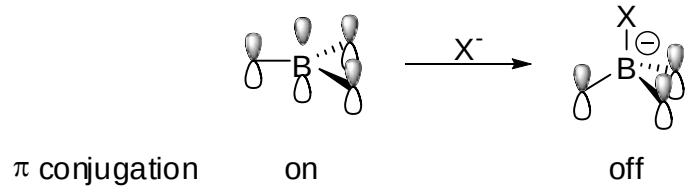

Figure 10: Change in π-conjugation of triarylboranes upon complexation.

The first reported triarylborane based fluoride receptor is the tri(9-anthryl)borane, **3**, reported by Yamaguchi and Tamao.[40] Compound **3** was found to change color from orange to light yellow upon treatment of fluoride in THF (Figure 11). By monitoring the decrease of the absorbance at 470 nm upon incremental addition of fluoride anions, the fluoride binding constant of **3**, 2.8 x 10^5 M^{-1} in THF, can be determined. The process has also been shown to be reversible upon the addition of water into THF solutions of the fluoroborate.

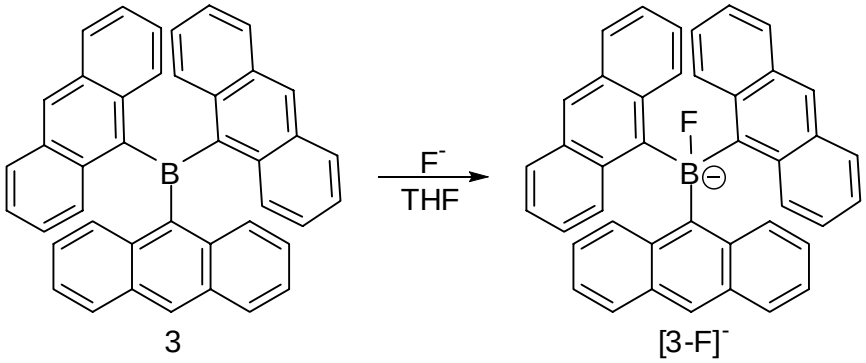

Figure 11: Fluoride complexation of **3**.

Yamaguchi has also prepared triarylborane derivatives featuring a different π-system. For example, his group has investigated the fluoride binding properties of a series of borafluorenes [41] (Figure 12). In this system, fluoride complexation removes the contribution of boron p_π orbital from the LUMO resulting in a significant increase in HOMO-LUMO gap. Since the LUMO of the resulting fluoroborate anion is still delocalized over the extended carbon backbone, the photophysical response of **4** upon fluoride binding occurs in the visible region. Due to the antiaromatic character of the

borafluorene moiety, **4** is more electron deficient, thus, the fluoride affinity of **4** is slightly higher than that observed for **3**.

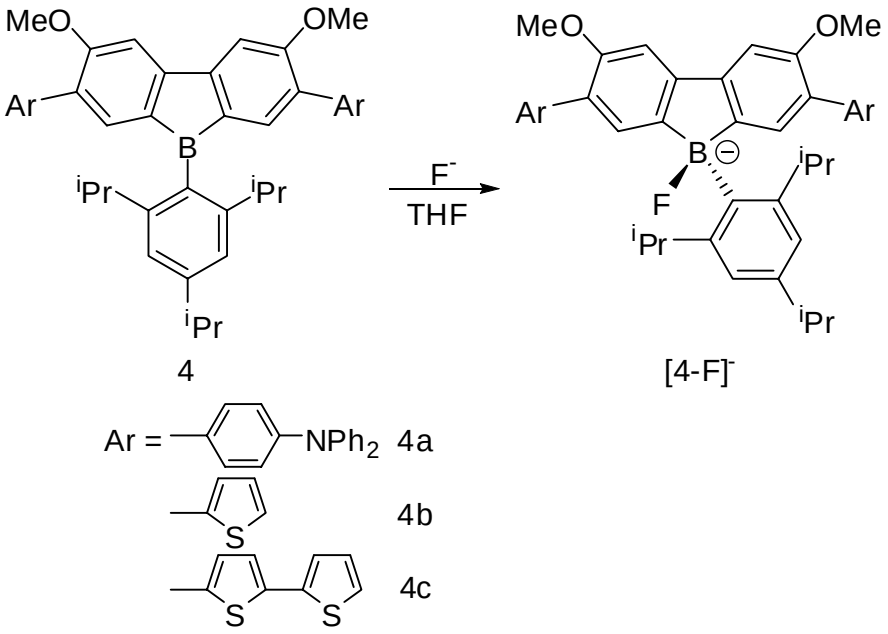

Figure 12: Fluoride complexation of **4**.

In the presence of appropriate electron donors, triarylboranes tend to display an intramolecular charge-transfer transition.[36] Although this property has been extensively studied, the use of these types of molecules in fluoride sensing was not investigated until recently. Wang and co-workers have developed a series of anion receptors featuring triarylamino and triarylboryl moieties that respectively serve as electron donor and acceptor units.[47, 100] Photo-excitation of these molecules results in an intramolecular charge-transfer emission, which can be quenched or perturbed upon fluoride binding at the boron center. Since the luminescence of the molecule is altered

due to the formation of a fluoroborate, the fluoride binding constant of the borane receptor can be determined by a fluorescence titration. The effect of the relative position of the donor and acceptor groups has also been investigated. In the linear molecule **5**, fluoride addition results in the quenching of the luminescence in THF (Figure 13).

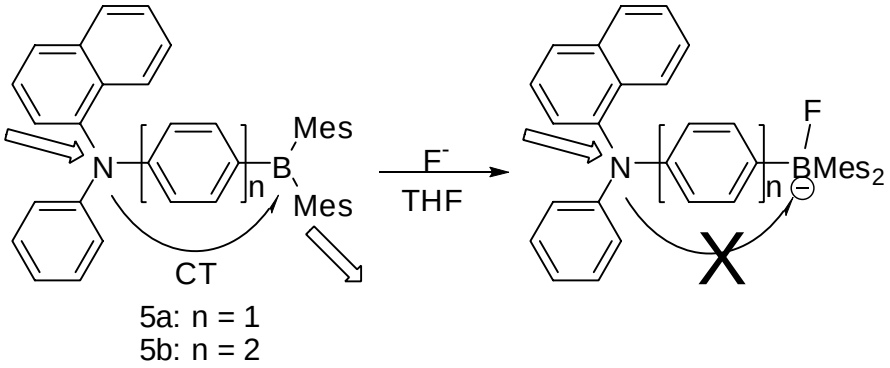

Figure 13: Fluoride complexation of **5**.

However, in the U shape molecule **6**, two emission mechanisms are observed, the through space donor-acceptor charge-transfer emission and the π-π* transition localized on the triarylamino moiety. In the presence of fluoride, the quantum yield of the π-π* transition is enhanced because of a quenching of the charge-transfer emission pathway (Figure 14). Moreover, the B-N separation in the U shape molecule affects not only the efficiency of the charge transfer, but also the fluoride binding ability of the triarylboryl moiety. For example, as the B-N distance increases from 6.7 Å in **6a** to 9.7 Å in **6b**, the fluoride binding constant increases from 1.4 x 10^4 M^{-1} to 4 x 10^4 M^{-1} in THF, respectively.

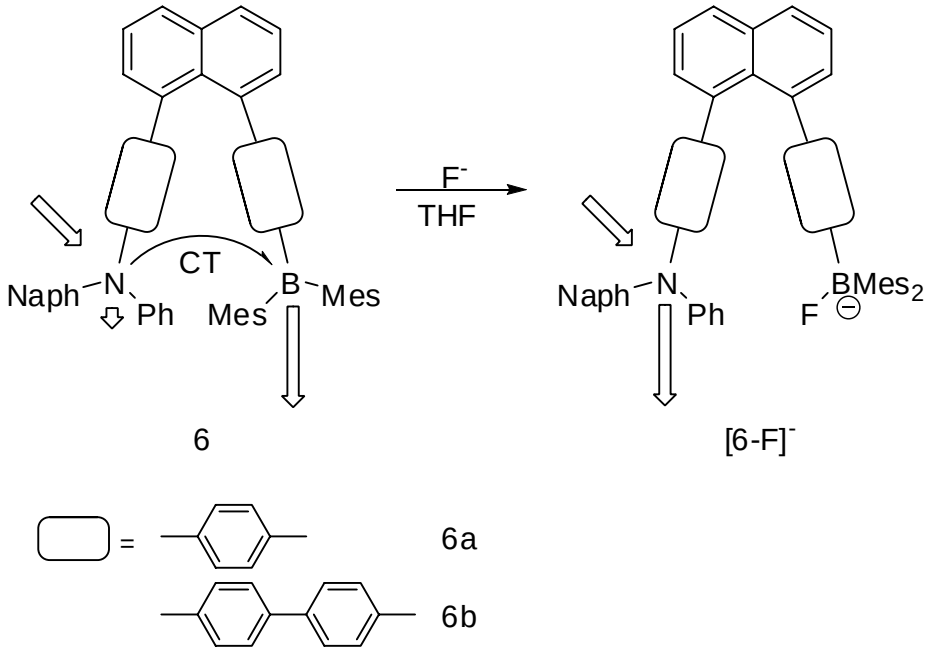

Figure 14: Fluoride complexation of **6**.

Recently, Wang's group has synthesized a series V shape receptors **7**, which exhibit two luminescence mechanisms similar to their U shape analogues, but with higher sensitivity toward fluoride binding.

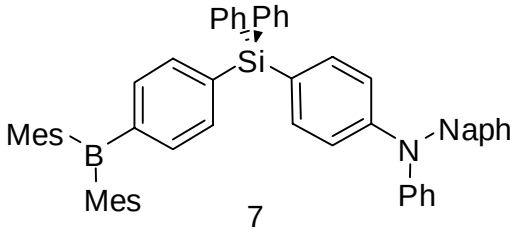

In addition to their single-photon related absorption and emission properties, several triarylborane derivatives were recently found to display an unusual two-photon excited fluorescence (TPEF). TPEF is especially attractive for imaging purposes in biological system because low energy light, which has a greater penetration depth in biological tissues, can be used to excite the compound. The TPEF property of **8** has also been used in fluoride recognition by Li and Fang (Figure 15).[46] As evidenced by obtaining the same fluoride binding constant of 2 x 10^5 M^{-1} from both single-photon excited fluorescence (SPEF) and TPEF, the origin for the spectral changes observed in both techniques derive from the same chemical event.

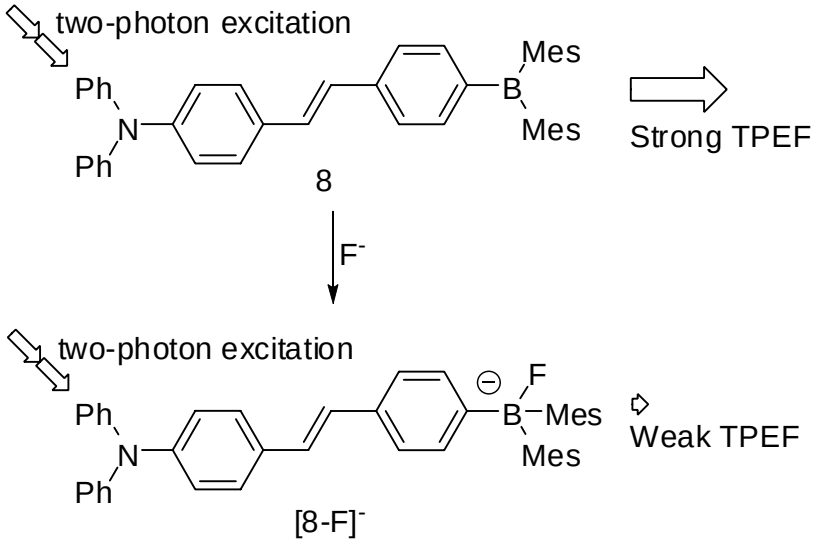

Figure 15: Fluoride complexation of **8**.

In addition to simple boranes, several polyfunctional boranes containing various molecular linkers have been investigated. Yamaguchi has reported a polyfunctional borane, **9**, that contains four boron atoms capable of binding fluoride. The fluoride binding constants were determined to be 6.9 x 10^4 M^{-1}, 9.0 x 10^2 M^{-1}, and 2.1 x 10^2 M^{-1} for the first, second and third fluoride ion, respectively.[35] This result indicates that the fluoride affinity of **9** is significantly decreased after the first fluoride binding event. Besides, the UV-vis spectrum of [**9**-$\mathbf{F_3}$]$^{3-}$ is very close to that observed form **3** suggesting that fluoride complexation only occurs at the terminal boron sites.

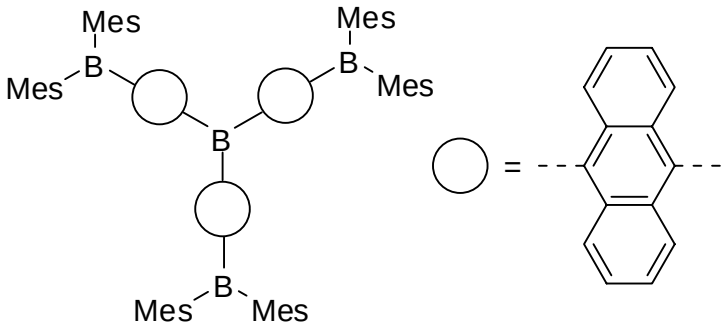

9

The photophysical response of diborane **10** upon addition of fluoride ions has also been studied.[46] Two stages of fluoride complexation were observed by a UV-vis titration experiment in THF, and the fluoride binding constants were determined to be 3.2 x 10^5 M^{-1} and 1.3 x 10^5 M^{-1} for first and second binding site, respectively. In addition to the change in the absorption spectrum, **10** also display strong SPEF and TPEF that can be used to monitor fluoride binding. However, only the first stage of

fluoride complexation can be observed using SPEF and TPEF. Indeed, after addition of one equivalent of fluoride, no further changes can be observed in the luminescence spectrum due to the low quantum yield of [**10-F**]$^-$.

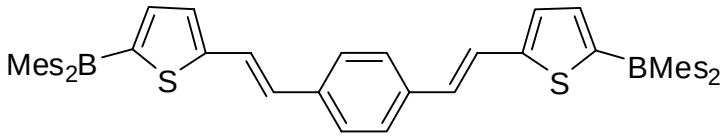

10

It is noteworthy that the fluoride affinity of the aforementioned polyfunctional boranes is not significantly different from that of monofunctional boranes. This phenomenon comes from the lack of cooperative binding between two boron centers or the presence of electron withdrawing functionalities in the molecule. In order to increase the anion affinity of polyfunctional borane receptors, main group chemists have investigated the synthesis of more electron deficient diboranes species that contain proximal boryl functionalities. Piers's group reported 1,2-bis(bis(pentafluorophenyl)boryl)benzene (**11**) and its use as a Lewis activator in olefin polymerization reactions. This diborane complexes a number of anions including hydroxide, methoxide[101], azide[102], chloride[103] and fluoride[101] (Figure 16). Although the stability constant of these adducts have not been reported, it can be assumed that this anionic chelate complexes are highly stable.

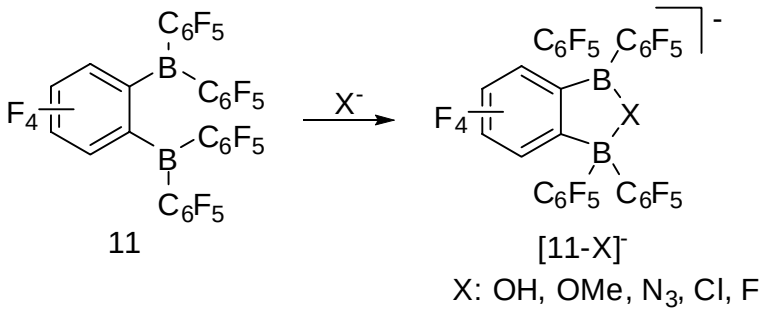

Figure 16: Anion complexations of **11**.

In 2004, Gabbaï's group reported the use of naphthalene based diboranes for fluoride complexation.[43, 104] The UV-vis titration of **1** in THF reveals that the absorbance decreases linearly with an increase in fluoride concentration and reaches the baseline after addition of one equivalent of fluoride (Figure 17). This result indicates the formation of a 1:1 complex between **1** and fluoride with a binding constant exceeding the measurable range ($>10^8$ M^{-1}). Therefore, the fluoride binding constant of diborane **1** exceeds of mono-functional boranes by at least three orders of magnitude in organic solvents. This enhancement is attributed to a chelate effect occurring in this type of systems and may also originate from a relief of steric repulsion between two boryl groups upon fluoride binding.[104] Unlike the fluoroborate derivatives [**3-F**]$^-$, addition of water to THF solutions of [**1-F**]$^-$ complexes does not result in dissociation of the B-F bond.

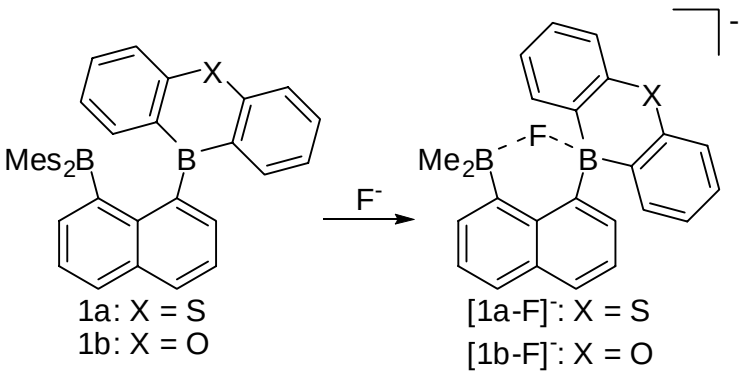

Figure 17: Fluoride complexation of **1**.

In addition to the bidentate diborane derivatives, Gabbaï's group also investigated the heteronuclear bidentate Lewis acid **2** which features a dimesitylboryl and a pentafluorophenylmercury group at the *peri*-position of naphthalene [52]. In addition to participating in fluoride binding,[105, 106] mercury can also serve to induce the room temperature phosphorescence of hydrocarbon chromophores via spin-orbit coupling effects.[107] As in other triarylboranes, the empty p-orbital of the boron atom of **2** mediates conjugation between the naphthalenediyl and mesityl substituents, which collectively behave as a single chromophore. Photoexcitation of **2** gives rise to an emission at λ_{max} = 531 nm in solid state corresponding to the phosphorescence of the dimesitylborylnaphthalenediyl chromophore (Figure 18). Upon fluoride complexation, a new intense signal appears at 480 nm whose energy and vibronic progressions is very close to those observed in the phosphorescence spectrum of pure naphthalene. This indicates that fluoride binding results in the loss of conjugation and isolates the naphthalenediyl chromophore, which readily phosphoresces due to the spin-orbit coupling induced by the mercury atom. The fluoride binding constant of **2** was

determined to be greater than 10^8 M^{-1} in organic solvent and 2.3 x 10^4 M^{-1} in a 9:1 THF/H_2O mixed solvent system, which substantiates the cooperative binding of fluoride by the boron and mercury atoms. At the time of this report, **2** was the first triarylborane capable of binding fluoride ions in water containing media.

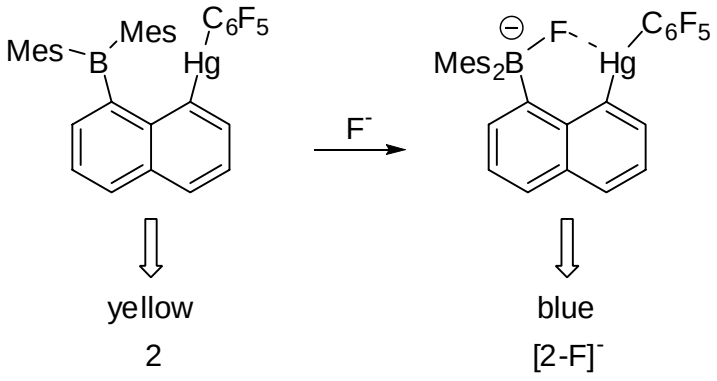

Figure 18: Fluoride complexation of **2**.

Another strategy to increase the fluoride affinity of diboranes is the incorporation of electron withdrawing molecular linker between two boryl groups. Diborane **12** reported by Wang and co-workers containing a 2,2'-bipyridyl linker displays an enhanced fluoride affinity due to the presence of electronegative nitrogen atoms.[108] As indicated by cyclic voltammetry, **12** undergoes reduction at potential which is 270 mV more positive than that of its biphenyl analog **13**. Moreover, the separation between the first and second reduction waves in the cyclic voltammogram of **12** is 130 mV greater than that observed for **13**. This observation indicates that the bipyridyl linker is more efficient in mediating electronic communication between the two boryl units. The higher Lewis acidity of **12** is also manifested by its unusually high fluoride affinity. This diborane binds a first fluoride anion with binding constant greater than 10^8 M^{-1} and second one at 10^6 M^{-1}. These values are much higher than those typically measured for triarylboranes.

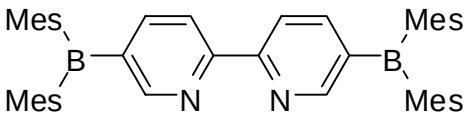

12

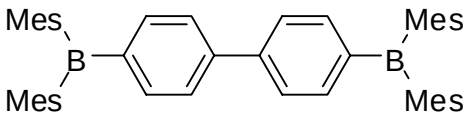

13

Coordination of Cu(I) or Pt(II) moieties to the bipyridyl ligand of this diborane leads to the formation of orange complexes **14a-c**, which feature Metal to Ligand Charge Transfer band. This MLCT band can also be used to monitor fluoride binding.

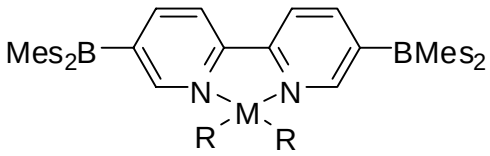

14a: M = Pt, R = Ph
14b: M = Pt, R = Me
14c: M = Cu, R = PPh_3

Despite the attractive photophysical properties and the substantial fluoride affinity of triarylboranes (Table 1), their use for practical applications remains problematic. In particular, none of the aforementioned boranes are capable of binding fluoride in aqueous media, nor are they able to overcome the hydration energy of fluoride. For example, although the fluoride adduct of compound [**3**-F]$^-$ shows a stability constant of 10^5 in organic solvent, addition of water into the system leads to complete dissociation of fluoroborate. The chelating diborane **1**, whose fluoride binding constant exceeds that of mono-functional borane by 3 orders of magnitude, cannot bind fluoride in protic environments and undergoes hydrolysis in the presence of water. The heteronuclear bidentate receptor **2**, which captures fluoride in a 9:1 THF/H_2O mixed solvent system, does not capture fluoride from pure water.

Table 1: Fluoride binding constant of triarylboranes

	Solvent	K_1 (M^{-1})	K_2 (M^{-1})	K_3 (M^{-1})
1	THF	$\geq 10^8$	-	-
2	THF/H_2O 9:1	2.3×10^4	-	-
3	THF	$2.8(\pm0.3) \times 10^5$	-	-
4c	THF	$1.4(\pm0.3) \times 10^6$	-	-
5	THF	N.A.	-	-
6a	THF	1.4×10^4	-	-
6b	THF	4×10^4	-	-
7	THF	N.A.	-	-
8	THF(SPEF)	$2.1(\pm0.4) \times 10^5$	-	-
	THF(TPEF)	$2.8(\pm0.6) \times 10^5$	-	-
9	THF	$6.9(\pm0.2) \times 10^4$	$9.0(\pm0.6) \times 10^2$	$2.1(\pm0.4) \times 10^2$
10	THF	$3.2(\pm0.3) \times 10^5$	$1.3(\pm0.2) \times 10^5$	-
12	CH_2Cl_2	$\geq 10^8$	$\sim 10^6$	-
	THF/EtOH 7:3	6×10^4	-	-
14a	CH_2Cl_2	$\geq 10^9$	$\sim 10^6$	-
	CH_2Cl_2/MeOH 4:1	4×10^3	-	-

2.2 Electroreduction of mono-functional and poly-functional boranes

Triaryl borane radical anions, which can be generated by reduction of triaryl boranes with alkali metals are isoelectronic to triarylmethyl neutral radicals. Because these relationship, such radical anions have attracted a great deal of attention since their discovery. However, salts of these radical anions are proved hard to crystallize and have been studied mostly by UV-vis or EPR spectroscopy.

The stability of the boron radical anions is strongly dependent on the steric shielding provided by the aryl groups. Attempts to generate the radical anion of triphenylborane in THF have been unsuccessful because of the formation of ion cluster. However, $[Mes_3B]^{\bullet-}$ (Mes = 2,4,6-trimethylphenyl) is obtained as a stable monomeric radical anion with a hyperfine coupling constant $a(^{11}B)$ of 10 gauss. While the $[Mes_3B]^{\bullet-}$ is stable for weeks in solution, $[Ph_3B]^{\bullet-}$ undergoes reductive cleavage and produces the arene or biaryl radical anions.[74]

According to EPR studies, the unpaired electron, which is largely localized on the boron center, is stabilized by delocalization on the aryl ligands. This is further confirmed by the solid state structural characterization of the $[Mes_3B]^{\bullet-}$ reported by Power's group in 1986.[75] According to the single crystal X-ray analysis of $[Li(12\text{-crown-4})]^{+}[Mes_3B]^{\bullet-}$, the boron atom adopts a trigonal planar geometry as indicated by the sum of C-B-C angles of 360º. Structural comparison of $[Mes_3B]^{\bullet-}$ and Mes_3B reveals that the additional electron results in virtually no changes in the molecular structure, except a slight lengthening of the B-C bond distance.

Similar studies have been carried out on $(C_6F_5)_3B$. Despite the fact that $(C_6F_5)_3B$ has been used to oxidize various transition metal complexes,[99, 109] $[(C_6F_5)_3B]^{\bullet-}$ has never been observed during those reactions nor isolated after reduction with Na/K.[109] Attempts to generate $[(C_6F_5)_3B]^{\bullet-}$ using cobaltocene also failed due to attack of the electrophilic boron center by the Cp ring. Finally, by using the more bulky Cp_2^*Co instead of Cp_2Co, side reactions are precluded and the EPR signal of $[(C_6F_5)_3B]^{\bullet-}$ is obtained as a 14 line-pattern spectrum centered at g_{iso} = 2.010. Analysis of the spectrum reveals that the unpaired electron is not only coupled to the ^{11}B nucleus by 10.5 G, but also to the *ortho*-, *meta*-, and *para*-fluorine atoms with $a(^{19}F)$ value of 4.60 G, 1.30 G, and 5.30 G, respectively.[77]

In addition to EPR studies, the reduction of triarylboranes can also be studied by electrochemical methods including cyclic voltammogram (CV). The reduction potential and reversibility of the reduction wave obtained from a CV measurement provide useful information concerning the Lewis acidity of a given borane and the stability of its corresponding radical anion. The electrochemistry of a series of triarylboranes reported by Kaim and co-workers has demonstrated that the steric bulk around the boron center is essential for the observation of a reversible reduction.[110, 111] As shown in Table 2, the reduction potential of boranes is quite sensitive to the electron donating ability of the aryl groups (NMe_2 > Me > H). The reduction wave of triphenylborane can be altered from irreversible to reversible by simply replacing one of the phenyl groups by a mesityl group. However, the cyclic voltammogram of Mes_3B

contains one reversible reduction wave followed by an irreversible one thus indicating that the doubly reduced boron dianion is not stable and subject to decomposition.

Table 2: Reduction potential of triarylboranes in THF

	Ph_3B	Ph_2MesB	$PhMes_2B$	Mes_3B	$(4\text{-}Me_2N\text{-}C_6H_4)BMes_2$
E_{red}[a] (V)	-1.63 (qr)[b]	-1.79	-1.85	-1.94	-2.16

a) Potential reported vs. SCE. b) (qr) = quasi-reversible

Since attempts to determine the reduction potential of highly reactive $(C_6F_5)_3B$ failed, Norton and co-workers decided to use an indirect method to estimate the reduction potential of $(C_6F_5)_3B$ in THF.[78] In order to do so, they experimentally determined the reduction potential of $Mes_2B(C_6F_5)$, $MesB(C_6F_5)_2$ and Mes_3B in THF to be -1.19 V, -1.57 V and -2.20 V, respectively. By assuming a linear relationship between the number of C_6F_5 rings and the reduction potential of the boranes in THF, the reduction potential of $(C_6F_5)_3B$ was estimated to be -0.64 V vs. SCE in THF.

In addition to monofunctional triarylboranes, the electroreduction of bifunctional boranes has also attracted a lot of attention. The one electron reduction of diboranes featuring co-facially oriented triarylboryl moieties has been shown to produce radicals with as B-B one electron σ–bond (Type A, Figure 19).[112, 113] When the two boron centers are linked by a B-B σ-bond, the one electron reduction produces a radical anion featuring a one electron B-B π-bond (Type B, Figure 19).[83] Finally, the reduction of several diboranes in which the two boryl groups are connected by aromatic linkers has

been reported. In this case, the resulting radical anion tends to be delocalized over the entire system (Type C, Figure 19).[110, 111, 114, 115]

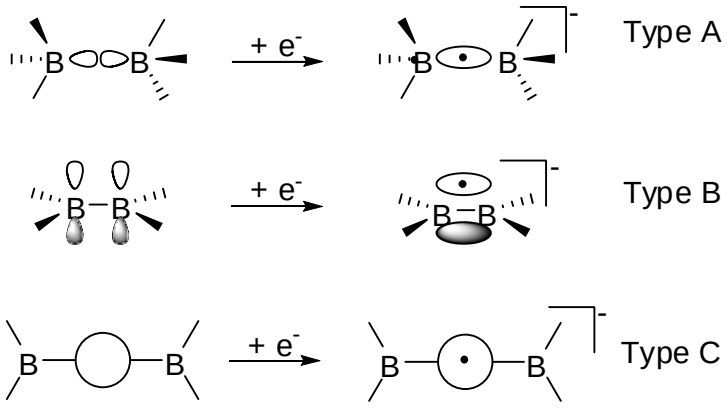

Figure 19: Reduction of diboranes.

During the electrochemical studies, it was proposed that $[Ph_3B]^{\bullet-}$ reacted with its neutral derivative to generate the diborane radical anion, $[Ph_3BBPh_3]^{\bullet-}$, in which the unpaired electron occupied a σ-orbital formed by the overlapping empty p orbitals of each boron atom. [116] Although similar bonding interaction have been observed in $[(MeO)_3BB(OMe)_3]^{\bullet-}$ and $[H_3BBH_3]^{\bullet-}$, these radical anions have only be observed at low temperatures or transiently. [112, 113] In order to pre-orient the p-orbitals, Gabbaï's group studied the synthesis of 1,8-diboryl-naphthalenediyl derivatives (**1**, **15** and **16**), in which two diarylboryl groups are in close proximity with a B-B distance ranging from 3.0 to 3.4 Å. [43, 87, 88, 117]

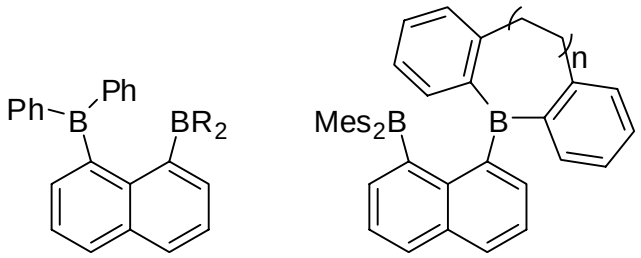

15a: R = Ph
15b: R = Mes

16a: n = 0
16b: n = 1

Electro-reduction of these diboranes suggests the formation of two stable reduction species as indicated by two reversible reduction waves in the CV. The reduction behavior of these diboranes is different from that observed for triarylboranes, which undergo one reversible reduction followed by an irreversible one. After the first reduction, the unpaired electron enters the empty σ-orbital between the two boron centers and forms a one electron B-B σ-bond. The presence of a one electron B-B σ-bond in [**15a**]$^{\bullet-}$ was confirmed by EPR.[87] A seven line splitting pattern with $a(^{11}B)$ = 5.9 G was observed as the result of equal sharing of electron between two boron atoms. The second reduction wave of **15a** corresponds to the formation of a dianion, which may exist as a diamagnetic species with a boron-boron σ-bond or as diradical (Figure 20). Unfortunately, attempts to generate the dianions chemically have not been successful; therefore, the identity of the dianion remains uncertain.

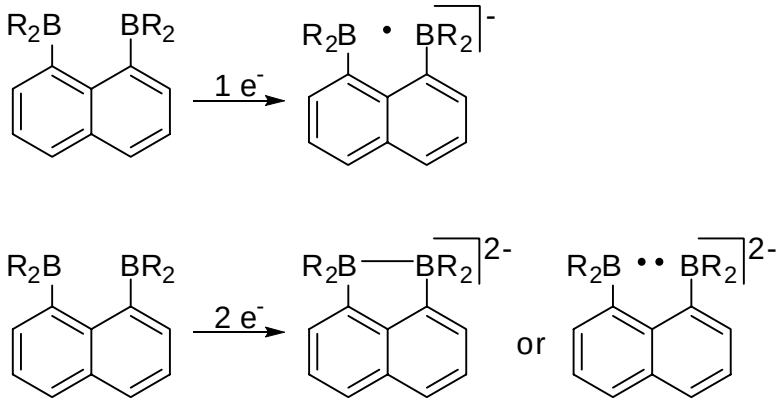

Figure 20: One- and two-electron reduction of 1,8-bis(diarylboryl)naphthalene.

Tetraaryldiboranes, which are isoelectronic to 1,1,2,2-tetraarylethylene dications,[118] have been extensively studied via electrochemistry.[84, 86] The diborane, **17**, can be reduced by one or two electrons to afford the corresponding radical anion and dianion, as shown in Figure 21.[84, 86] One electron reduction of **17** results in the formation of the diborane radical anion [**17**]$^{\bullet-}$, and the detection of seven line EPR signal with $a(^{11}B)$ = 13G suggests the delocalization of the unpaired electron in the B-B π bonding orbital. Further reduction of the diborane affords the B=B double bonded species [**17**]$^{2-}$. The conformational changes accompanying the stepwise population of the B-B π bonding orbital were also studied by X-ray crystallography. The structural results show that the B-B bond distance and the dihedral angle between the two boron containing planes are decreased on going from **17** to [**17**]$^{2-}$, in accordance with the formation of B=B double bond.

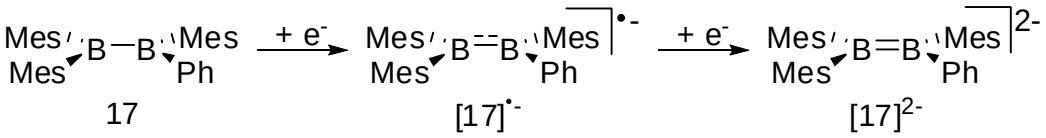

Figure 21: Reduction of diborane **17**.

The reduction chemistry of diboranes featuring *para*-phenylene or 4,4'-biphenyl linkers have also been studied.[110] As indicated by cyclic voltammetry, both compounds undergo two reversible reductions corresponding to the formation of radical anions and dianions in DMF ($E^1_{1/2}$ = -1.55 V, $E^2_{1/2}$ = -2.25 V for **18**; $E^1_{1/2}$ = -1.47 V, $E^2_{1/2}$ = -1.72 V for **13**). The greater separation of the two reduction waves in **18** suggests a stronger electronic communication between two boron centers.

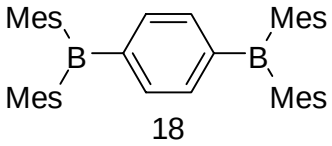

Although none of the reduced derivatives have been structurally characterized, the ab initio computation using model complex **19** shed light on the possible structural changes accompanying the reduction (Figure 22).[114] As indicated by the optimized geometry, the B-C bond undergoes a steady decrease on going from **19** to [**19**]$^{2-}$ (1.557 Å in **19**; 1.502 Å in [**19**]$^{\bullet-}$; 1.459 Å in [**19**]$^{2-}$). Therefore, the successive reduction of **18** affords a quinonoid derivative with localized C=C and C=B double bonds.

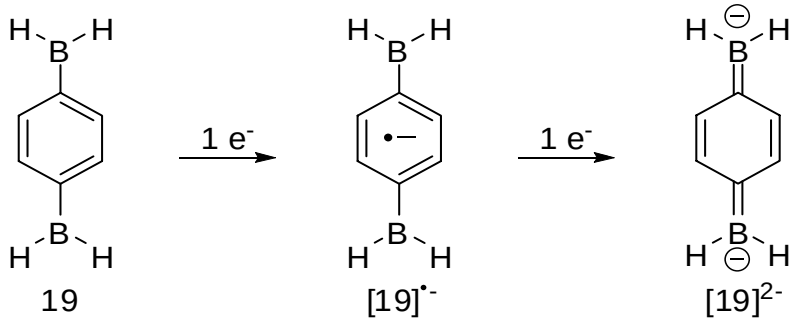

Figure 22: Reduction of diboranes **19**.

In addition to the *para*-phenylene backbone, the *meta*-analog **20** has also been synthesized and the reduction chemistry investigated (Figure 23).[119] Diborane **20** possesses two reversible reduction processes at -2.02 and -2.64 V vs. Fc/Fc^{+} in THF. However, in contrast to the closed shell quinonoid derivative $[\mathbf{18}]^{2-}$, the two electron reduction of **20** results in the formation of the triplet diradical dianion, $[\mathbf{20}]^{\bullet\bullet 2-}$.

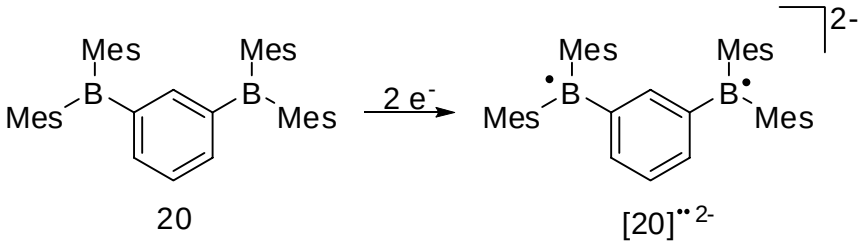

Figure 23: Reduction of diboranes **20**.

Recently, 4,6-dilithiodibenzofuran was isolated and used for the synthesis of 4,6-bis(dimesitylboryl)dibenzofuran **21**.[115] The CV of **21** also exhibits two reversible reduction waves detected at -2.45 and -2.81 V vs. Fc/Fc^+ in THF. The potential difference ($\Delta E_{1/2}$) of 0.36 V between the two reduction waves observed in **21** is larger than that obtained from **13** ($\Delta E_{1/2}$ = 0.25 V), indicating substantial electronic coupling of the two boron centers in **21**. The DFT calculation reveals that the LUMO of **21** has equal contribution from both boron atoms suggesting an antiferromagnetic coupling of the spin carriers between the two boryl groups attached to the 4- and 6-positions of dibenzofuran.

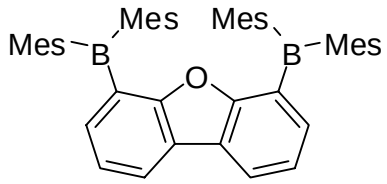

21

CHAPTER III

SYNTHESIS, CHARACTERIZATION AND ANION COMPLEXATION OF CATIONIC BORANES*

3.1 Introduction

Owing to its small size and high polarizing ability, fluoride has the highest hydration enthalpy of all water stable anions.[5, 8, 11, 20] For this reason, its complexation by molecular receptors in water is extremely challenging. A majority of the current research is focused on the design of receptors which interact with the anionic guest via hydrogen-bonds. Unfortunately, such receptors are not compatible with aqueous environments because water competes with the hydrogen-bond donor groups of the receptors.[21] These limitations, which can sometimes be circumvented by immobilization of the receptors, have led a number of researchers to investigate the use of Lewis acidic triarylborane receptors.[39-41, 120] Such receptors present attractive photophysical properties and capture fluoride with association constants in the 10^5-10^6 M^{-1} range in organic solvents. Like their hydrogen-bond donor counterparts, these boron-based fluoride receptors do not tolerate aqueous environments.

---

* Reproduced in part with permission from *J. Am. Chem. Soc.* **2006**, *128*, 14248, Chiu, C.-W.; Gabbaï, F. P., "Fluoride ion capture from water with a cationic borane", Copyright 2006 American Chemical Society.

To increase the binding constant of borane-based receptors, we and others have explored the use of naphthalene-based bidentate boranes that chelate fluoride.[43, 49-53] Although the fluoride binding constants of such a receptor exceeds that of monofunctional analogues by 3 or 4 orders of magnitude, their use in protic environments remains problematic. For example, chelating diboranes such as **1**[43] will undergo a slow hydrolysis in the presence of water. Compound **2**[52] which captures fluoride in THF/water 90/10 vol, does not capture fluoride from pure water.

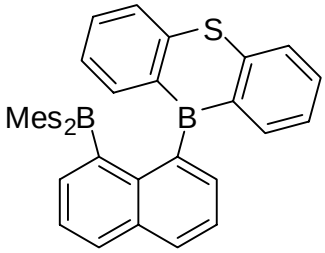

1

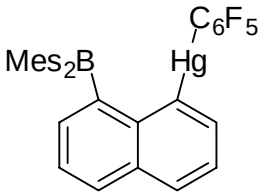

2

In an effort to overcome these challenges, we decided to investigate the cationic boranes which would have improved water compatibility In this chapter, we describe the synthesis of a cationic Lewis acidic borane which forms a highly stable zwitterionic ammonium/ fluoroborate complex possessing a C-H···F-B hydrogen bond. We also demonstrate how this cationic borane can be used for the extraction of fluoride from water.

3.2 Synthesis and characterization of ammonium borane

3.2.1 Synthesis of the aminoborane

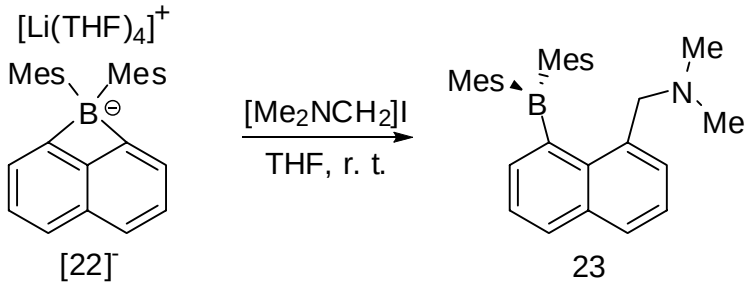

Figure 24: Synthesis of **23**.

The $[Li(THF)_4]^+$ salt of dimesityl-1,8-naphthalenediylborate ($[\mathbf{22}]^-$) was allowed to react with $[Me_2NCH_2]I$ to afford borane **23** (Figure 24). The ^1H NMR spectrum of borane **23** exhibits four distinct aromatic CH resonances from the mesityl groups indicating a highly congested structure. In accordance with this conclusion, the methylene hydrogen atoms of **23** are diastereotopic and give rise to two signals at 3.04 and 3.46 ppm. The ^{11}B signal detected at 69 ppm is comparable to other triarylboranes suggesting a coordination free boron center in solution.

A colorless single crystal suitable for the X-ray analysis was obtained by evaporating a CH_2Cl_2/hexane solution at room temperature. **23** crystallizes in the monoclinic space group $P2_1/c$ with four molecules in the unit cell (Figure 25, Table 3). The carbon-boron bond lengths of **23** are unremarkable and the boron adopts a trigonal planar geometry ($\Sigma_{angles} = 359.0°$). The methylene carbon atom C(01) of the CH_2NMe_2 moiety is separated from the boron atom B(1) by only 3.121 Å indicating significant steric congestion. As a result, the B(1)-C(1)-C(9) (128.7(2)°) and C(01)-C(8)-C(9) (123.7(2)°) angles substantially deviate from the ideal value of 120º.

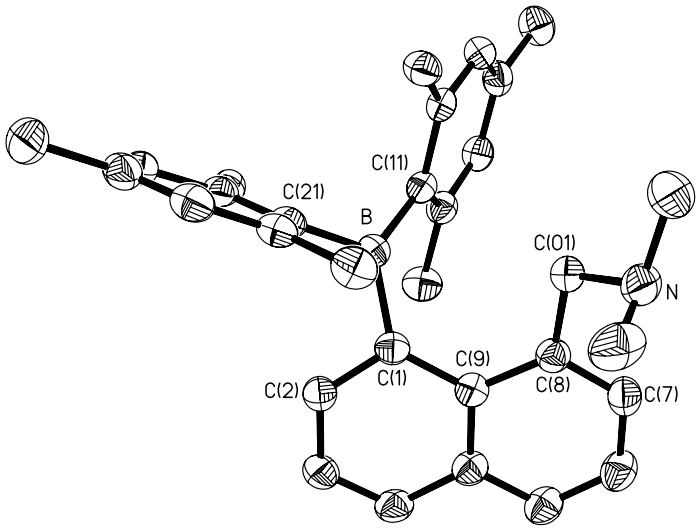

Figure 25: ORTEP plot of the molecular structure of **23** with thermal ellipsoids set at 50% probability level. Hydrogen atoms are omitted for clarity. Selective bond distances [Å] and bond angles [°]: B-C(1) 1.571(3), B-C(11) 1.577(3), B-C(21) 1.587(3), C(1)-C(2) 1.384(3), C(1)-C(9) 1.449(3), C(7)-C(8) 1.379(3), C(8)-C(9) 1.427(3), C(8)-C(01) 1.517(2), C(1)-B-C(11) 121.97(18), C(1)-B-C(21) 116.50(18), C(11)-B-C(21) 120.53(18), C(2)-C(1)-C(9) 117.48(18), C(2)-C(1)-B 111.81(19), C(9)-C(1)-B 128.65(18), C(7)-C(8)-C(9) 119.47(19), C(7)-C(8)-C(01) 116.85(18), C(9)-C(8)-C(01) 123.63(18).

Table 3: Crystal data and structure refinement for **23**

Crystal data	**23**
Formula	$C_{31}H_{36}BN$
M_r	433.42
Crystal size (mm^3)	0.42 x 0.27 x 0.16
Crystal system	Monoclinic
Space group	*P*2(1)/c
a (Å)	15.8202(13)
b (Å)	10.2595(8)
c (Å)	17.3207(14)
α (º)	90.00
β (º)	116.6200(10)
γ (º)	90.00
V ($Å^3$)	2513.5(3)
Z	4
ρ_{calc} (gcm^{-3})	1.145
μ(Mo K_α) (mm-1)	0.064
F(000) (e)	936
Data collection	
T/K	110
Scan mode	ω
hkl range	-19→15, -12→11, -20→20
Measured refl.	12734
Unique refl., [R_{int}]	4544, [0.0660]
Refl. Used for refinement	4544
Refinement	
Refined parameters	295
R_1, wR_2 [all data]	0.0815, 0.1399
ρ_{fin} (max/min) (e $Å^{-3}$)	0.417/-0.358

3.2.2 Synthesis of ammonium boranes

The ammonium boranes were synthesized using Brønsted acids to give the tertiary ammonium boranes or alkylation reagents to generate the quaternary ammonium boranes (Figure 26).

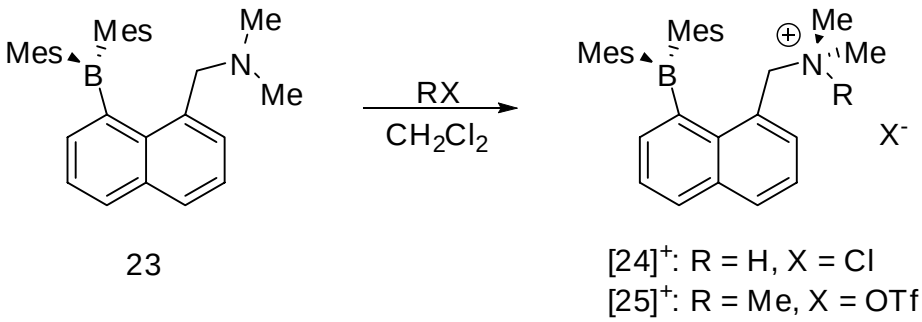

Figure 26: Synthesis of cationic borane.

The tertiary ammonium borane [**24**]$^+$ was synthesized in quantitative yield by protonation of **23** with HCl, and isolated as a chloride salt. The formation of the tertiary ammonium ion was confirmed by ^{1}H NMR spectroscopy.

The ^{1}H NMR spectrum of [**24**][Cl] shows the aromatic CH and methyl group resonances from the mesityl groups are all non-equivalent indicating a crowded environment around the boron atom. The ^{11}B NMR signal of [**24**]$^{+}$ detected at 69 ppm suggests a trigonal planar geometry around the boron center and the absence of chloride-boron interaction in solution.

Single crystals of [**24**][Cl] were obtained by vapor diffusion of hexane into a $CHCl_3$ solution at room temperature. [**24**][Cl] crystallizes in the monoclinic space group P2(1)/n as a $CHCl_3$ solvate (Figure 27). All bond distances and bond angles for [**24**]$^{+}$ are typical with the exception of the B(1)-C(1)-C(9) angle of 131.0(2)°, which substantially deviates from the ideal value of 120º. The sum of the angles around B(1) (Σ_{angles} = 359.4°) and the long B(1)-Cl(1) distance (6.958 Å) show that there is no interaction between boron and chloride. These structural features re-emphasize the steric congestion around the boron atom in [**24**]$^{+}$ that precludes complexation of large anions.

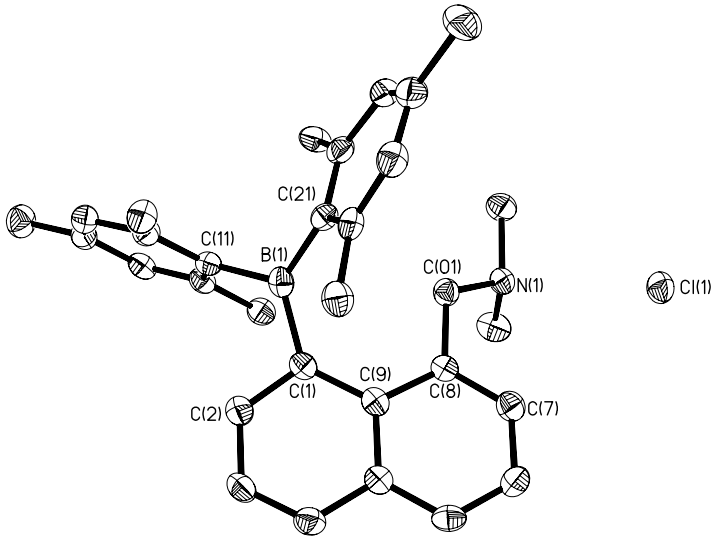

Figure 27: Crystal structure of [**24**]$^+$ with thermal ellipsoids set at the 50% probability level. Hydrogen atoms are omitted for clarity. Selected bond lengths [Å] and bond angles [º]: B(1)-C(1) 1.566(4), B(1)-C(11) 1.578(4), B(1)-C(21) 1.586(4), C(1)-C(2) 1.402(4), C(1)-C(9) 1.451(4), C(7)-C(8) 1.373(4), C(8)-C(9) 1.435(4), C(8)-C(01) 1.515(4), C(1)-B(1)-C(11) 117.0(2), C(1)-B(1)-C(21) 123.2(2), C(11)-B(1)-C(21) 119.2(3), C(2)-C(1)-C(9) 117.2(3), C(2)-C(1)-B(1) 110.5(2), C(9)-C(1)-B(1) 131.0(2), C(7)-C(8)-C(9) 120.6(3), C(7)-C(8)-C(01) 118.6(2), C(9)-C(8)-C(01) 120.7(2).

Table 4: Crystal data and structure refinement for [**24**][OTf]

Crystal data	**[24][OTf]•$CHCl_3$**
Formula	$C_{32}H_{38}BNCl_4$
M_r	596.21
Crystal size (mm^3)	0.2 x 0.09 x 0.07
Crystal system	Monoclinic
Space group	P2(1)/n
a (Å)	16.788(4)
b (Å)	9.139(2)
c (Å)	20.569(4)
α (º)	90.00
β (º)	101.575(4)
γ (º)	90.00
V ($Å^3$)	3091.4(11)
Z	4
ρ_{calc} (gcm^{-3})	1.281
μ(Mo K_α) (mm-1)	0.406
F(000) (e)	1244
Data collection	
T/K	110
Scan mode	ω
hkl range	-2121, -128, -2722
Measured refl.	17849
Unique refl., [R_{int}]	7048, [0.0604]
Refl. Used for refinement	7048
Refinement	
Refined parameters	366
R_1, wR_2 [all data]	0.1174, 0.1963
ρ_{fin} (max/min) (e $Å^{-3}$)	1.102/-0.367

Compound **23** can also be methylated with MeOTf to afford the quaternary ammonium borane [**25**]$^+$ which was isolated as a triflate salt. The ^{1}H NMR spectrum of [**25**]$^+$ exhibits four distinct aromatic CH resonances and six methyl CH resonances arising from the mesityl groups, indicating a highly congested environment around the boron center. The methylene hydrogen atoms of [**25**]$^+$ are also diastereotopic and give rise to two signals at 3.69 and 4.81 ppm emphasizing the sterically inhered environment at the *peri*-positions of naphthalene. The presence of a base free tricoordinate boron center in solution was confirmed by the detection of a ^{11}B NMR resonance at 68 ppm.

The crystal structure of [**25**][OTf] has been determined. This salt crystallizes in the monoclinic *P*-1 space group with two independent molecules in the asymmetric unit (Figure 28, Table 5). Both independent molecules, arbitrarily denoted as molecule A and molecule B, feature very similar structures. The boron atoms of each molecule adopt a trigonal planar geometry ($\Sigma_{(C\text{-}B\text{-}C)}$ = 359.3°, molecule A; $\Sigma_{(C\text{-}B\text{-}C)}$ = 359.3°, molecule B) and are separated from the methylene carbon atom by only 3.215(7) (A) and 3.189(7) Å (B). This short separation indicates that the unsaturated boron centers are sterically encumbered. This observation is in agreement with the large B(1)-C(1)-C(9) (125.6(4)° (A), 126.2(4)° (B)) angle which substantially deviates from the ideal value of 120°.

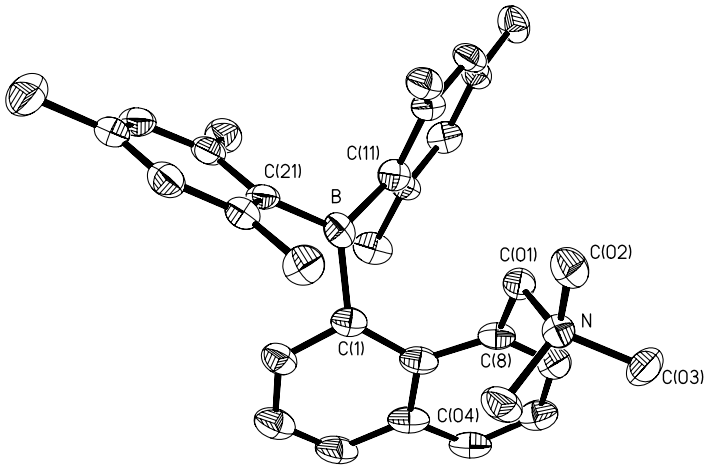

Figure 28: Crystal structure of [**25**]$^+$ with thermal ellipsoids set at the 50% probability level. Hydrogen atoms are omitted for clarity. Selected bond lengths [Å] and bond angles [º]: B-C(1) 1.580(7), B-C(11) 1.570(7), B-C(21) 1.578(7), B-C(01) 3.215(7), C(1)-C(2) 1.379(6), C(1)-C(9) 1.457(7), C(7)-C(8) 1.383(6), C(8)-C(9) 1.425(7), C(1)-B-C(11) 119.6(5), C(1)-B-C(21) 118.5(4), C(11)-B-C(21) 121.2(4), C(2)-C(1)-C(9) 117.3(5), C(2)-C(1)-B 112.8(4), C(9)-C(1)-B 125.6(4), C(7)-C(8)-C(9) 119.5(5), C(7)-C(8)-C(01) 118.8(5), C(9)-C(8)-C(01) 121.4(4).

Table 5: Crystal data and structure refinement for [**25**][OTf]

Crystal data	**[25][OTf]**
Formula	$C_{33}H_{39}BF_3NO_3S$
M_r	597.52
Crystal size (mm^3)	
Crystal system	Triclinic
Space group	P-1
a (Å)	14.135(3)
b (Å)	15.099(3)
c (Å)	16.702(3)
α (º)	65.970(4)
β (º)	72.914(4)
γ (º)	81.375(4)
V ($Å^3$)	3110.2(10)
Z	4
ρ_{calc} (gcm^{-3})	1.276
μ(Mo K_α) (mm-1)	0.156
F(000) (e)	1264
Data collection	
T/K	110
Scan mode	ω
hkl range	-14→17, -15→18, -17→20
Measured refl.	14506
Unique refl., [R_{int}]	11334, [0.0478]
Refl. Used for refinement	11334
Refinement	
Refined parameters	757
R_1, wR_2 [I>2σ(I)]	0.0765, 0.1376
ρ_{fin} (max/min) (e $Å^{-3}$)	

A fluorescent anthracenyl moiety can also be introduced by allowing **23** to react with excess iodomethylanthracene in a $CHCl_3$/acetone for three days (Figure 29).

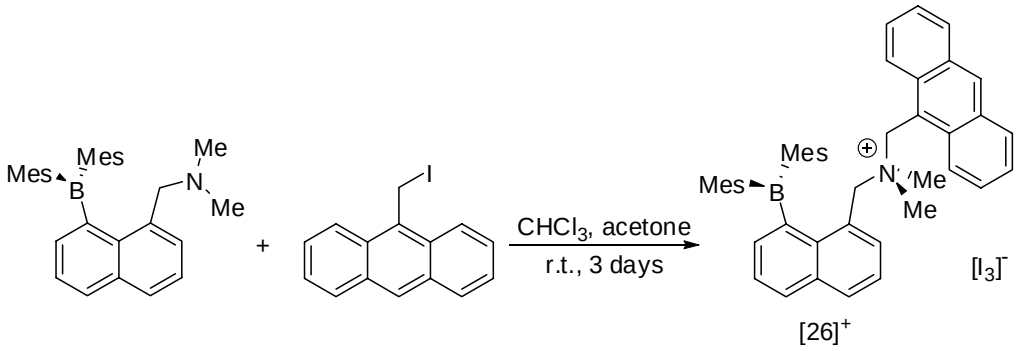

Figure 29: Synthesis of [**26**][I_3].

Slow evaporation of a CH_2Cl_2/ether solution of [**26**][I_3] yields a dark red crystalline solid with triiodide as the counter anion in moderate yield. In the ^{1}H NMR spectrum of [**26**][I_3], the aromatic CH from the anthracene, naphthalene and mesityl groups are all non-equivalent indicating a crowded structure. The ^{11}B resonance at 70 ppm is comparable to other triarylboranes.

The crystal structure of [**26**][I_3] has been determined (Figure 30, Table 1). [**26**][I_3] crystallizes in the monoclinic space group P2(1)/c with four molecules in the unit cell. The boron-carbon bond lengths of [**26**]$^+$ are unremarkable and the boron atom adopts a trigonal planar geometry ($\Sigma_{(C\text{-}B\text{-}C)}$ = 359.7°). The distance between the methylene carbon C(01) and the boron atom B(1) is only 3.223(5)Å suggests substantial steric congestion at the *peri* positions of naphthalene.

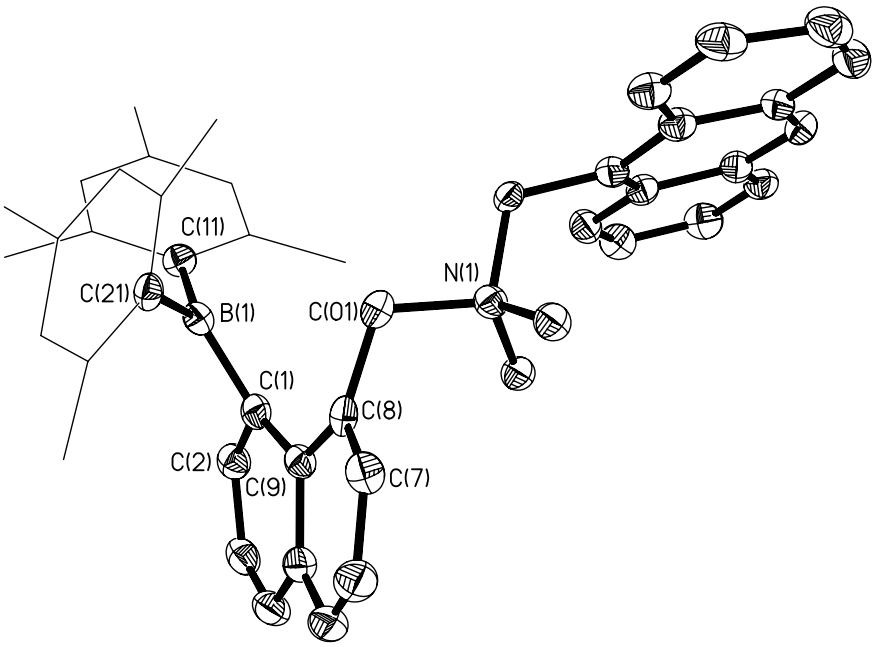

Figure 30: Crystal structure of [**26**]$^+$ with thermal ellipsoids set at the 50% probability level. Hydrogen atoms are omitted for clarity. Selected bond lengths [Å] and bond angles [º]: B(1)-C(1) 1.573(5), B(1)-C(11) 1.575(5), B(1)-C(21) 1.583(5), B(1)-C(01) 3.223(5), C(1)-C(2) 1.386(5), C(1)-C(9) 1.450(5), C(7)-C(8) 1.370(5), C(8)-C(9) 1.433(5), C(8)-C(01) 1.514(5), C(1)-B(1)-C(11) 122.2(3), C(1)-B(1)-C(21) 116.5(3), C(11)-B(1)-C(21) 121.0(3), C(2)-C(1)-C(9) 118.1(3), C(2)-C(1)-B(1) 112.8(3), C(9)-C(1)-B(1) 124.9(3), C(7)-C(8)-C(9) 119.8(3), C(7)-C(8)-C(01) 119.8(3), C(9)-C(8)-C(01) 120.2(3).

Table 6: Crystal data and structure refinement for [**26**][I_3]

Crystal data	**[26][I_3]**
Formula	$C_{46}H_{47}BI_3N$
M_r	1005.36
Crystal size (mm^3)	
Crystal system	Monoclinic
Space group	P2(1)/c
a (Å)	20.6707(12)
b (Å)	13.8171(8)
c (Å)	14.8433(8)
α (º)	90.00
β (º)	106.4910(10)
γ (º)	90.00
V ($Å^3$)	4065.0(4)
Z	4
ρ_{calc} (gcm^{-3})	1.643
μ(Mo K_α) (mm-1)	2.339
F(000) (e)	1976
Data collection	
T/K	110
Scan mode	ω
hkl range	-27→22, -18→17, -18→18
Measured refl.	24167
Unique refl., [R_{int}]	9379, [0.0338]
Refl. Used for refinement	9379
Refinement	
Refined parameters	460
R_1, wR_2 [all data]	0.0657, 0.01493
ρ_{fin} (max/min) (e $Å^{-3}$)	

3.3 Cyclic voltammetry

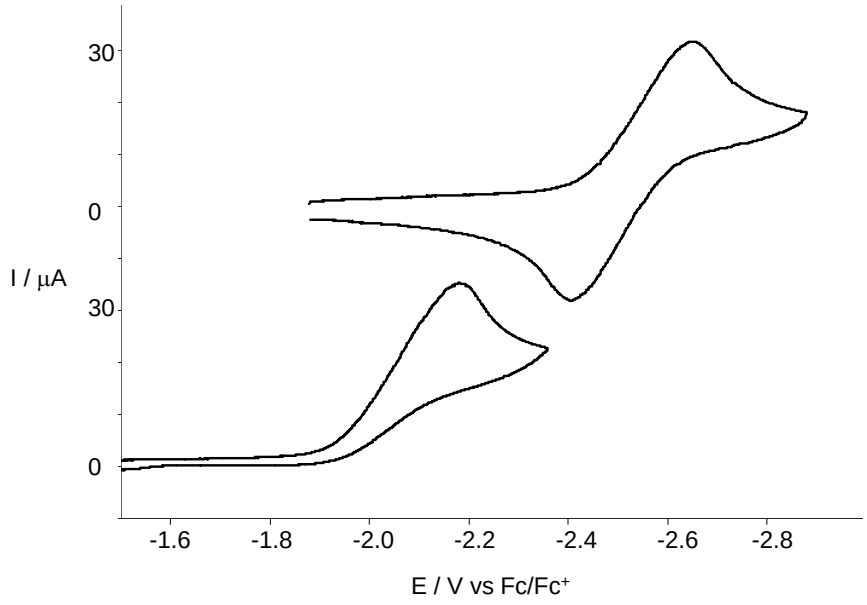

Figure 31: Cyclic voltammograms of **23** (top) and [**25**]$^+$ (bottom) in THF with a glassy-carbon working electrode (0.1 M nBu$_4$NPF$_6$). Scan rates: ν = 300 mV s^{-1} for **23** and 100 mVs^{-1} for [**25**]$^+$.

In an attempt to better understand the chemical properties of **23** and [**25**]OTf, we have studied their electrochemistry (Figure 31). The cyclic voltammogram of **23** in THF shows a reversible reduction wave at $E_{1/2}$ -2.53 V (vs. Fc/Fc$^+$) which is followed by undefined irreversible processes. The redox behavior of this derivative is similar to that of other triarylboranes which typically display a single reversible reduction wave corresponding to the formation of a radical anion.[71-78, 81, 82] The reduction potential of

23 is slightly more negative than that reported for dimesityl-1-naphthylborane (-2.41 V, vs. Fc/Fc^+) in agreement with the electron releasing properties of the CH_2NMe_2 substituent present at the 8-position.[88] Interestingly, the cyclic voltammogram of $[\mathbf{25}]^+$ in THF only shows an irreversible wave at E_{peak} -2.18 V (vs. Fc/Fc^+).

A comparison with the reduction peak potential of -2.66 V recorded for **23** indicates that $[\mathbf{25}]^+$ is substantially more electrophilic than **23**. This observation can be easily reconciled by considering the fact that $[\mathbf{25}]^+$ is a cation which is therefore expected to be more electrophilic. The irreversibility of the reduction of $[\mathbf{25}]^+$ suggested that the resulting radical anion decomposes possibly through loss of NMe_3.

3.4 Anion complexation

3.4.1 Fluoride complexation

Compound **23** does not show any appreciable affinity for fluoride. For example, the ^1H NMR spectrum of a mixture of **23** and TBAF in $CHCl_3$ only contains resonances corresponding to the free borane. Addition of TBAF to a $CHCl_3$ solution of $[\mathbf{24}]^+$ leads to deprotonation on the $NHMe_2$ group and forms compound **23** in quantitative yield. The reaction between $[\mathbf{26}]^+$ with anions, such as fluoride and thiosulfate, leads to decomposition of the molecule. Nevertheless, $[\mathbf{25}]^+$ is swiftly and quantitatively converted into zwitterionic **25**-F when treated with TBAF or TASF in $CHCl_3$ (Figure 32) . No changes are observed in the presence of other halides indicating that the complexation is selective.

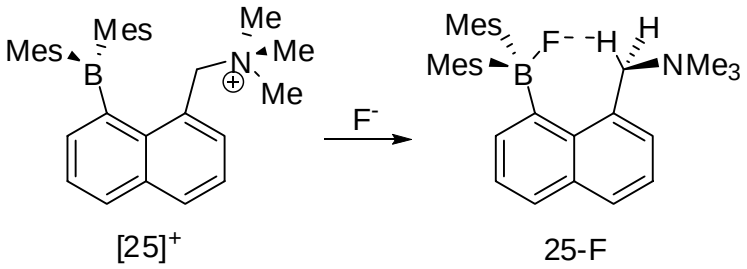

Figure 32: Fluoride complexation of [**25**]$^{+}$.

The ^{11}B NMR signal of **25**-F appears at 12.2 ppm as expected for a tetrahedral boron atom. The ^{19}F NMR spectrum features a broad signal at -152 ppm which is comparable to the chemical shift observed in other triarylfluoroborate complexes. [43, 49-53] Formation of this fluoride complex noticeably affects the ^{1}H NMR resonances of the diastereotopic methylene hydrogen atom. In particular, one of the two resonances is shifted downfield and appears at 6.50 ppm. Moreover, this methylene resonance shows coupling to the fluorine nucleus ($^{1}J_{H\text{-}F}$ = 9.2 Hz) and appears as a doublet of doublets ($^{2}J_{H\text{-}H}$ = 12.9 Hz) (Figure 33).

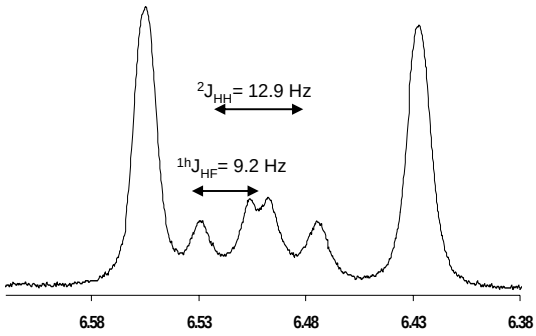

Figure 33: Portion of the ^{1}H-NMR of **25**-F showing the resonance of the hydrogen atom hydrogen-bonded to the fluorine atom.

This spectroscopic feature indicates the presence of a C-H···F-B hydrogen bond that persists in solution. Altogether, these results suggest that fluoride binding at boron may in fact be assisted by the formation of a hydrogen bond with a neighboring hydrogen bond donor group. This situation is reminiscent to that encountered in the ammonium fluoroborate [(η^5-C_5H_5)Fe{ η^5-C_5H_3(BF_3)(CH_2-NMe_2H)}] which features a N-H···F-B hydrogen bond.[24]

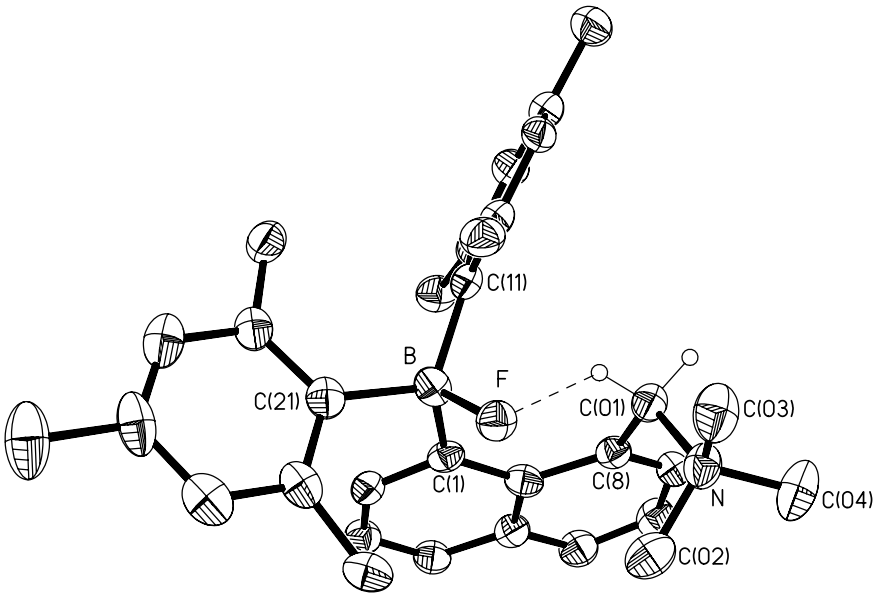

Figure 34: Crystal structure of **25**-F with thermal ellipsoids set at the 50% probability level. Hydrogen atoms are omitted for clarity. Selected bond lengths [Å] and bond angles [º]: F-B 1.486(4), F-C(01) 2.826(4), B-C(1) 1.678(5), B-C(11) 1.656(5), B-C(21) 1.667(5), C(1)-C(2) 1.390(4), C(1)-C(9) 1.465(4), C(7)-C(8) 1.377(4), C(8)-C(9) 1.456(4), C(8)-C(01) 1.506(4), B-F-C(01) 92.30(18), C(1)-B-C(11) 113.4(3), C(1)-B-C(21) 111.0(3), C11-B-C21 116.3(3), C(2)-C(1)-C(9) 115.4(3), C(2)-C(1)-B 113.9(3), C(9)-C(1)-B 130.6(3), C(7)-C(8)-C(9) 120.4(3), C(7)-C(8)-C(01) 115.0(3), C(9)-C(8)-C(01) 124.6(3).

Table 7: Crystal data and structure refinement for **25**-F

Crystal data	**25**-F
Formula	$C_{32}H_{39}BFN$
M_r	467.45
Crystal size (mm^3)	0.04 x 0.02 x 0.02
Crystal system	Orthorhombic
Space group	P2(1)2(1)2(1)
a (Å)	8.4633(10)
b (Å)	17.444(2)
c (Å)	17.727(2)
α (º)	90.00
β (º)	90.00
γ (º)	90.00
V ($Å^3$)	2617.0(5)
Z	4
ρ_{calc} (gcm^{-3})	1.186
μ(Mo K_α) (mm-1)	0.072
F(000) (e)	1008
Data collection	
T/K	110
Scan mode	ω
hkl range	-11→11, -22→9, -23→23
Measured refl.	15618
Unique refl., [R_{int}]	5947, [0.0619]
Refl. Used for refinement	5947
Refinement	
Refined parameters	316
R_1, wR_2 [all data]	0.1049, 0.1292
ρ_{fin} (max/min) (e $Å^{-3}$)	

Colorless crystals of **25**-F were obtained by evaporation of a Et_2O solution of **25**-F. As indicated by the X-ray crystal structure (Figure 34, Table 7), the fluorine atom is trapped between the boron atom and the methylene group. The B-F bond length of 1.486(4) Å is not significantly longer than those found in triarylfluoroborate anions (1.47 Å), thus indicating the presence of a usual polar covalent B-F linkage. Accordingly, the sum of the coordination angles at boron ($\Sigma_{(C\text{-}B\text{-}C)}B = 340.71°$) indicates substantial pyramidalization. The distance of 2.826(4) Å separating the fluorine atom and the methylene carbon atom confirms the presence of a C-H···F-B hydrogen bond. Hydrogen bonds involving C(sp^3)-H groups are rare[121, 122] especially for fluoroborate species.[123]

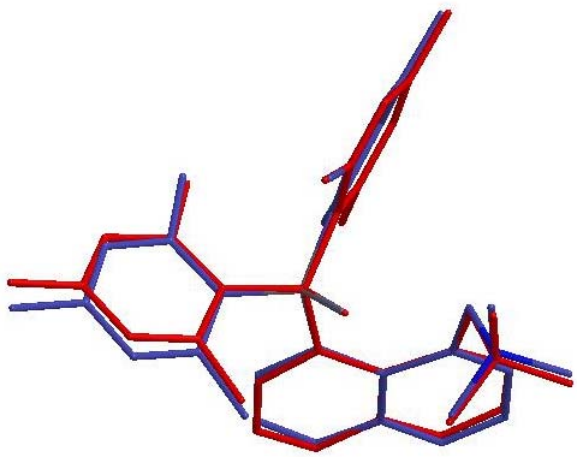

Figure 35: An overlap of the DFT optimized structure (blue) and crystal structure (red) of **25**-F.

In an effort to better understand this unusual C-H···F-B linkage, the structure of **25**-F was optimized using DFT methods (B3LYP, 6-31+g(d') for the boron and fluorine, 6-31g for all other atoms). The optimized structure is close to that determined experimentally (Figure 35). In particular, the calculated B-F (1.528 Å) and F-C(01) (2.818 Å) distances are within a few hundreds of an angstrom from that observed in the crystal (1.486 and 2.826 Å, respectively).

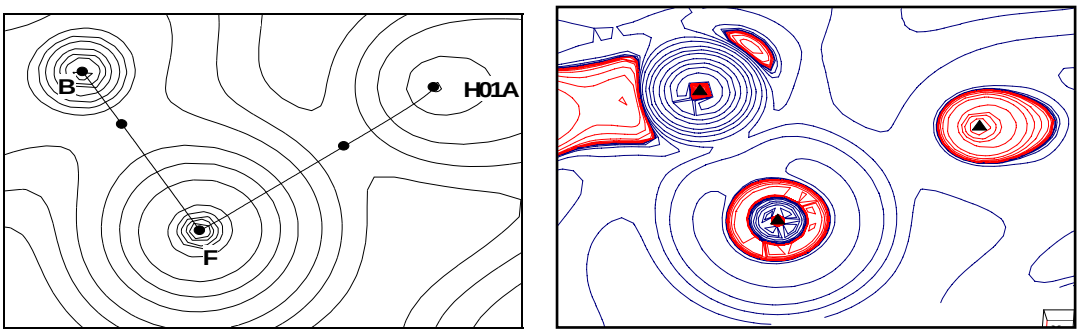

Figure 36: Left: Contour plot of the electron density of **25**-F in the H01A-F-B1 plane. Right: Contour plot of $-\frac{1}{4}\nabla^2 \rho(r)$ for **25**-F in the same plane illustrating the dative nature of both B-F and H-F bond. The blue and red lines represent negative and positive contours, respectively.

Analysis of the topology of the electron density using the AIM2000 program[124] shows the presence of a bond path between the hydrogen and fluorine atom of the C-H···F-B bridge (Figure 36). Moreover, the value of the electron density ($\rho(r)$ = 2.5 x 10^{-2} e bohr^{-3}) and the Laplacian value ($-1/4\nabla^2 \rho(r)$ = -2.4 x 10^{-2} e bohr^{-5}) at the H···F bond critical point fall within the expected range for a moderately strong hydrogen

bond.[125] Although moderately strong, this interaction may serve to increase the stability of the fluoroborate motif.[126]

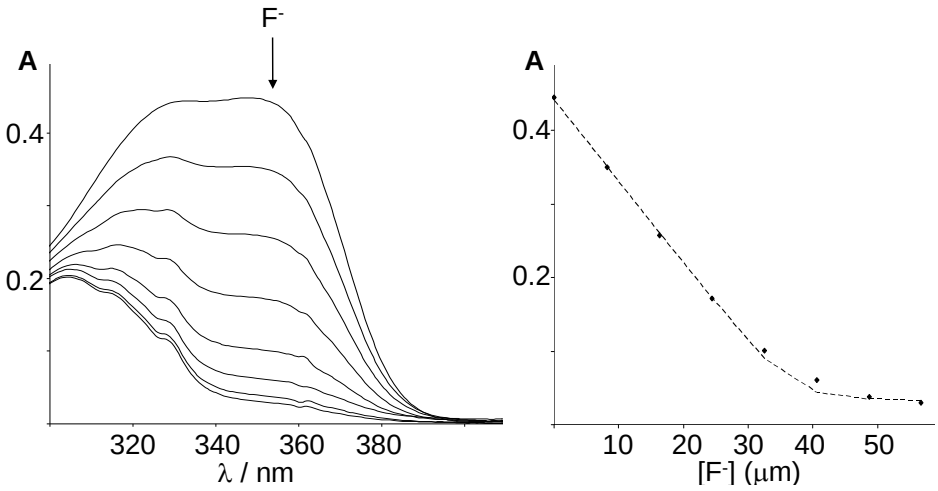

Figure 37: Absorption spectrum of a solution of [**25**]$^+$ (THF/MeOH 75/25) upon addition of fluoride. Plot of absorbance at 353 nm vs. concentration of fluoride.

The fluoride binding constant of [**25**]$^+$ in 75/25 (vol) THF/MeOH is equal to 5.0 ± (0.5) x 10^6 M^{-1} as indicated by a UV titration experiment carried out by monitoring the absorption of [**25**]$^+$ at λ_{max}) 352 nm (ε = 11850) (Figure 37). Under these conditions, Mes_3B does not form any detectable quantities of $[Mes_3BF]^-$. Encouraged by these results, we attempted to test the water compatibility of [**25**]$^+$. Although water stable, cation [**25**]$^+$ does not react with fluoride in pure water. Nevertheless, when dissolved in $CHCl_3$, [**25**]$^+$ captures fluoride from water to form **25**-F. For example, shaking a biphasic mixture consisting of TBAF in D_2O (2.7 x 10^{-1} M, 0.5 mL) and [**25**]OTf in

$CDCl_3$ (6.9 x 10^{-2} M, 0.5 mL) results in a 82% conversion of [**25**]OTf into **25**-F after a few minutes (Figure 38). To our knowledge, such a biphasic fluoride capture is unprecedented for any boron-based fluoride receptors. To provide additional comparative data, we have carried out the same experiments using **1** and **2,** and found that these chelating boranes fail to capture fluoride under these biphasic conditions.

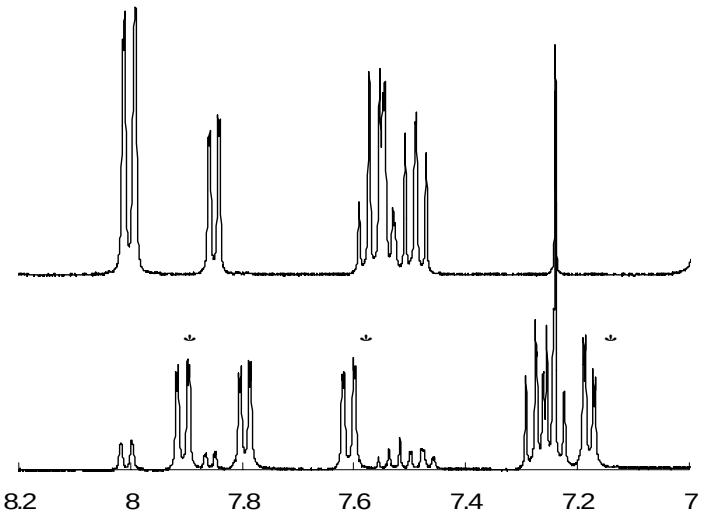

Figure 38: Fluoride abstraction using [**25**]$^+$ in water/chloroform biphasic condition. Top figure is the ^{1}H-NMR spectrum of the chloroform phase before shaking; bottom figure is the spectrum after shaking. Resonance from **25**-F are marked with *.

3.4.2 Cyanide complexation

Encouraged by the high affinity that [**25**]$^+$ displays for fluoride,[68] we decided to investigate its reaction with cyanide ions. This cationic borane is swiftly converted into zwitterionic **25**-CN when treated with NaCN in MeOH (Figure 39). The ^{11}B NMR signal of **25**-CN appears at -12.2 ppm as expected for a tetrahedral boron atom. Formation of this cyanide complex noticeably affects the ^{1}H NMR resonances of the diastereotopic methylene hydrogen atom. The two resonances are shifted downfield and appear at 4.66 and 5.46 ppm (vs. 3.69 and 4.81 ppm in [**25**]$^+$).

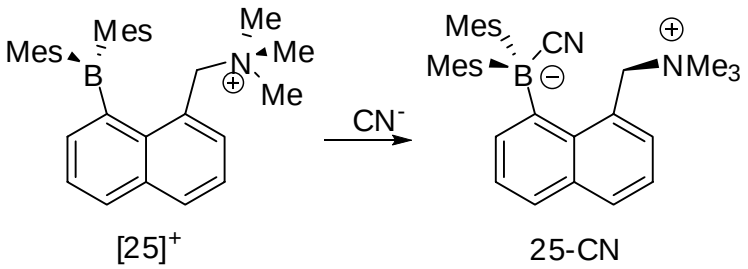

Figure 39: Cyanide complexation of [**25**]$^+$.

Formation of **25-**CN can also be monitored using differential pulsed voltammetry. Indeed, addition of cyanide ions to a solution of [**25**]OTf in THF with nBu$_4$NPF$_6$ as a supporting electrolyte leads to a progressive decrease of the peak corresponding to the reduction of the boron center (Figure 40). This decrease is caused by binding of the cyanide ion to the boron center which can no longer be reduced because of its coordinative saturation. Similar observations have been made upon addition of fluoride ions to bidentate boranes.[104]

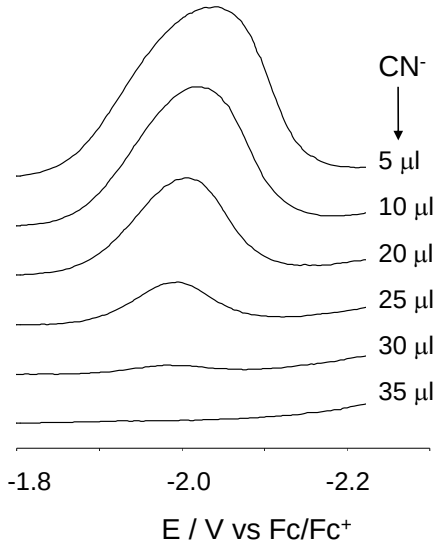

Figure 40: Changes in the differential pulsed voltammogram of [**25**]OTf (0.001 M) observed upon the addition of nBu$_4$NCN (0.087 M in CH_2Cl_2) to a THF solution.

The crystal structures of **25**-CN has been determined (Figure 41, Table 8). This compound crystallizes in the monoclinic space group $P2_1/c$ with four molecules in the unit cell. The sum of the C_{aryl}-B-C_{aryl} angles ($\Sigma_{(C\text{-}B\text{-}C)}$ = 343.5°) indicates substantial pyramidalization of the boron atom which is more acute than that observed in **25**-F ($\Sigma_{(C\text{-}B\text{-}C)}$ = 340.7°).[68] The B(1)-C(30) bond connecting the carbon atom of the cyanide anion to the boron center (1.527(6) Å) is significantly shorter than those typically found in triarylcyanoborate anions such as $[Ph_3BCN]^-$ (1.65 Å).[127] It is also important to note that the B(1)-C(1) bond length of 1.791(7) Å is abnormally long, especially when compared to the B(1)-C(1) bond lengths of 1.678(5) Å measured in **25**-F and 1.573 Å measured in [**25**]OTf. The B(1)-C(1)-C(9) angle of 132.8(4)° in **25**-CN is also larger than that present in **25**-F (130.6(3)°). These unusual metrical parameters and, in particular, the length of the B(1)-C(1) bond indicates that the steric congestions present in **25**-CN are more important than in **25**-F. The larger size of the cyanide anion is certainly responsible for this effect.

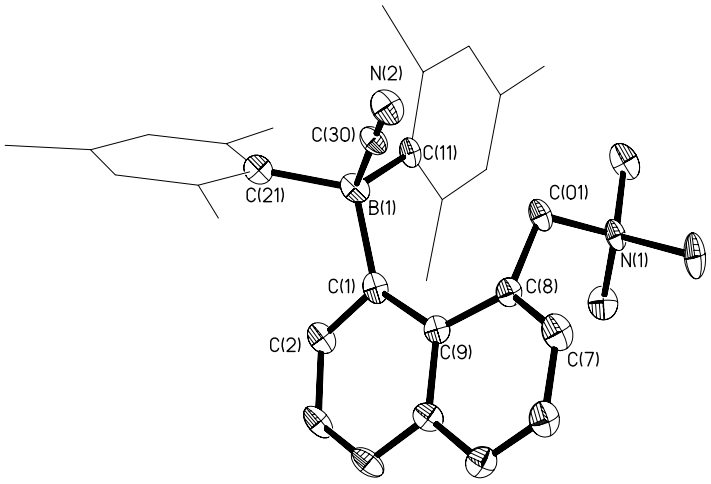

Figure 41: ORTEP plot of the molecular structure of **25**-CN with thermal ellipsoids set at 50% probability level. Hydrogen atoms are omitted for clarity. Selective bond distances [Å] and bond angles [°]: B(1)-C(1) 1.791(7), B(1)-C(11) 1.633(6), B(1)-C(21) 1.726(7), B(1)-C(30) 1.527(6), N(2)-C(30) 1.074(5), C(1)-C(2) 1.354(6), C(1)-C(9) 1.457(6), C(7)-C(8) 1.328(6), C(8)-C(9) 1.405(6), C(8)-C(01) 1.527(6), B(1)-C(30)-N(2) 117.0(5), C(1)-B(1)-C(11) 113.1(4), C(1)-B(1)-C(21) 112.9(4), C(11)-B(1)-C(21) 117.5(4), C(2)-C(1)-C(9) 110.2(4), C(2)-C(1)-B(1) 116.3(4), C(9)-C(1)-B(1) 132.8(4), C(7)-C(8)-C(9) 117.0(4), C(7)-C(8)-C(01) 117.8(4), C(9)-C(8)-C(01) 125.0(4).

Table 8: Crystal data and structure refinement for **25**-CN

Crystal data	**25**-CN
Formula	$C_{33}H_{39}BN2$
M_r	474.47
Crystal size (mm^3)	0.21 x 0.06 x 0.03
Crystal system	Monoclinic
Space group	*P*2(1)/c
a (Å)	16.009(3)
b (Å)	10.329(2)
c (Å)	17.540(4)
α (º)	90.00
β (º)	111.12(3)
γ (º)	90.00
V ($Å^3$)	2705.5(9)
Z	4
ρ_{calc} (gcm^{-3})	1.165
μ(Mo K_α) (mm-1)	0.066
F(000) (e)	1024
Data collection	
T/K	110
Scan mode	ω
hkl range	-19→19, -11→12, -14→20
Measured refl.	13047
Unique refl., [R_{int}]	4757, [0.0763]
Refl. Used for refinement	4757
Refinement	
Refined parameters	326
R_1, wR_2 [all data]	0.1393, 0.1961
ρ_{fin} (max/min) (e $Å^{-3}$)	0.444/-0.594

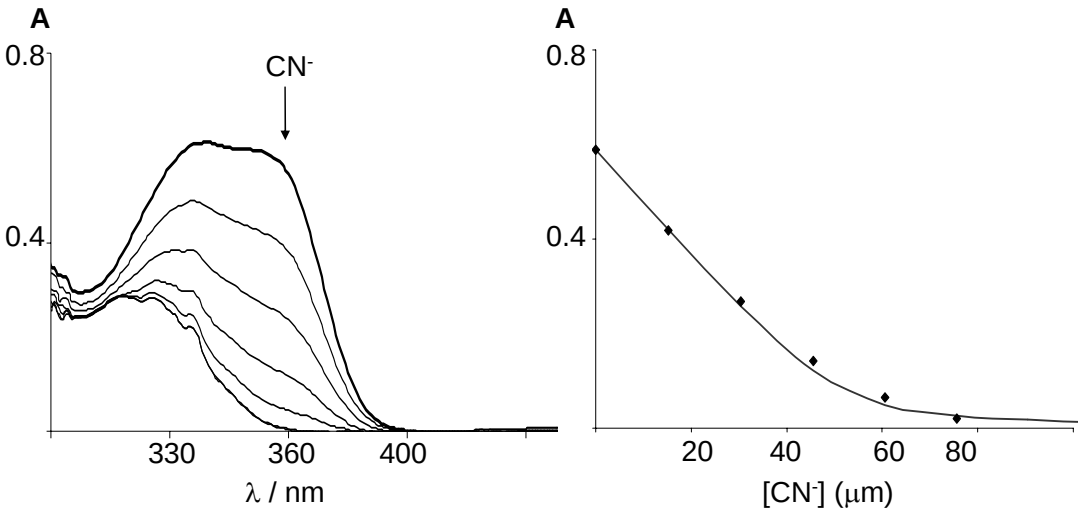

Figure 42: Changes in the UV-vis absorption spectra of a solution of $[\mathbf{25}]^+$ (5.16 x 10^{-5}M in THF) upon the addition of a NaCN solution (9.14 x 10^{-3}M in methanol).

A UV titration experiment carried out by monitoring the absorption of $[\mathbf{25}]^+$ at λ_{max} 352 nm (ε = 11435) shows that the cyanide binding constant of $[\mathbf{25}]^+$ in THF is equal to $8.0(\pm0.5)\times10^5$ M^{-1} (Figure 42). Under the same conditions, the fluoride binding constant of $[\mathbf{25}]^+$ cannot be accurately measured and exceeds 10^8 M^{-1}. These results indicate that $[\mathbf{25}]^+$ shows a greater selectivity for fluoride than cyanide which is surprising since cyanide (pKa = 9.3) is more basic than fluoride (pKa = 3.18). Presumably, the larger size of the cyanide anion impedes binding to the sterically crowded boron center of $[\mathbf{25}]^+$. Similar effects have been observed in the case of $[o\text{-}Mes_2B\text{-}C_6H_4\text{-}NMe_3]^+$ which binds fluoride but not cyanide in aqueous media.[128] In an effort to assess the influence of the cationic nature of $[\mathbf{25}]^+$ on its cyanide binding ability, we have also studied the cyanide affinity of **23**. UV-vis titrations carried out in

THF indicate that the cyanide binding constant of **23** is at least three orders of magnitude lower than that of [**25**]$^+$ thus suggesting that favorable Coulombic effects are essential to the cyanide binding ability of [**25**]$^+$. Although cation [**25**]$^+$ does not react with cyanide in water, it is able to transport it into organic phases. For example, shaking a biphasic mixture consisting of NaCN in D_2O (0.5 ml, 7.6 x 10^{-2} M) and [**25**]OTf in $CDCl_3$ (0.5 ml, 7.21 x 10^{-2}M) results in a 32% conversion of [**25**]OTf into **25**-CN after a few minutes (Figure 43).

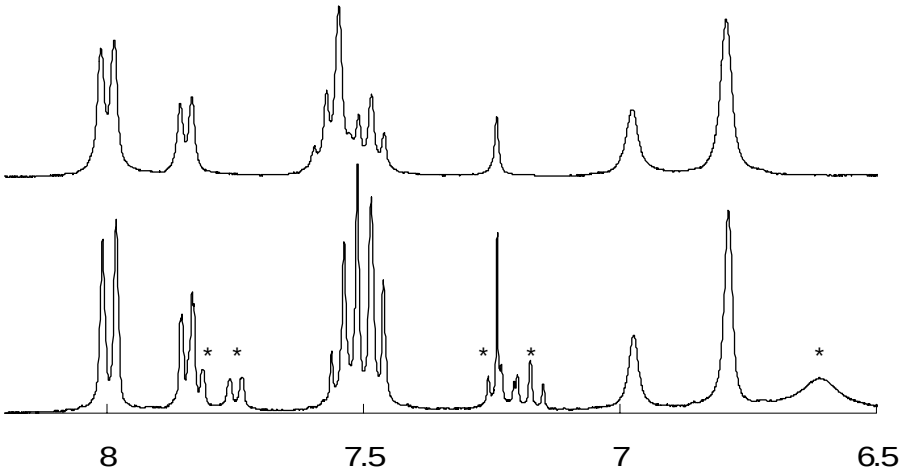

Figure 43: Cyanide abstraction using [**25**]$^+$ in water/chloroform biphasic condition. Top figure is the ^{1}H-NMR spectrum of the chloroform phase before shaking; bottom figure is the spectrum after shaking. Resonance from **25**-CN are marked with *.

3.5 Conclusion

The results that we present in this chapter indicate that cationic boranes such as [**25**]$^+$ may be well suited as molecular recognition units for fluoride and cyanide ions in water under biphasic conditions. We propose that the high fluoride/cyanide affinity of [**25**]$^+$ results from favorable Coulombic forces which stabilize the B-F/B-CN bond against heterolysis. This conclusion is also in agreement with the redox properties of [**25**]$^+$ which is more easily reduced than its neutral precursor **23**. Last but not least, these results allow us to establish that [**25**]$^+$ has a higher affinity for fluoride than cyanide. Keeping in mind that cyanide is much more basic than fluoride, the observed selectivity arises, at least in part, from steric effects which impedes cyanide binding to the sterically congested boron center of [**25**]$^+$.

3.6 Experimental section

Synthesis of borane 23: To the suspension of eschenmoser's salt (840 mg, 4.54 mmol) in THF was added dimesityl-1,8-naphthalenediylborate (3g, 4.47 mmol) THF solution at room temperature. After stirring for 1 hour, the reaction was quenched with water and extracted with CH_2Cl_2. The combined organic phase was washed with water, brine and dried over $MgSO_4$. The solvent were removed under reduced pressure and light yellow oil was obtained. Upon adding hexane to the oil residual, compound 1 was obtained as white powders, which were recrystallized from dichloromethane/hexane solution to give pure product (1.33g, yield 69%). Single crystals of **23** for X-ray structural analysis were obtained by evaporation of dichloromethane/hexane solution. ^{1}H NMR ($CDCl_3$, 400

MHz): 0.77 (s, 3H, Mes-CH_3), 1.88 (s, 3H, Mes-CH_3), 2.08 (s, 6H, Mes-CH_3), 2.14 (s, 3H, Mes-CH_3), 2.17 (s, 3H, Mes-CH_3), 2.33 (s, 3H, NMe_2-CH_3), 2.42 (s, 3H, NMe_2-CH_3), 3.04 (d, 1H, $^2J_{H-H}$ = 14.4 Hz, nap-CH_2-NMe_2), 3.46 (d, 1H, $^2J_{H-H}$ = 14.4 Hz, nap-CH_2-NMe_2), 6.42 (s, 1H, Mes-CH), 6.75 (s, 1H, Mes-CH), 6.81 (s, 1H, Mes-CH), 6.91 (s, 1H, Mes-CH), 7.35 (dd, 1H, $^3J_{H-H}$ = 8.1 Hz, $^3J_{H-H}$ = 6.9 Hz, nap-CH), 7.48-7.54 (m, 2H, nap-CH), 7.77-7.82 (m, 2H, nap-CH), 7.95 (dd, 1H, $^3J_{H-H}$ = 8.1 Hz, $^4J_{H-H}$ = 1.4 Hz, nap-CH). ^{13}C NMR ($CDCl_3$, 100.5 MHz): δ 21.1 (Mes-*p*-CH_3), 21.3 (Mes-*p*-CH_3), 22.1 (Mes-*o*-CH_3), 23.2 (Mes-*o*-CH_3), 24.1 (Mes-*o*-CH_3), 25.3 (Mes-*o*-CH_3), 44.9 (NMe_2), 64.7 (nap-CH_2-N), 124.8, 125.8, 127.3, 128.1, 128.2, 128.7, 128.9, 129.0, 132.9, 133.8, 134.3, 136.0, 136.9, 138.6, 139.2, 140.5, 141.2, 141.3, 141.5, 142.5, 144.3, 147.8. ^{11}B NMR ($CDCl_3$, 128.2 MHz): δ 69. Anal. Calcd. for $C_{31}H_{36}BN$: C, 85.90; H, 8.37. Found: C, 85.76; H, 8.50

Synthesis of cationic borane [24][Cl]: To a chloroform solution of **23** (100 mg, 0.2 mmol) was added excess HCl and stirred for 1h. After reaction, ether was added and resulted in the precipitation of [**24**]$^+$[Cl]$^-$ as light yellow solid (85 mg, yield 78%). Single crystals of [**24**][Cl] were obtained by vapor diffusion of diethyl ether into a solution of dichloromethane. ^{1}H NMR ($CDCl_3$, 400 MHz): 0.63 (s, 3H, Mes-CH_3), 1.84 (s, 3H, Mes-CH_3), 2.01 (s, 3H, Mes-CH_3), 2.20 (bs, 6H, Mes-CH_3), 2.33 (s, 3H, Mes-CH_3), 2.41 (s, 3H, $NHMe_2^+$), 2.75 (d, 3H, $^3J_{H-H}$ = 4.8 Hz, $NHMe_2^+$), 3.75 (d, 1H, $^2J_{H-H}$ = 13.2 Hz, nap-CH_2-$NHMe_2^+$), 4.16 (dd, 1H, $^2J_{H-H}$ = 13.2 Hz, $^3J_{H-H}$ = 9.2 Hz, nap-CH_2-$NHMe_2^+$), 6.44 (s, 1H, Mes-CH), 6.77 (s, 1H, Mes-CH), 6.83 (s, 1H, Mes-CH), 6.93 (s, 1H, Mes-CH), 7. 43 (m, 1H, nap-CH), 7.60 -7.70 (m, 2H, nap-CH), 7.92 (d, 1H, $^3J_{H-H}$ = 8.4

Hz, nap-CH), 8.00 (d, 1H, $^{3}J_{H-H}$ = 8.0 Hz, nap-CH), 8.38 (d, 1H, $^{3}J_{H-H}$ = 7.2 Hz, nap-CH), 12.26 (bs, 1H, $NHMe_2^+$). ^{11}B NMR ($CDCl_3$, 128.2 MHz): δ 69.

Synthesis of cationic borane [25][OTf]: To a dichloromethane solution of **23** (502 mg, 1.16 mmol) was added excess methyl triflate in glove box. After stirring for 1h, ether was added and resulted in the precipitation of [**25**][OTf] as light yellow solid (610 mg, yield 88%). Single crystals of [**25**][OTf] were obtained by vapor diffusion of diethyl ether into a solution of dichloromethane. ^{1}H NMR ($CDCl_3$, 400 MHz): 0.34 (s, 3H, Mes-CH_3), 1.70 (s, 3H, Mes-CH_3), 2.13 (s, 3H, Mes-CH_3), 2.19 (s, 3H, Mes-CH_3), 2.33 (s, 3H, Mes-CH_3), 2.60 (s, 3H, Mes-CH_3), 2.84 (s, 9H, NMe_3^+-CH_3), 3.69 (d, 1H, $^{2}J_{H-H}$ = 13.4 Hz, nap-CH_2-NMe_3^+), 4.81 (d, 1H, $^{2}J_{H-H}$ = 13.4 Hz, nap-CH_2-NMe_3^+), 6.35 (s, 1H, Mes-CH), 6.79 (s, 2H, Mes-CH), 6.98 (s, 1H, Mes-CH), 7.48 (dd, 1H, $^{3}J_{H-H}$ = 8.1 Hz, $^{3}J_{H-H}$ = 7.2 Hz, nap-CH), 7.52-7.60 (m, 2H, nap-CH), 7.84 (dd, 1H, $^{3}J_{H-H}$ = 6.9 Hz, $^{4}J_{H-H}$ = 1.4 Hz, nap-CH), 8.00 (dd, 2H, $^{3}J_{H-H}$ = 8.1 Hz, $^{4}J_{H-H}$ = 1.4 Hz, nap-CH). ^{13}C NMR ($CDCl_3$, 100.5 MHz): δ 21.0 (Mes-*p*-CH_3), 21.2 (Mes-*p*-CH_3), 21.3 (Mes-*o*-CH_3), 22.5 (Mes-*o*-CH_3), 23.3 (Mes-*o*-CH_3), 25.7 (Mes-*o*-CH_3), 52.5 (NMe_3), 69.1 (nap-CH_2-N), 118.9, 122.1, 125.1, 125.3, 126.6, 128.7, 128.9, 129.2, 130.8, 132.7, 134.3, 134.5, 138.4, 139.1, 139.3, 139.6, 140.0, 140.3, 140.6, 141.4, 142.5, 144.6. ^{11}B NMR ($CDCl_3$, 128.2 MHz): ^{19}F NMR ($CDCl_3$, 375.95 MHz) Anal. Calcd. for $C_{33}H_{39}BF_3NO_3S$: C, 66.33; H, 6.58. Found: C, 65.83; H, 6.56

Synthesis of cationic borane [26][I_3]: 9-bromomethyl-anthracene and NaI were stirred at room temperature for 4 hours in acetone in the absence of light to generate the 9-iodomethyl-anthracene. After reaction, the solvent was removed under reduced

pressure and chloroform was added to the mixture. The chloroform solution was cannulated to another flask that contained compound **23** and stirring for 2 days in dark. After reaction, the mixture was washed with water and brine, and then dried over $MgSO_4$. The crude product was obtained by removing solvents and was purified by re-crystallization form CH_2Cl_2/ether solution to give [**26**][I_3] as dark red solid (605 mg, yield 52%). Single crystals of [**26**][I_3] were obtained by vapor diffusion of diethyl ether into a solution of dichloromethane. ^{1}H NMR ($CDCl_3$, 500 MHz): 0.46 (s, 3H, Mes-CH_3), 1.81 (s, 3H, Mes-CH_3), 2.36 (s, 9H), 2.56 (s, 3H), 2.63 (s, 3H), 2.84 (s, 3H, NMe_2^+), 4.65 (d, 1H, $^2J_{H-H}$ = 13.0 Hz), 4.98 (d, 1H, $^2J_{H-H}$ = 14.5 Hz), 5.20-5.40 (m, 2H), 6.51 (s, 1H, Mes-CH), 6.85 (s, 1H, Mes-CH), 7.04 (s, 1H, Mes-CH), 7.09 (s, 1H, Mes-CH), 7.38 (d, 1H, $^3J_{H-H}$ = 8.5 Hz), 7.44-7.50 (m, 2H), 7.52-764 (m, 3H), 7.76 (d, 1H, $^3J_{H-H}$ = 8.0 Hz), 7.85 (m, 1H), 7.92-8.02 (m, 3H), 8.09-8.16 (m, 2H), 8.21 (d, 1H, $^3J_{H-H}$ = 7.0 Hz), 8.54 (s, 1H, Ant-CH). ^{13}C NMR ($CDCl_3$, 100.5 MHz): δ 21.2 (Mes-*p*-CH_3), 21.4 (Mes-*p*-CH_3), 21.9 (Mes-*o*-CH_3), 22.6 (Mes-*o*-CH_3), 23.9 (Mes-*o*-CH_3), 26.1 (Mes-*o*-CH_3), 50.3, 51.7, 57.0, 70.4, 116.1, 122.6, 125.2, 125.6, 125.8, 126.8, 128.6, 128.8, 129.0, 129.3, 130.1, 130.3, 131.1, 132.5, 132.7, 132.9, 133.0, 134.5, 134.6, 138.9, 139.2, 139.7, 140.5, 141.1, 141.4, 142.8, 144.7. ^{11}B NMR ($CDCl_3$, 128.2 MHz): δ 70. Anal. Calcd. for $C_{46}H_{47}BI_3N$: C, 54.95; H, 4.71. Found: C, 54.84; H, 4.65

Synthesis of 25-F: To a solution of [**25**][OTf] (44 mg, 0.07 mmol) in CH_2Cl_2 was added one equivalent of TSAF (20 mg, 0.07 mmol) in glovebox. After stirring at room temperature for 10 minutes, the solvent were removed under reduced pressure and the residual white solid was extracted with ether. The combined ether solution was dried to give the **25**-F as white powder (22 mg, yield 64%). Single crystals of **25**-F were obtained from evaporation of an ether solution. ^{1}H NMR (acetone-d^{6}, 233K): 0.82 (s, 3H, Mes-CH_3), 1.53 (s, 3H, Mes-CH_3), 2.14 (s, 6H, Mes-CH_3), 2.33 (d, 3H, $^{1h}J_{H-F}$ = 6.9 Hz, NMe_3^+-CH_3), 2.97 (s, 6H, Mes-CH_3), 3.35 (s, 6H, NMe_3^+-CH_3), 3.82 (dd, 1H, $^{2}J_{H-H}$ = 12.9 Hz, nap-CH_2-NMe_3^+), 6.17 (s, 1H, Mes-CH), 6.43 (s, 1H, Mes-CH), 6.50 (dd, 1H, $^{2}J_{H-H}$ = 12.9 Hz, $^{1h}J_{H-F}$ = 9.2 Hz, nap-CH_2-NMe_3^+), 6.56 (s, 1H, Mes-CH), 6.67 (s, 1H, Mes-CH), 7.16 (t, 1H, $^{3}J_{H-H}$ = 7.5 Hz, nap-CH), 7.37 (dd, 1H, $^{3}J_{H-H}$ = 7.8 Hz, $^{3}J_{H-H}$ = 7.1 Hz, nap-CH), 7.45 (dd, 1H, $^{3}J_{H-H}$ = 7.1 Hz, $^{4}J_{H-H}$ = 1.6 Hz, nap-CH), 7.68 (d, 2H, $^{3}J_{H-H}$ = 7.5 Hz, nap-CH), 7.98 (dd, 1H, $^{3}J_{H-H}$ = 7.9 Hz, $^{4}J_{H-H}$ = 1.4 Hz, nap-CH). ^{13}C NMR (acetone-d^{6}, 233K): δ 20.8 (Mes-*p*-CH_3), 24.5 (Mes-*o*-CH_3), 24.8 (Mes-*o*-CH_3), 25.3 (d, J_{C-F} = 10.3 Hz, Mes-*o*-CH_3), 26.4 (d, J_{C-F} = 13.0 Hz, Mes-*o*-CH_3), 51.9 (NMe_3), 68.9 (d, d, J_{C-F} = 17.6 Hz, nap-CH_2-N), 122.7, 126.4, 127.7, 128.7, 129.0, 129.4, 129.8, 132.2, 132.3, 132.5, 133.7, 136.4, 136.5, 141.1, 141.2, 141.3, 143.3, 143.7. ^{11}B NMR (acetone-d^{6}, 233K): δ 12.2. ^{19}F NMR (acetone-d^{6}, 233K): δ -152. Anal. Calcd. for $C_{32}H_{39}BFN$: C, 82.22; H, 8.41.

Synthesis of 25-CN: [**25**][OTf] (100 mg, 0.17 mmol) was mixed with eight equivalent of NaCN (66 mg, 1.35 mmol) in methanol at room temperature. After stirring for 1 hour, the solvent was removed under reduced pressure and the residual white solid was extracted with ether. The combined ether solution was dried to give the **25**-CN as white powder (58 mg, yield 72%). Single crystals of **25**-CN were obtained from evaporation of an methanol solution. ^{1}H NMR ($CDCl_3$, 399.59MHz, 263K): δ 1.21 (s, 3H, Mes-CH_3), 1.79 (s, 3H, Mes-CH_3), 2.15 (s, 3H, Mes-CH_3), 2.19 (s, 3H, Mes-CH_3), 2.20 (s, 3H, Mes-CH_3), 2.24 (s, 9H, NMe_3), 2.46 (s, 3H, Mes-CH_3), 4.66 (d, 1H, $^{2}J_{H-H}$ = 12.8 Hz, nap-CH_2-NMe^{3+}), 5.46 (d, 1H, $^{2}J_{H-H}$ = 12.8 Hz, nap-CH_2-NMe^{3+}), 6.55 (s, 2H, Mes-CH), 6.61 (s, 1H, Mes-CH), 6.90 (s, 1H, Mes-CH), 7.16 – 7.23 (m, 2H, nap-CH), 7.48 (d, 1H, $^{3}J_{H-H}$ = 6.4 Hz, nap-CH), 7.54 (d, 1H, $^{3}J_{H-H}$ = 7.2 Hz, nap-CH), 7.76 (d, 1H, $^{3}J_{H-H}$ = 6.4 Hz, nap-CH), 7.85 (d, 1H, $^{3}J_{H-H}$ = 8.4 Hz, nap-CH). ^{13}C NMR ($CDCl_3$, 100.5 MHz, 263K): δ 20.6 (Mes-p-CH_3), 23.8 (Mes-*o*-CH_3), 25.0 (Mes-*o*-CH_3), 25.8 (Mes-*o*-CH_3), 30.1 (d, JC-F = 13.0 Hz, Mes-*o*-CH3), 51.9 (NMe3), 71.3 (nap-CH_2-N), 121.6, 125.0, 125.4, 126.9, 128.6, 129.0, 129.8, 132.7, 133.1, 133.8, 134.3, 138.3, 141.3, 142.9, 143.1, 143.4, 144.9. ^{11}B NMR ($CDCl_3$, 128.2 MHz, 263K): δ -12.2. IR ν_{CN} = 2163 cm^{-1}.

UV-vis titration in THF-MeOH (75/25) with fluoride: A solution of [**25**][OTf] (3 mL, 3.72 x 10^{-5} M, THF-MeOH (75/25)) was placed in the cuvet and titrated with incremental amounts of fluoride anions by addition of a solution of nBu_4NF in THF (4.77 x 10^{-3} M). The absorption was monitored at λ_{max} = 352 nm (ε = 11900 for $[\mathbf{25}]^+$). The experimental data obtained was fitted to a 1:1 binding isotherm which indicated that the fluoride binding constant of $[\mathbf{25}]^+$ is about 1.3 x 10^6 M^{-1} in THF-MeOH (75/25).

UV-vis titration in THF with fluoride: A THF solution of [**25**][OTf] (4.95 x 10^{-5}M, 3 ml) was titrated with incremental amounts of fluoride by addition of TBAF in THF (4.46 x 10^{-3}M). The absorbance was monitored at λ_{max} = 352 nm (ε = 11435 for $[\mathbf{25}]^+$, ε = 135 for 25-F). The experimental data obtained was fitted to a 1:1 binding isotherm which indicated that the fluoride binding constant of $[\mathbf{25}]^+$ is greater than 1 x 10^8 M^{-1}.

UV-vis titration in THF with cyanide: A THF solution of [**25**][OTf] (5.16 x 10^{-5}M, 3 ml) was titrated with incremental amounts of cyanide by addition of NaCN in methanol (9.14 x 10^{-3}M). The absorbance was monitored at λ_{max} = 352 nm (ε = 11435 for $[\mathbf{25}]^+$, ε = 394 for **25**-CN). The experimental data obtained was fitted to a 1:1 binding isotherm which indicated that the cyanide binding constant of $[\mathbf{25}]^+$is 8.0(± 0.5) x 10^5 M^{-1}.

CHAPTER IV

ELECTRO-REDUCTION OF A CATIONIC BORANE TO A NEUTRAL RADICAL AND A BORATAALKENE*

4.1 Introduction

Owing to their negative charge and the large radius of boron, borataalkenes (type A^-) are usually very reactive and have only been isolated on a few occasions.[88, 129, 130] The derivative $[Mes_2B{=}CH_2]^-$ (Mes=2,4,6-trimethylphenyl) is one of the simplest examples, and was isolated by deprotonation of the corresponding methyl compound. [129, 131-133] While the chemistry of borataalkenes has not been widely investigated, studies have shown that they can act as nucleophilic reagents or as ligands in transition-metal complexes.[134-136] Electrogenerated diborataalkenes, such as $[p\text{-}(Mes_2B)C_6H_4(BMes_2)]_2^-$, have also been detected using spectroelectrochemistry.[110, 111, 114] Interestingly, however, the structural changes accompanying the stepwise population/depopulation of a boron-carbon π bond have not been studied experimentally.

---

* Reproduced in part with permission from *Angew. Chem. Intl. Ed.* **2007**, *46,* 1723, Chiu, C.-W.; Gabbaï, F. P., "A 9-borylated acridinyl radical," *Angew. Chem. Intl. Ed.* **2007**, *46*, 6878, Chiu, C.-W.; Gabbaï, F. P., "Structural changes accompanying the stepwise population of a B-C π-bond," Copyright 2007 Wiley InterScience.

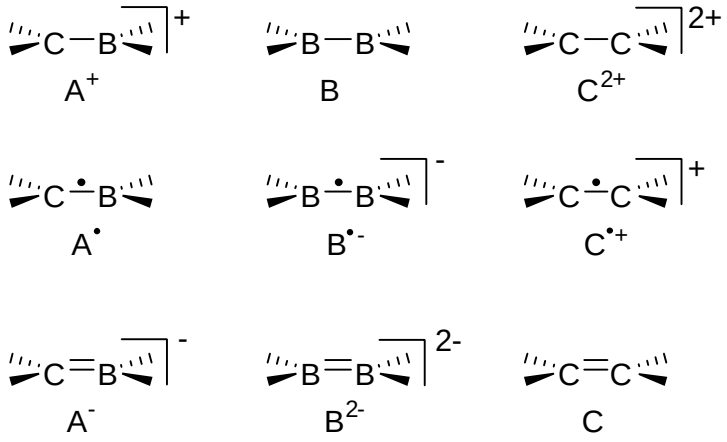

Figure 44: Electron population of B=C, B=B, and C=C double bond.

Examination of the literature indicates that such structural data is available for tetraaryldiboranes (Figure 44, type B) such as $Mes_2BBMesPh$ which undergoes two one-electron reductions to afford the corresponding radical anion (Figure 44, type $B^{\bullet-}$) and dianion (Figure 44, type B^{2-}).[84-86, 137] Structural studies carried out on $[Mes_2BBMesPh]^{\bullet-}$ and $[Mes_2BBMesPh]^{2-}$ confirm that reduction of the neutral diborane leads to population of the boron-boron π bond. Comparable studies have also been carried out on isoelectronic carbon derivatives.[118, 138] For example, tetraarylalkenes (Figure 44, type C), such as tetraanisylethylene, can be oxidized to afford the corresponding radical cations (Figure 44, type $C^{\bullet+}$) and dication (Figure 44, type C^{2+}) whose structures have also been determined.[118] A common feature observed in the structure of these redox-active species is a lengthening of the boron-boron bond (Figure 44, type B^{2-}) or ethylenic carbon-carbon bond (Figure 44, type C) upon oxidation, in agreement with the stepwise removal of the central π bonding electrons.

In this series of compounds, the radicals of type $A^{\bullet}$, $B^{\bullet-}$ and $C^{\bullet+}$ have an open-shell electronic configuration and are expected to be inherently unstable. This situation applies to radical anion of diboranes (Figure 44, type $B^{\bullet-}$), for which the existence of a one-electron π bond has been proposed.[74, 83, 139] While spectroscopic evidence for such radicals was obtained early on, their stabilization and isolation in the condensed state have only been achieved once.[84, 85] Radical cations of alkenes (Figure 44, type $C^{\bullet+}$) are also too unstable to isolate[140-142] unless appropriate substituents are employed.[118, 143] One of the added complications which jeopardize the stability of radicals of type $B^{\bullet-}$ and type $C^{\bullet+}$ is their charged character and associated reducing or oxidizing nature. Although neutral radicals of type $A^{\bullet}$ should not suffer from these destabilizing effects and are there predicted to be stable. To date, however, such species are unknown.

In previous chapters, we presented the synthesis of a series of triarylboranes containing an ammonium functionality, and showed that $[25]^{+}$ is able to abstract fluoride[68] and cyanide[144] from aqueous solution under biphasic conditions. However, the reduction of this ammonium borane does not result in the formation of a neutral radical but lead to the cleavage of the C-N bond. In this chapter, we describe the synthesis of an α–borylated carbocation and its reduction chemistry. Keeping in mind that 9,9'-bisacridnium undergoes clean stepwise reduction at low temperature,[138, 145] we decided to focus on the synthesis of a 9-boryl-acridinium derivative.

4.2 Synthesis and characterization of dimesityl-(*N*-methyl-acridinyl) borane

Treatment of 9-lithioacridine with Mes_2BF affords the corresponding acridinyl borane which could be easily alkylated in CH_2Cl_2 using MeOTf (Figure 45).

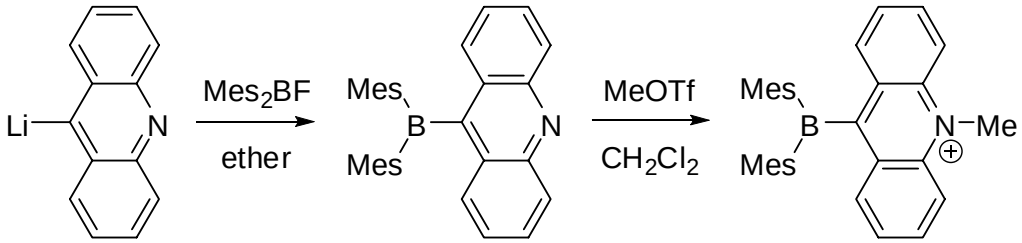

Figure 45: Synthesis of [**27**]$^+$.

The resulting acridinium borane [**27**]$^+$ has been isolated as a triflate salt which can be stored in air for extended periods of time. This novel derivative has been fully characterized. While the ^{1}H NMR spectra shows all the expected resonance, the ^{11}B NMR signal detected at 77 ppm confirms the presence of a base-free trigonal planar boron center. The ^{13}C resonance of the C-9 carbon atom of the acridinium unit is detected at 175 ppm which is close to that detected in other acridinium derivatives. We note in passing that the acridinium borane [**27**]$^+$ (form a, Figure 46) can be alternatively described as a α-boryl methylium (form b) or borenium[146] carbene adduct (form c). The chemical shift of the C(9) carbon nucleus is similar to that reported for the methylium center of $[(4\text{-}Me_2NC_6H_4)_3C]^+$ (δ = 179 ppm),[147] which points to the relevance of form b.

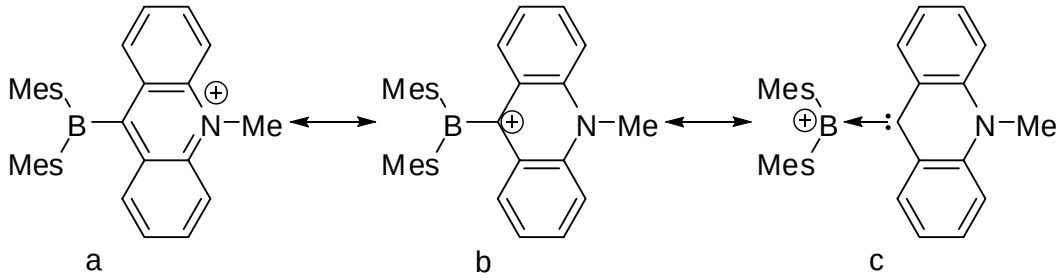

Figure 46: Resonance structures of [**27**]$^+$.

The single crystals of [**27**]OTf were obtained by vapor diffusion of diethyl ether into a dichloromethane solution. According to the single crystal X-ray analysis of [**27**][OTf] (Figure 47, Table 9), there is no short contact between the cationic and anionic components that is in agreement with the solution study. The boron and methylium carbon atoms adopt a trigonal planar geometry ($\Sigma_{(C\text{-}B\text{-}C)}B(1)$ = 359.9°; $\Sigma_{(C\text{-}C\text{-}C)}C(9)$ = 360.0°) with a dihedral angle of 62.4° between the trigonal planes containing B(1) and C(9), respectively. The B(1)-C(9) bondlength (1.627(5)Å) is noticeable lengthened compared to that in bulky triarylboranes (1.59 Å).[148] The electrostatic repulsion existing between the carbocationic center and the electropositive boron center is probably responsible for the observation of bond lengthening. Because of the existence of this long B(1)-C(9) bond, [**27**]$^+$ can also be described as a borenium carbene adduct (Figure 46, form c). [149, 150]

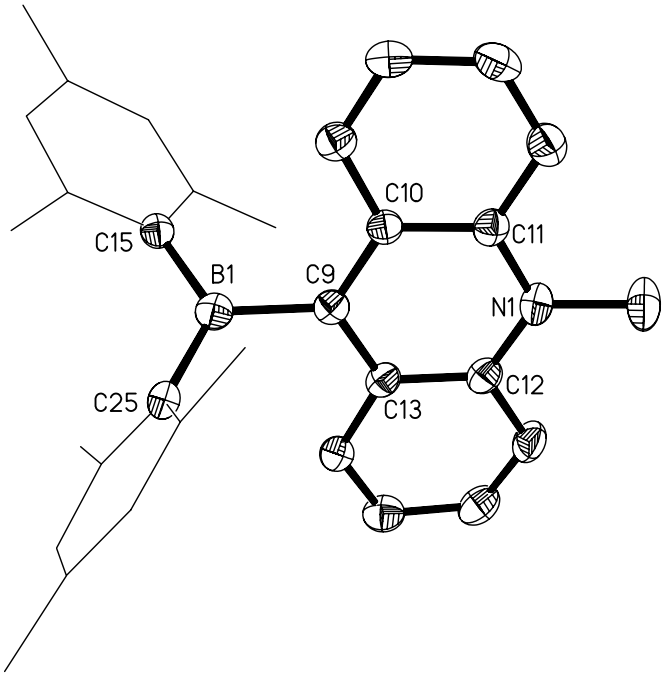

Figure 47: Crystal structure of [**27**]$^+$ with thermal ellipsoids set at the 50% probability level. Hydrogen atoms are omitted for clarity. Selected bond lengths [Å] and bond angles [º]: B(1)-C(9) 1.627(5), B(1)-C(15) 1.584(5), B(1)-C(25) 1.589(5), C(9)-C(10) 1.425(4), C(9)-C(13) 1.426(4), N(1)-C(11) 1.388(4), N(1)-C(12) 1.386(4), N(1)-C(14) 1.498(4), C(9)-B(1)-C(15) 119.0(3), C(9)-B(1)-C(25) 116.8(3), C(15)-B(1)-C(25) 124.1(3), B(1)-C(9)-C(10) 121.3(3), B(1)-C(9)-C(13) 120.3(3), C(10)-C(9)-C(13) 118.4(3), C(11)-N(1)-C(12) 121.6(3), C(11)-N(1)-C(14) 120.1(3), C(12)-N(1)-C(14) 118.1(3).

Table 9: Crystal data and structure refinement for [**27**][OTf]

Crystal data	[**27**][OTf]
Formula	$C_{33}H_{33}BF_3NO_3S$
M_r	591.47
Crystal size (mm^3)	0.17 x 0.05 x 0.02
Crystal system	Monoclinic
Space group	P2(1)/n
a (Å)	14.163(3)
b (Å)	8.2625(17)
c (Å)	26.232(5)
α (º)	90.00
β (º)	97.51(3)
γ (º)	90.00
V ($Å^3$)	3043.3(11)
Z	4
ρ_{calc} (gcm^{-3})	1.291
μ(Mo K_α) (mm-1)	
F(000) (e)	1240
Data collection	
T/K	110(2)
Scan mode	ω
hkl range	
Measured refl.	19205
Unique refl., [R_{int}]	4711, [0.0557]
Refl. Used for refinement	4711
Refinement	
Refined parameters	379
R_1, wR_2 [all data]	0.0886, 0.1474
ρ_{fin} (max/min) (e $Å^{-3}$)	0.7980/0.9727

In order to further understand the nature of the bonding in [**27**]$^+$, the spin restricted DFT calculation were performed on the *N*,*N*-dimethylimidazol-2-ylidene (**28**) and the *N*-methylacridin-9-ylidene (**29**) at the B3LYP/6-31g level of theory.

As shown in Figure 48, the HOMO of both systems undoubtedly depicts the characteristic orbital of a singlet carbene molecule, while the LUMO+1 of **28** and LUMO of **29** represent the remaining empty p orbital of the carbon atom. One of the most distinctive features in these two models is that the LUMO of the **29** is significantly lower in energy when compared to **28**. This low laying LUMO makes the energy difference between the σ-donating and the π-accepting orbital in **29** 4.49 eV smaller than that in **28**, suggesting a much stronger electron acceptor ability of **29** when compared to **28**. In the light of this theoretical finding, it can be concluded that **29** is an electron deficient carbene ligand. In turn, [**1**]$^+$ could be described as a borenium cation with the general formula of R_2BL^+, in which the ligand is **29**.

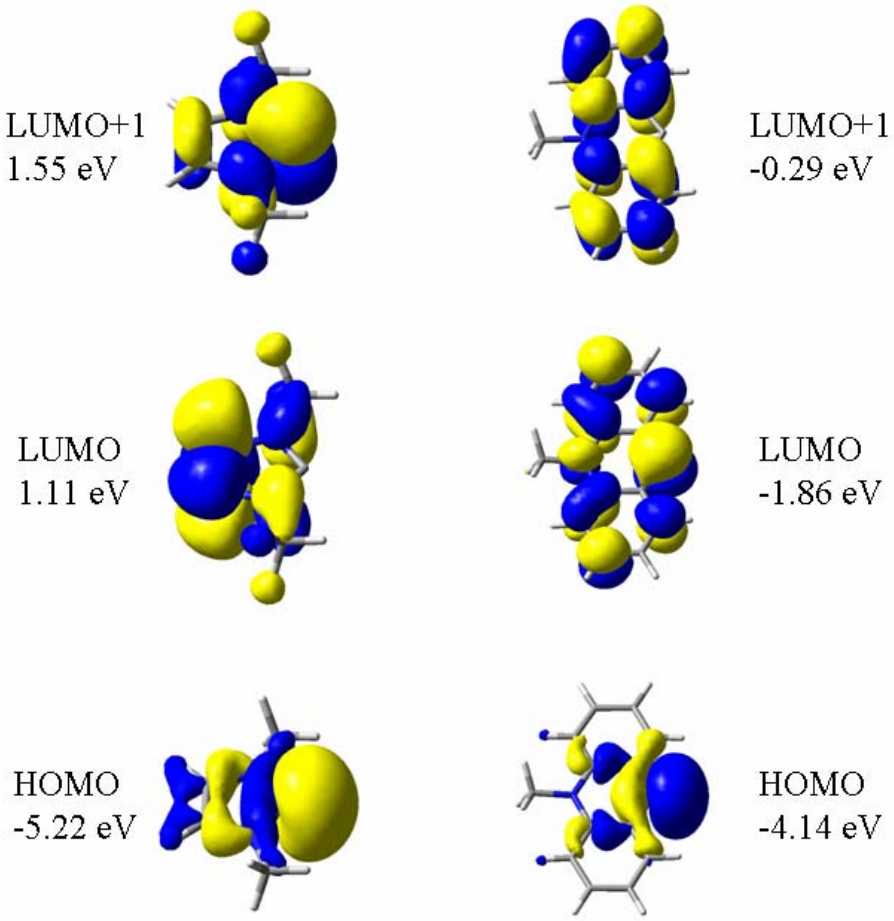

Figure 48: Frontier molecular orbitals and energy of **28** and **29**.

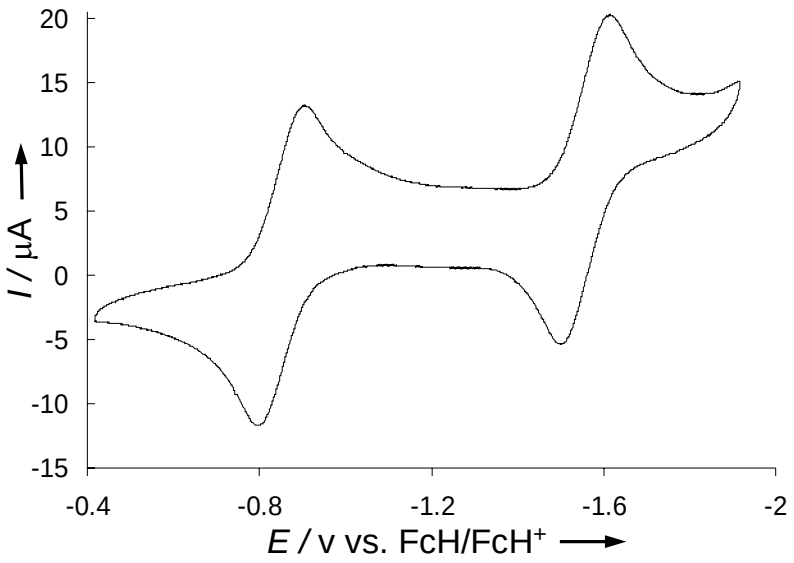

Figure 49: Cyclic voltammogram of [**27**]OTf in CH_2Cl_2 with a Pt working electrode: scan rate 100 mV/sec, 0.1 M NBu_4PF_6.

As indicated by cyclic voltammetry, $[\mathbf{27}]^+$ undergoes two reversible reductions at -0.86 V and -1.56 V vs. Fc/Fc^+ (Figure 49) thus suggesting the formation of $\mathbf{27}^\bullet$ and $[\mathbf{27}]^-$ as stable reduction species. This behavior contrasts with that of other triarylboranes which typically undergo a single reversible reduction wave followed by an irreversible one.[78] Moreover, the potential of the first reduction wave is distinctly more positive than that of triarylboranes which is typically observed at -2.6 V vs. Fc/Fc^+.[78] It is also more positive than that of *N*-methylacridinium which is reduced at -0.89 V vs. Fc/Fc^+. Encouraged by these results which suggest the formation a stable reduction species, we attempted their isolation.

4.3 One electron reduction of [**27**]$^{+}$ to form a neutral radical **27**$^{\bullet}$

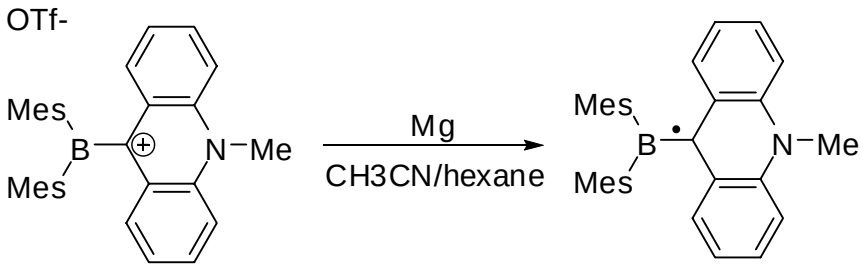

Figure 50: Synthesis of **27**$^{\bullet}$.

Treatment of [**27**]OTf with Mg in acetonitrile/hexane produces a deep blue hexane solution which can be separated from the acetonitrile layer (Figure 50). Upon cooling to -40°C, the hexane solution affords single crystals of the neutral radical **27**$^{\bullet}$. The crystal structure of **27**$^{\bullet}$ has been experimentally determined (, Table 10). The boron atom B(1) and the carbon atom C(9) adopt a trigonal planar geometry. The B(1)-C(9) bond of 1.559(5) Å is shorter than the B-C bond observed in bulky triarylboranes such as 9,10-bis(dimesitylboryl)anthracene (1.59 Å).[148]

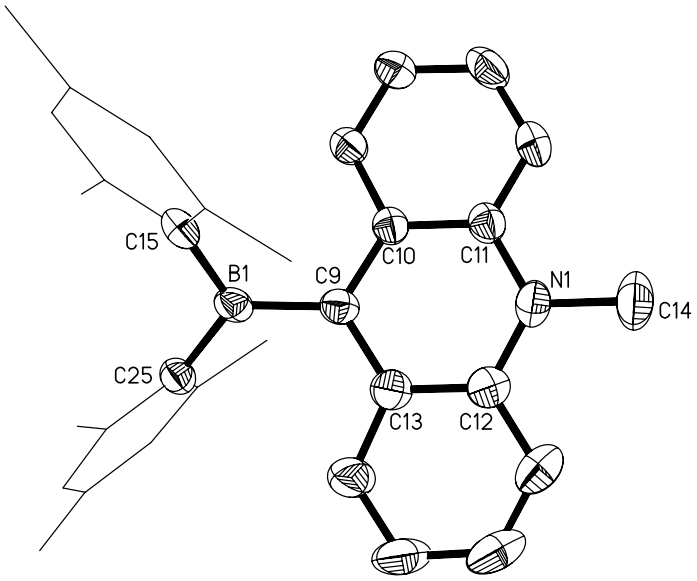

Figure 51: Crystal structure of **27**$^{\bullet}$ with thermal ellipsoids set at the 50% probability level. Hydrogen atoms are omitted for clarity. Selected bond lengths [Å] and bond angles [º]: B(1)-C(9) 1.559(5), B(1)-C(15) 1.581(5), B(1)-C(25) 1.593(5), C(9)-C(10) 1.430(4), C(9)-C(13) 1.447(4), N(1)-C(11) 1.403(4), N(1)-C(12) 1.384(4), N(1)-C(14) 1.477(4), C(9)-B(1)-C(15) 119.3(3), C(9)-B(1)-C(25) 121.2(3), C(15)-B(1)-C(25) 119.4(3), B(1)-C(9)-C(10) 121.4(3), B(1)-C(9)-C(13) 122.5(3), C(10)-C(9)-C(13) 116.2(3), C(11)-N(1)-C(12) 121.2(3), C(11)-N(1)-C(14) 119.2(3), C(12)-N(1)-C(14) 119.4(3).

Table 10: Crystal data and structure refinement for **27**$^{\bullet}$

Crystal data	**27**$^{\bullet}$
Formula	$C_{32}H_{33}BN$
M_r	442.40
Crystal size (mm^3)	0.13 x 0.11 x 0.02
Crystal system	monoclinic
Space group	P2(1)/n
a (Å)	15.979(3)
b (Å)	9.0599(18)
c (Å)	18.109(4)
α (º)	90.00
β (º)	104.34(3)
γ (º)	90.00
V ($Å^3$)	2540.0(9)
Z	4
ρ_{calc} (gcm^{-3})	1.157
μ(Mo K_α) (mm-1)	0.490
F(000) (e)	948
Data collection	
T/K	110
Scan mode	ω
hkl range	-17→17, -9→10, -20→20
Measured refl.	17755
Unique refl., [R_{int}]	3573, [0.0793]
Refl. Used for refinement	3573
Refinement	
Refined parameters	308
R_1, wR_2 [all data]	0.0985, 0.1819
ρ_{fin} (max/min) (e $Å^{-3}$)	0.345/-0.284

However, it is longer than that typically observed in borataalkenes[129] such as 8,10,11a-trimethyl-7-mesityl-11*aH*-7-boratabenzo[de]anthracene, which features a B-C double bond of length 1.48 Å.[88] It is also intermediate between that observed for $[Mes_2BBMesBPh]^{\bullet-}$ (1.65Å)[84] and $[An_2CCAn_2]^{\bullet+}$ (1.42Å; An = 4-$MeOC_6H_5$)[118] radicals. Other salient structural features include: 1) a twist angle α of 44.8º for the B(1)-C(9) bond and 2) a slight puckering of the central C_5N ring of the acridine moiety leading to the displacement of the C(9) and N(1) atoms by 0.12 and 0.16 Å, respectively, above the C(10)-C(11)-C(12)-C(13) plane.

Radical **27**$^{\bullet}$ has been analyzed by EPR spectroscopy in hexane at room temperature. The observed EPR spectrum could be satisfactorily simulated based on the hyperfine coupling constant shown in Figure 52. This fitting suggests delocalization of the spin on the acridinyl moiety with a non-negligible contribution from the boron atom ($a(^{11}B)$ = 2.55 G). The value of this hyperfine coupling is smaller than that reported for diborane radical anions, which is in agreement with delocalization of the unpaired electron on the electrophilic acridinium moiety.

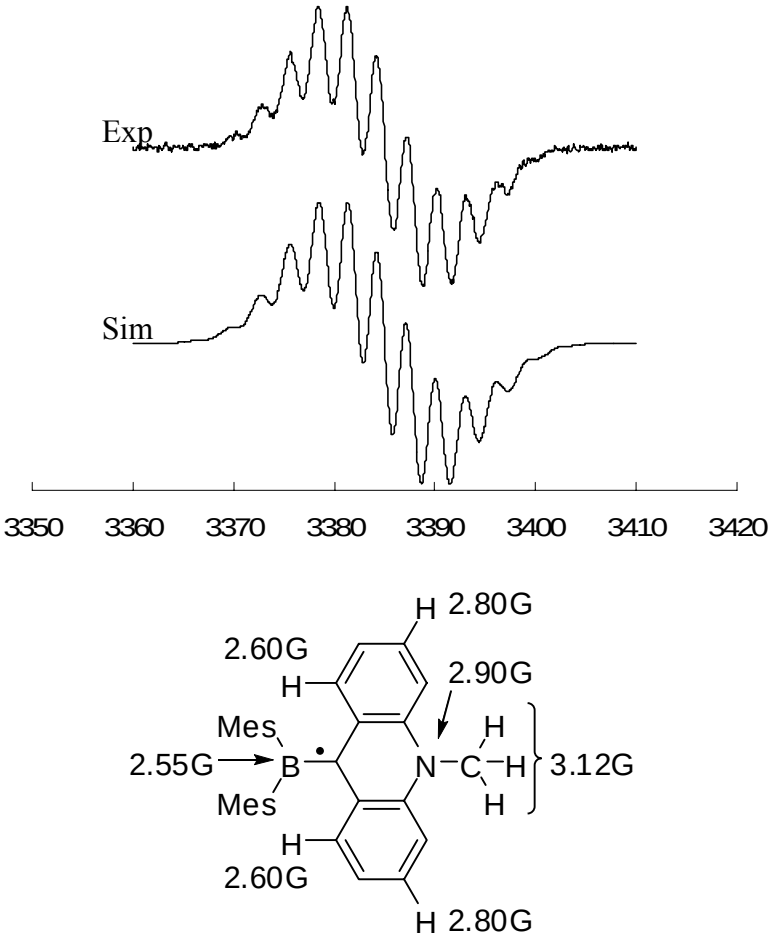

Figure 52: Top: the EPR spectrum of **27**$^{\bullet}$ in hexane at room temperature and the simulated EPR spectrum. Bottom: the hyperfine coupling constant used for simulation.

The computed spin density of **27**$^{\bullet}$ (Figure 53) also shows substantial localization of the unpaired electron in a polarized B-C π-bonding orbital. In accordance with the results obtained from structural data and EPR spectrum of **27**$^{\bullet}$, **27**$^{\bullet}$can be regarded as possessing a one electron boron-carbon π bond.

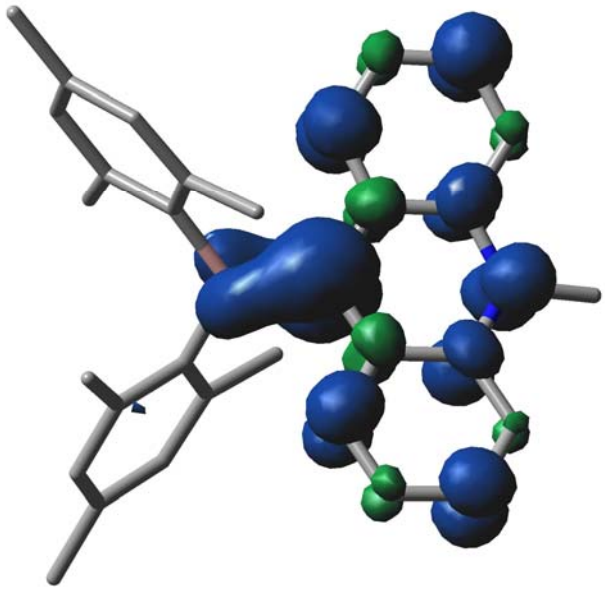

Figure 53: DFT-optimized geometry of **27**$^{\bullet}$ with an overlay of the computed spin density (isovalue = 0.0025).

4.4 Two electron reduction of [**27**]$^{+}$ to form a borataalkene [**27**]$^{-}$

When treated with potassium in a THF/dibenzo-18-crown-6 (db-18-c-6) mixture, [**27**]$^{+}$ is converted into [**27**]$^{-}$ which has been isolated as the [K(db-18-c-6)(THF)$_2$]$^{+}$ salt (Figure 54). The ^{11}B NMR resonances (40 ppm) is close to those reported for [Mes$_2$BCH$_2$]$^{-}$[129] and 8,10,11a-trimethyl-7-mesityl-11aH-7-boratabenzo[de]anthracene[88]

thus suggesting that [**27**]$^-$ is a borataalkene with a formal B=C double bond. The ^{1}H resonance of the *N*-methyl group (3.1 ppm) is 1.9 ppm upfield shifted compared to that of [**27**]$^+$ (5.0 ppm), consistent with the lost of aromaticity of the central ring in the acridinyl moiety and the formation of borataalkene complex.

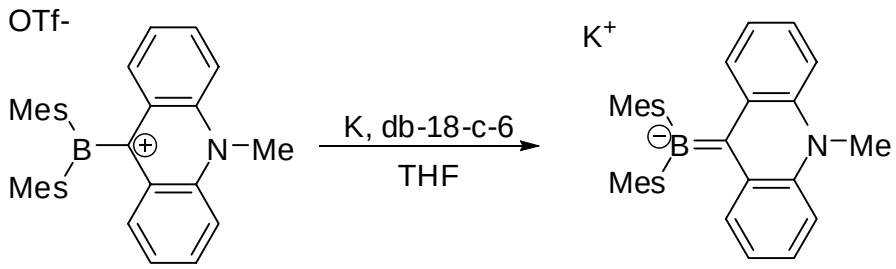

Figure 54: Synthesis of [**27**]$^-$**.**

The dark red crystal of [**27**][K(db-18-c-6)(THF)$_2$] was obtained as a THF/0.5 hexane solvate by vapor diffusion of hexane into a THF solution. According to the single crystal X-ray analysis of [**27**][K(db-18-c-6)(THF)$_2$] (Figure 55, Table 11), the boron and methylium carbon atoms B(1) and C(9) retain a trigonal planar geometry ($\Sigma_{(C\text{-}B\text{-}C)}$B(1) = 359.8°; $\Sigma_{(C\text{-}C\text{-}C)}$C(9) = 360.0°). The twist angle α of 15.3° about the B(1)-C(9) bond is small. While the boron and methylium carbon atoms adopt the similar geometry as in [**27**]$^+$ and **27**$^\bullet$, the nitrogen atom undergoes a significant pyramidalization as indicated by the sum of the angle of 353.4°. The B(1)-C(9) bond length (1.462(8) Å) is comparable to that reported for other borataalkene featuring B=C double bonds, such as [Mes$_2$BCH$_2$]$^-$ (1.444(8) Å) and [CH$_2$C$_6$H$_2$(3,5-Me$_2$)(4-BMes$_2$)]$^-$ (1.522(10) Å).

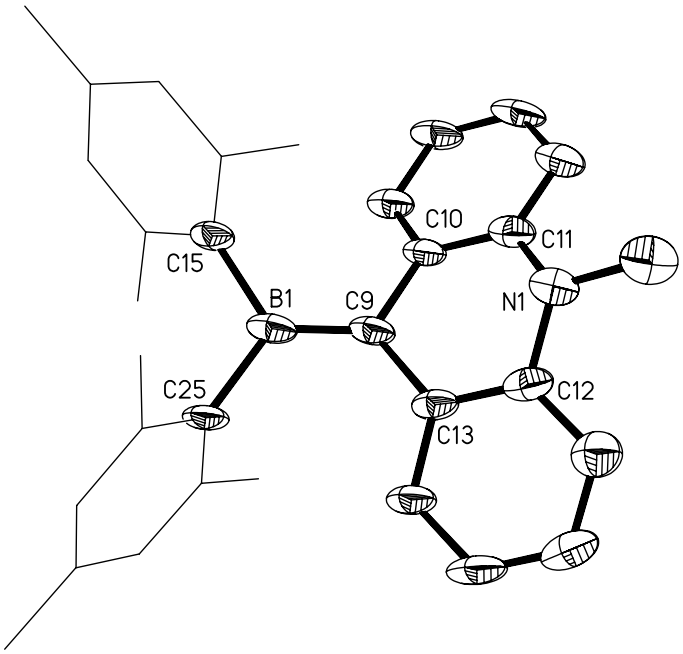

Figure 55: Crystal structure of [**27**]$^-$ with thermal ellipsoids set at the 50% probability level. Hydrogen atoms are omitted for clarity. Selected bond lengths [Å] and bond angles [º] (as compared to calculated values in brackets): B(1)-C(9) 1.462(8) , B(1)-C(15) 1.626(8) , B(1)-C(25) 1.628(8), C(9)-C(10) 1.502(7), C(9)-C(13) 1.475(7), N(1)-C(11) 1.419(7), N(1)-C(12) 1.435(6), N(1)-C(14) 1.448(7), C(9)-B(1)-C(15) 123.7(5), C(9)-B(1)-C(25) 124.4(5), C(15)-B(1)-C(25) 111.7(5), B(1)-C(9)-C(10) 120.8(5), B(1)-C(9)-C(13) 128.5(5), C(10)-C(9)-C(13) 110.7(5), C(11)-N(1)-C(12) 114.8(4), C(11)-N(1)-C(14) 119.7(5), C(12)-N(1)-C(14) 118.9(5).

Table 11: Crystal data and structure refinement for [**27**][K(db-18-c-6)(THF)$_2$]

Crystal data	[**27**][K(db-18-c-6)(THF)$_2$] (THF)(hexane)$_{0.5}$
Formula	$C_{67}H_{88}BKNO_9$
M_r	1101.29
Crystal size (mm^3)	
Crystal system	Triclinic
Space group	P-1
a (Å)	13.544(3)
b (Å)	14.278(3)
c (Å)	18.858(4)
α (º)	91.46(3)
β (º)	110.26(3)
γ (º)	114.29(3)
V (Å^3)	3057.4(11)
Z	2
ρ_{calc} (gcm^{-3})	1.196
μ(Mo K$_\alpha$) (mm-1)	
F(000) (e)	1186
Data collection	
T/K	150(2)
Scan mode	ω
hkl range	
Measured refl.	25198
Unique refl., [R_{int}]	6741, [0.0699]
Refl. Used for refinement	6741
Refinement	
Refined parameters	712
R_1, wR_2 [all data]	0.1043, 0.1870
ρ_{fin} (max/min) (e Å^{-3})	0.9623/0.9986

4.5 Structural changes observed upon reduction of the acridinium borane

In all three structures, the boron atom B(1) and the carbon atom C(9) adopt a trigonal planar geometry. The B(1)-C(9) bond undergoes a noticeable shortening on going from $[\mathbf{27}]^+$ to $\mathbf{27}^\bullet$ to $[\mathbf{27}]^-$. More importantly, the B(1)-C(9) bond length of 1.559(5) Å measured for $\mathbf{27}^\bullet$, is almost exactly intermediate between that measured in $[\mathbf{27}]^+$ (1.627(5) Å) and $[\mathbf{27}]^-$ (1.462(8) Å).

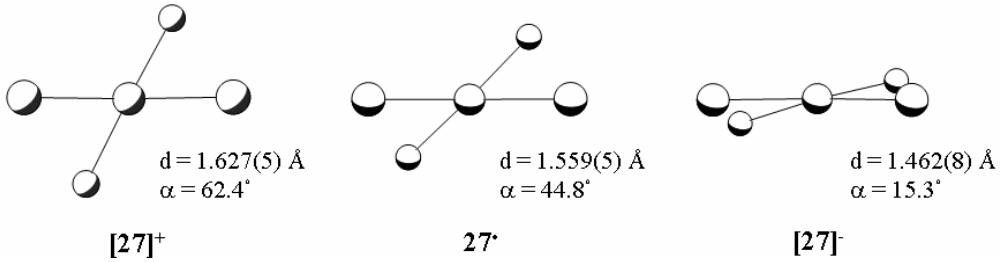

Figure 56: View of the central core of $[\mathbf{27}]^+$, $\mathbf{27}^\bullet$, and $[\mathbf{27}]^-$ along the B(1)-C(9) vector showing the B(1)-C(9) distance d and the dihedral angle α formed by the trigonal planes containing B(1) and C(9).

In accordance with the above, we note that the dihedral angle formed by the trigonal planes containing B(1) and C(9), respectively, undergoes a steady decrease. As shown in Figure 56, the perspective views along the B(1)-C(9) bond of $[\mathbf{27}]^+$, $\mathbf{27}^\bullet$, and $[\mathbf{27}]^-$ highlight the increasing of planarity of molecules with the dihedral angle decreasing from 62.4° in $[\mathbf{27}]^+$, to 44.8° in $\mathbf{27}^\bullet$, and to 15.3° in $[\mathbf{27}]^-$. Conversion of $[\mathbf{27}]^+$ into $\mathbf{27}^\bullet$ and $[\mathbf{27}]^-$ is also accompanied by an increase in the puckering of the central C_5N ring of the acridinyl moiety. This puckering is reflected by the

displacement of C(9) and N(1) atoms above the plane containing the C(10)-C(11)-C(12)-C(13) atoms (displacements in Å for C(9): 0.04 in $[\mathbf{27}]^+$, 0.12 in $\mathbf{27}^\bullet$, 0.33 $[\mathbf{27}]^-$; and for N(1): 0.04 in $[\mathbf{27}]^+$, 0.16 in $\mathbf{27}^\bullet$, 0.42 $[\mathbf{27}]^-$).

4.6 Computational analysis of the B-C bonding

In order to better appreciate the origin of the structural changes induced by reduction of $[\mathbf{27}]^+$, the structure of $[\mathbf{27}]^+$, $\mathbf{27}^\bullet$ and $[\mathbf{27}]^-$ have been optimized at the B3LYP/6-31g(d) level of theory. Despite of the slight deviation of the B(1)-C(9) bond length of the optimized structures to those experimentally determined values, DFT computation applied to the counter-ion free molecules reproduce the same trend in the changes of the B-C bond length and the dihedral angles, indicating the critical features of bonding are captured in these models (Table 12).

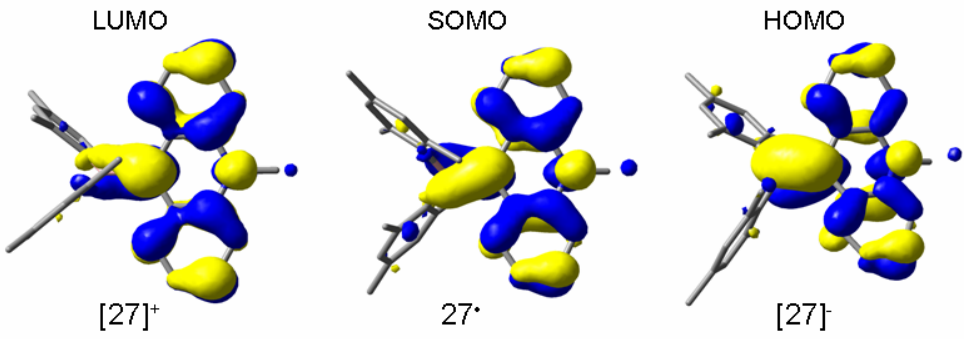

Figure 57: The B3LYP/6-31g optimized geometry of $[\mathbf{27}]^+$, $\mathbf{27}^\bullet$ and $[\mathbf{27}]^-$ with overlay of frontier molecular orbital (isovalue = 0.03).

Table 12: Experimental and calculated bond distance and angles for $[\mathbf{27}]^+$, $\mathbf{27}^\bullet$, and $[\mathbf{27}]^-$

	$[\mathbf{27}]^+$ X-ray	$[\mathbf{27}]^+$ B3LYP	$\mathbf{27}^\bullet$ X-ray	$\mathbf{27}^\bullet$ B3LYP	$[\mathbf{27}]^-$ X-ray	$[\mathbf{27}]^-$ B3LYP
B(1)-C(9)	1.627(5)	1.613	1.559(5)	1.566	1.462(8)	1.497
B(1)-C(15)	1.584(5)	1.568	1.581(5)	1.589	1.626(8)	1.621
B(1)-C(25)	1.589(5)	1.569	1.593(5)	1.593	1.628(8)	1.627
C(9)-C(10)	1.425(4)	1.425	1.430(4)	1.455	1.502(7)	1.487
C(9)-C(13)	1.426(4)	1.425	1.447(4)	1.455	1.475(7)	1.482
N(1)-C(11)	1.388(4)	1.387	1.403(4)	1.404	1.419(7)	1.420
N(1)-C(12)	1.386(4)	1.387	1.384(4)	1.403	1.435(6)	1.414
N(1)-C(14)	1.498(4)	1.485	1.477(4)	1.467	1.448(7)	1.452
C(9)-B(1)-C(15)	119.0(3)	118.3	119.3(3)	119.6	123.7(5)	124.6
C(9)-B(1)-C(25)	116.8(3)	119.1	121.2(3)	122.0	124.4(5)	122.0
C(15)-B(1)-C(25)	124.1(3)	122.6	119.4(3)	118.4	111.7(5)	113.3
B(1)-C(9)-C(10)	121.3(3)	120.9	121.4(3)	121.0	120.8(5)	125.9
B(1)-C(9)-C(13)	120.3(3)	121.5	122.5(3)	122.9	128.5(5)	121.4
C(10)-C(9)-C(13)	118.4(3)	117.6	116.2(3)	116.1	110.7(5)	112.5
C(11)-N(1)-C(12)	121.6(3)	121.4	121.2(3)	120.8	114.8(4)	118.8
C(11)-N(1)-C(14)	120.1(3)	119.3	119.2(3)	119.6	119.7(5)	120.1
C(12)-N(1)-C(14)	118.1(3)	119.2	119.4(3)	119.6	118.9(5)	119.9

Examination of the frontier molecular orbital shows that the LUMO of [**27**]$^{+}$ is mostly localized over the acridinium moiety (). However, with a contribution from the B(1) and C(9) atomic orbitals of 27.25%, the LUMO of [**27**]$^{+}$ shows a non-negligible contribution of the B(1)-C(9) empty π-bond. Upon reduction, the LUMO of [**27**]$^{+}$ becomes the SOMO of **27**$^{\bullet}$ (). Despite the addition of an electron, the SOMO of **27**$^{\bullet}$ only slightly differs from the LUMO of [**27**]$^{+}$. In particular, the B(1) and C(9) atomic orbitals make up 27.62% of this molecular orbital indicating a comparable contribution of the B(1)-C(9) π-bond. Addition of a second electron to this molecular orbital induces some noticeable changes. In particular, the contribution of the B(1) and C(9) atomic orbitals increases to 31.3% in the HOMO of [**27**]$^{-}$. For the SOMO of **27**$^{\bullet}$ and the HOMO of [**27**]$^{-}$, we note that the contribution of the C(9) atomic orbitals (22.7% for **27**$^{\bullet}$, 21.67% for [**27**]$^{-}$) is much greater than that of the B(1) atomic orbitals (8.05% for **27**$^{\bullet}$, 9.63% for [**27**]$^{-}$). These contributions suggest that the π-electron density localized about the B(1)-C(9) linkage is polarized toward the carbon atom. Altogether these computational results suggest that reduction of [**27**]$^{+}$ into **27**$^{\bullet}$ and [**27**]$^{-}$ leads to the progressive population of the B(1)-C(9) π-orbital. It also suggest that as the molecule becomes more electron rich, the relative occupation of the B(1)-C(9) π-bonding combination increases.

Bonding in [**27**]$^{+}$, **27**$^{\bullet}$ and [**27**]$^{-}$ has been analyzed with the Natural Bond Orbital (NBO) method using the aforementioned optimized geometries and a 6-31g(d) basis set for all atoms ().[151, 152] In the case of [**27**]$^{+}$, one σ-bonding orbital occupied by 1.95 electrons connects the B(1) and C(9) atoms in agreement with existence of a B-C single

bond (Figure 58). NBO analysis of [**27**]$^-$ affords one σ- and one π-bonding orbital spanning the B(1)-C(9) linkage (Figure 58). These orbitals are occupied by 1.95 and 1.67 electrons respectively. It is interesting to note the contour plot of the π-bond shows a polarization toward the carbon atom of the B=C linkage. Hence, the π-bond of this borataalkene may be viewed as originating from donation of a carbanion lone pair into the empty p-orbital of the adjacent boron atom. Because of its open-shell electronic configuration, NBO analysis of radical **27**$^\bullet$ affords orbitals both in the α- and β-spin manifold. The B(1) and C(9) atoms are connected by two σ-bonding orbitals. These two orbitals respectively belong to the α- and β-spin manifold and are each occupied by 0.98 electrons. In addition to these two sigma interactions, the NBO analysis indicates that there is a π-bonding interaction between B(1) and C(9) in the α spin manifold, which is occupied by 0.81 electrons with a strong polarization toward C(9) atom (83% on C and 17% on B). The combined occupancies of the orbitals connecting B(1) and C(9) in [**27**]$^+$, **27**$^\bullet$ and [**27**]$^-$ are respectively equal to 1.95, 2.77, and 3.62 which suggest an increase of the bond-order upon reduction. However, because some of these interactions are strongly polarized, the bond orders are likely to be less than 1, 1.5 and 2, a set of value that would be derived from simple valence bond theory. More realistic numbers may in fact be provided by the Wiberg bond indexes which are equal to 0.83 for [**27**]$^+$, 0.96 for **27**$^\bullet$ and 1.34 for [**27**]$^-$ ().

Table 13: Selected NBO output involving the B(1)-C(9) bonding interaction

	Occupancy	Hybridization	% Polarization
σ-NBO in [**27**]$^{+}$	1.95	B: $sp^{2.30}$ C: $sp^{1.69}$	B: 29.95% C: 70.05%
σ-NBO in [**27**]$^{-}$	1.95	B: $sp^{1.71}$ C: $sp^{1.30}$	B: 31.95% C:68.05%
π-NBO in [**27**]$^{-}$	1.67	B: p C: p	B: 27.78% C: 72.22%
α-spin σ–NBO in **27**$^{\bullet}$	0.98	B: $sp^{1.99}$ C: $sp^{1.55}$	B: 31.05% C: 68.95%
β-spin σ-NBO in **27**$^{\bullet}$	0.98	B: $sp^{1.96}$ C: $sp^{1.55}$	B: 31.64% C: 68.36%
α-spin π-NBO in **27**$^{\bullet}$	0.81	B: p C: p	B: 16.9% C: 83.1%

Table 14: Selected Wiberg bond index in Natural Atomic Orbital (NAO)

	B(1)-C(9)	B(1)-C(15)	B(1)-C(25)
[**27**]$^{+}$	0.83	0.94	0.94
27$^{\bullet}$	0.96	0.89	0.89
[**27**]$^{-}$	1.34	0.86	0.87

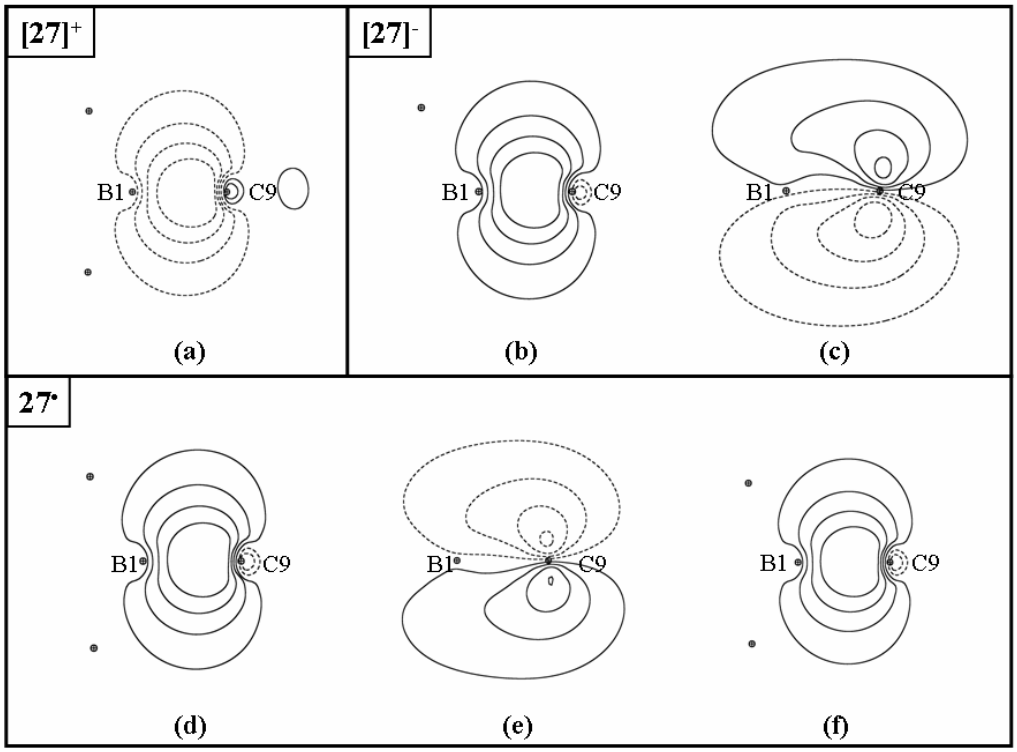

Figure 58: Selected natural bond orbital contours. $[\mathbf{27}]^{+}$: $\sigma_{B(1)\text{-}C(9)}$ (a). $[\mathbf{27}]^{-}$: $\sigma_{B(1)\text{-}C(9)}$ (b) and $\pi_{B(1)\text{-}C(9)}$ (c). $\mathbf{27}^{\bullet}$: $\sigma_{B(1)\text{-}C(9)}$ (d), $\pi_{B(1)\text{-}C(9)}$ (e) and $\sigma_{B(1)\text{-}C(9)}$ (f).

4.7 Conclusion

In this chapter, we describe the first α-borylated carbocation which may also be described as a borenium-carbene adduct. As indicated by cyclic voltammetry, this derivative undergoes two reversible reductions to produce the neutral radical **27**$^{\bullet}$ and the borataalkene [**27**]$^{-}$, respectively. The structural results indicate that reduction of [**27**]$^{+}$ results in the sequential population of the central boron-carbon π-bond of this derivative. Population of this orbital is substantiated by a clear shortening of the boron-carbon bond as well as a decrease of its twist angle. The computational results are in agreement with these experimental findings and confirm an increase of the order of the B-C bond upon reduction. Another important outcome of this work is the discovery that borataalkenes are amenable to reversible redox chemistry and can in fact be considered as the reduced form of α-borylated carbocations.

4.8 Experimental section

Synthesis of [27][OTf]: An hexane solution of n-BuLi (1.6 M, 3 mL, 4.8 mmol) was added to a solution of 9-bromoacridine (1 g, 4 mmol) in ether (60 mL), at -78°C. After 30 min, a solution of dimesitylboron fluoride (1.26 g, 4.7 mmol) in ether (15 mL) was added to the reaction mixture. The reaction mixture was allowed to warm to room temperature. After stirring for 12 hours, the reaction was quenched with water. The product was extracted with ether. The organic phase was washed with brine, dried over $MgSO_4$, filtered, and dried under vacuum to afford a viscous oil. Extraction of this oil with hexane afforded crude 9-dimesitylboryl-acridine as brown solid. Without further

purification this solid was dissolved in dichloromethane and allowed to react with methyl triflate in the glove box. After stirring for 1 hour, [**27**][OTf] was precipitated as a bright yellow solid by addition of ether (0.71 g, yield 30% based on 9-bromoacridine). ^{1}H NMR ($CDCl_3$, 499.95 MHz): δ 1.88 (s, 12H, Mes-CH3), 2.28 (s, 6H, Mes-CH3), 5.03 (s, 3H, NMe), 6.82 (s, 4H, Mes-CH), 7.65 (dd, 2H, $^{3}J_{H-H}$ = 5 Hz, $^{3}J_{H-H}$ = 8.5 Hz), 8.24 (d, 2H, $^{3}J_{H-H}$ = 8.5 Hz), 8.29 (dd, 2H, $^{3}J_{H-H}$ = 5 Hz, 3JH-H = 9.5 Hz), 8.73 (d, 2H, $^{3}J_{H-H}$ = 9.5 Hz). ^{13}C NMR (CDCl3, 125.7 MHz): δ 21.4 (Mes-*p*-CH3), 24.1 (Mes-*o*-CH3), 39.6 (NMe), 119.5, 127.5, 128.2, 129.9, 130.8, 138.9, 139.6, 141.0, 142.8, 143.9, 174.8 (methylium carbon). ^{11}B NMR (CDCl3, 128.2 MHz): δ 76.5. Anal. Calcd. for $C_{33}H_{33}BF_3NO_3S$: C, 67.01; H, 5.62. Found: C, 66.73; H, 5.53.

Synthesis of 27$^{\bullet}$: [**27**][OTf] (30 mg, 0.05 mmol) was allowed to react with excess Mg powder at room temperature in acetonitrile (2 mL). After stirring for 10 minutes, the dark green solution was extracted with hexane (3 x10 mL). The resulting dark blue hexane solution was concentrated to ca. 5 mL and cooled to -40°C to afford dark crystals of **27$^{\bullet}$** (8.5 mg, yield 38%). The yield was not optimized.

Synthesis of [27][K(db-18-c-6)(THF)$_2$]: [**27**][OTf] (50 mg, 0.08 mmol) was allowed to react with excess K at room temperature in THF (2 mL) in the presence of dibenzo-18-crown-6 (40 mg, 0.11 mmol). The color of solution changed from yellow to blue, and then to red after about 30 minutes. [**27**][K(db-18-c-6)(THF)$_2$] was obtained as a THF/0.5 hexane solvate in the from of dark red crystals. These crystals are very sensitive and decompose at room temperature in an inert atmosphere. ^{1}H NMR (pyridine-d5, 499.95 MHz): δ 2.20 (s, 6H, Mes-CH3), 2.86 (s, 12H, Mes-CH3), 3.09 (s, 3H, NMe), 3.64 (bs, 16H), 6.46 (d, 2H, $^3J_{H-H}$ = 7.5 Hz), 6.51 (t, 2H, $^3J_{H-H}$ = 7.5 Hz), 6.62 (t, 3H, $^3J_{H-H}$ = 7.5 Hz), 6.83 (s, 4H, Mes-CH), 6.93(bs, 8H), 7.49 (d, 2H, $^3J_{H-H}$ = 7.5 Hz). ^{13}C NMR (pyridine-d5, 125.7 MHz): δ 20.2 (Mes-*p*-CH3), 23.2 (Mes-*o*-CH3), 32.4 (NMe), 66.3 (crown), 68.1 (crown), 108.9, 110.5, 117.9, 119.5, 120.7, *1*23.4, 126.5, 130.8, 140.8, 143.4, 143.7, 146.0, 151.7. ^{11}B NMR (pyridine-d5, 160.4MHz): δ 40.

CHAPTER V

THE REDUCTION POTENTIAL OF CATIONIC TRIARYLBORANES

5.1 Introduction

As indicated in Chapter III, we have learned that the Lewis acidity of a triarylborane could be greatly increased by appending a positively charged group to the molecule. With a pendant ammonium group, the cationic borane $[25]^+$ is the first triarylborane capable of extraction of fluoride from water under biphasic conditions. This remarkable property arises from favorable Coulombic effects which stabilize the boron-fluorine bond against heterolysis.

Following this initial discovery, our group started to investigate the fluoride binding properties of various cationic boranes in protic media. The ultimate goal of these studies is to design a selective fluoride receptor that will function in water at physiological pH. In order to better understand how the nature of the cationic groups impact the Lewis acidic properties of the borane, we designed series of triarylboranes that contain ammonium or phosphonium functionality. Fluoride complexation studies carried out on $[\mathbf{30}]^+$ show that the incorporation of a *para*-methyldiphenylphosphonium substituent affords a borane which capture fluoride ions in H_2O/methanol (9:1) with a binding constant of 1000 M^{-1}.[153] Interestingly, the analogous *para*-trimethylammonium derivative $[\mathbf{31}]^+$ does not complex fluoride under these conditions, which may be assigned to the increased solvation of the trimethylammonium group. Better results were obtained with the *ortho*-trimethylammonium derivative $[\mathbf{32}]^+$ which was found to

complex fluoride ion in H_2O/DMSO (6:4) with a binding constant of 910 ± (50) M^{-1}. This drastic difference in behavior may result from the stronger acidity and smaller binding pocket of $[\mathbf{32}]^+$ when compared to $[\mathbf{31}]^+$.[128]

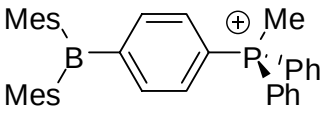

$[30]^+$

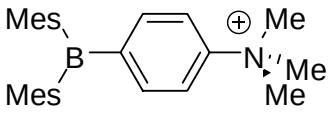

$[31]^+$

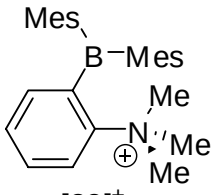

$[32]^+$

In order to better understand the Lewis acidic properties of this type of cationic boranes, we have now decided to investigate the effect induced by the presence of multiple cationic substituents. As recently shown by Norton and Jäkle, the reduction potential of Mes_3B, $Mes_2B(C_6F_5)$, and $MesB(C_6F_5)_2$ increases linearly with the number of electron-withdrawing pentafluorophenyl group (Figure 59).[78]

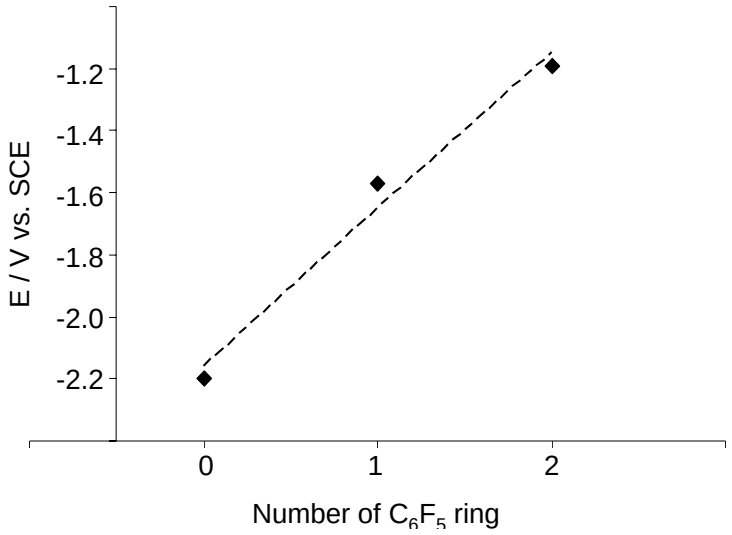

Figure 59: Reduction potential vs. number of C_6F_5 ring on boranes.

In this chapter, we have decided to determine whether the reduction potential of triarylboranes would show a similar dependence on the number of cationic substituents. To this end, we have synthesized and studied a series of cationic boranes that have similar steric bulk around the boron atom but a different number of pendant positively charged functionalities.

5.2 Synthesis of the cationic boranes

As shown by earlier electrochemical studies of triarylboranes, the reversibility of the reduction and hence the stability of the resulting radical depend on the steric property of the aryl substituents. For example, the cyclic voltammogram (CV) of Ph_3B, which possesses a fairly exposed boron center, features a quasi-reversible reduction wave at -1.63 V (vs. SCE) while the more sterically protected boranes Ph_2BMes, $PhBMes_2$ and

Mes_3B undergo a reversible reduction at -1.79 V, -1.85 V, and -1.94 V (vs. SCE).[111] For these reasons, we decided to synthesize and study compounds **33**, [**34**]$^{+}$, [**35**]$^{2+}$ and [**36**]$^{3+}$, which all feature a boron center protected by six *ortho*-methyl groups.

Mes_3B	Mes_2BAr^{N+}	$MesB(Ar^{N+})_2$	$B(Ar^{N+})_3$
33	$[34]^{+}$	$[35]^{2+}$	$[36]^{3+}$

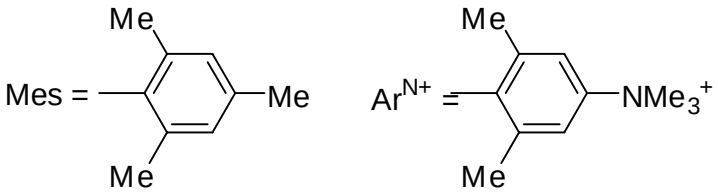

The salt cation [**34**][OTf] was obtained by reaction of one equivalent of 4-lithio-*N*,*N*,3,5-tetramethylanline with 1.5 equivalent of Mes_2BF in ether followed by methylation with MeOTf. Salt [**34**][OTf] is colorless and has been characterized by ^{1}H, ^{13}C and ^{11}B NMR. As indicated in ^{1}H NMR, the aromatic CH resonances of the Ar^{N+} group (Ar^{N+} = [4-(Me_3N)-2,6-Me_2-C_6H_2]$^{+}$) appears at 7.21 ppm while those of the mesityl groups are detected as two singlets at 6.73 ppm and 6.75 ppm. The detection of these two signals indicates that rotation of the aromatic substituents about the B-C bonds is slow on the NMR time scale. The ^{1}H NMR resonance of trimethylammonium group appears at 3.69 ppm thus confirming that cationic nature of [**34**]$^{+}$. The ^{11}B resonance of [**34**]$^{+}$ is detected at 83 ppm indicating the presence of a coordinatively unsaturated boron center.

In order to introduce two and three ammonium functionalities into the borane backbone, we first investigated the synthesis of bis(4-dimethylamino-2,6-dimethyl-phenyl)boron fluoride (Ar^N_2BF) (Figure 60).

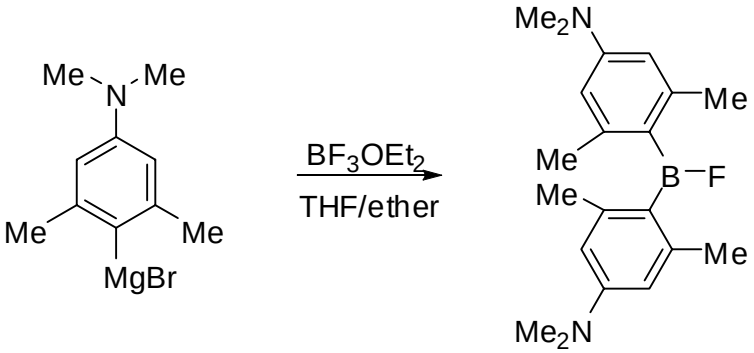

Figure 60: Synthesis of Ar^N_2BF.

By treating $BF_3 \cdot OEt_2$ with two equivalents of the Grignard reagent, the boron fluoride derivative Ar^N_2BF could be isolated as pale yellow solid in moderate yield. The ^{1}H-NMR spectrum of Ar^N_2BF contains three sharp singlets at 6.46, 3.06 and 2.39 ppm for the aromatic CH, NMe_2, and *ortho*-methyl groups on the phenyl ring, respectively. The ^{11}B NMR and ^{19}F NMR resonances which respectively appear at 52 ppm and -23 ppm are comparable to those Mes_2BF.[154] Ar^N_2BF is moisture sensitive and hydrolyzes to form the corresponding boron hydroxide immediately. The boron hydroxide compound, **37**, was also characterized in ^{1}H and ^{11}B NMR. Single crystals of **37** could be obtained from slow evaporation of a hexane solution and were subjected to an X-ray analysis (Figure 61, Table 15). The bond lengths and angles of **37** are

unremarkable. The boron atom adopts a trigonal planar geometry as expected for a three-coordinate boron hydroxide derivative. The B(1)-O(1) distant of 1.368(4)Å is almost identical to the value of 1.368(5) Å reported for Mes_2BOH.[155] The nitrogen atoms of the two NMe_2 groups remain pyramidal with sum of the C-N-C angle of 355.6º and 343.8 º for N(1) and N(2) atom, respectively.

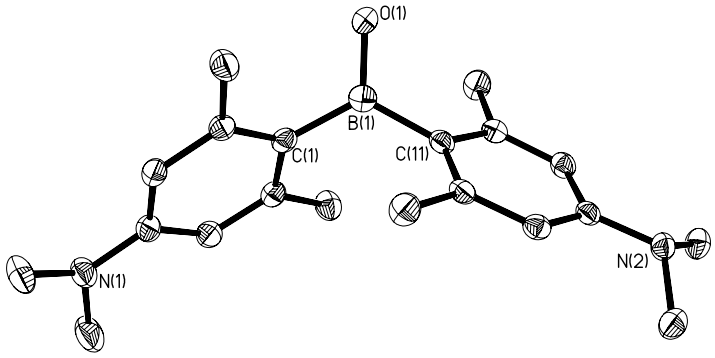

Figure 61: Crystal structure of **37** with thermal ellipsoids set at the 50% probability level. Hydrogen atoms are omitted for clarity. Selected bond lengths [Å] and bond angles [º]: B(1)-O(1) 1.368(4), B(1)-C(1) 1.577(4), B(1)-C(11) 1.595(5), N(1)-C(4) 1.388(4), N(1)-C(9) 1.443(4), N(1)-C(10) 1.451(4), N(2)-C(14) 1.417(4), N(2)-C(19) 1.461(4), N(2)-C(20) 1.464(4), O(1)-B(1)-C(1) 120.0(3), O(1)-B(1)-C(11) 116.7(3), C(1)-B(1)-C(11) 123.1(3), C(4)-N(1)-C(9) 118.4(3), C(4)-N(1)-C(10) 119.1(3), C(9)-N(1)-C(10) 118.1(3), C(14)-N(2)-C(19) 116.0(2), C(14)-N(2)-C(20) 115.8(2), C(19)-N(2)-C(20) 112.0(2).

Table 15: Crystal data and structure refinement for **37**

Crystal data	**37**
Formula	$C_{20}H_{29}BN_2O$
M_r	324.26
Crystal size (mm^3)	0.45 x 0.44 x 0.27
Crystal system	monoclinic
Space group	P2(1)/n
a (Å)	11.675(2)
b (Å)	10.943(2)
c (Å)	15.106(3)
α (º)	90.00
β (º)	103.74(3)
γ (º)	90.00
V ($Å^3$)	1874.6(6)
Z	4
ρ_{calc} (gcm^{-3})	1.149
μ(Mo K_α) (mm-1)	0.070
F(000) (e)	704
Data collection	
T/K	110
Scan mode	ω
hkl range	-13→13, -12→7, -17→17
Measured refl.	8331
Unique refl., [R_{int}]	2946, [0.0279]
Refl. Used for refinement	2946
Refinement	
Refined parameters	217
R_1, wR_2 [all data]	0.0794, 0.1728
ρ_{fin} (max/min) (e $Å^{-3}$)	0.605/-0.638

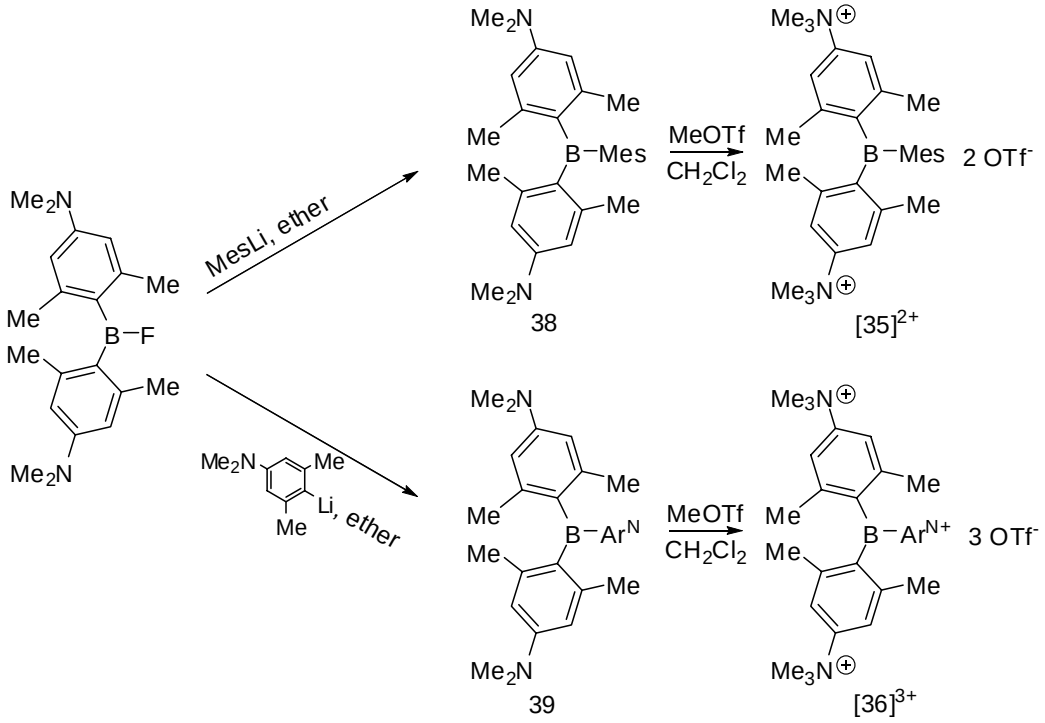

Figure 62: Synthesis of $[\mathbf{35}]^{2+}$ and $[\mathbf{36}]^{3+}$.

Treatment of $Ar^N{}_2BF$ with excess MesLi or 4-lithio-*N*,*N*,3,5-tetramethylaniline affords the corresponding boranes **38** and **39** (Figure 62). These two boranes can be methylated with methyl triflate to afford the corresponding dication $[\mathbf{35}]^{2+}$ or trication $[\mathbf{36}]^{3+}$ as triflate salts (Figure 62). Surprisingly, both $[\mathbf{35}][OTf]_2$ and $[\mathbf{36}][OTf]_3$ are air- and moisture-stable. This stability is somewhat surprising and may be assigned to the steric protection of the boron center. As indicated by the ^1H NMR of $[\mathbf{35}]^{2+}$, the aromatic CH of the Ar^{N+} and the mesityl group are detected at 7.40 and 6.89 ppm, respectively. The ^1H NMR resonance of $NMe_3{}^+$ group of the Ar^{N+} ligand observed at 3.52 ppm is comparable to that in $[\mathbf{34}]^+$. The ^1H NMR spectrum of $[\mathbf{36}]^{3+}$ contains

three sharp singlets at 7.44, 3.52 and 2.11 ppm for the aromatic CH, NMe_3^+, and *ortho*-methyl groups of the Ar^{N+} ring. The ^{11}B NMR resonance of $[\mathbf{35}]^{2+}$ and $[\mathbf{36}]^{3+}$ are respectively observed at 83 and 89 ppm which are slightly higher than that that typically observed in neutral triarylboranes. The cationic character of $[\mathbf{35}]^{2+}$ and $[\mathbf{36}]^{3+}$ is probably responsible for this observation.

5.3 Electrochemistry

In an attempt to assess the influence of the number of positive groups on the electron deficiency of the boranes, the reduction potential of **33**, $[\mathbf{34}]^+$, $[\mathbf{35}]^{2+}$, and $[\mathbf{36}]^{3+}$ have been measured. To this end, **33**, $[\mathbf{34}]^+$, $[\mathbf{35}]^{2+}$, and $[\mathbf{36}]^{3+}$ were analyzed by cyclic voltammetry in CH_3CN using a glassy carbon electrode and $[Bu_4N][PF_6]$ (0.1 M) as a supporting electrolyte. The analyte concentration was kept at 0.001 M in all four cases. The potentials were recorded at ambient temperature and reported against Fc/Fc^+. The cyclic voltammograms of **33**, $[\mathbf{34}]^+$and $[\mathbf{35}]^{2+}$ show a reversible reduction wave at $E_{1/2}$ -2.57 V, -2.33 V and -2.09 V vs. Fc/Fc^+, respectively. The reversible reduction behavior of $[\mathbf{34}]^+$ and $[\mathbf{35}]^{2+}$ indicate the formation of the stable radicals, namely $[\mathbf{34}]^{\bullet}$ and $[\mathbf{35}]^{\bullet+}$ (Figure 63) By contrast, the CV of $[\mathbf{36}]^{3+}$ features an irreversible reduction wave at E_{peak} -1.86 V (Figure 64).

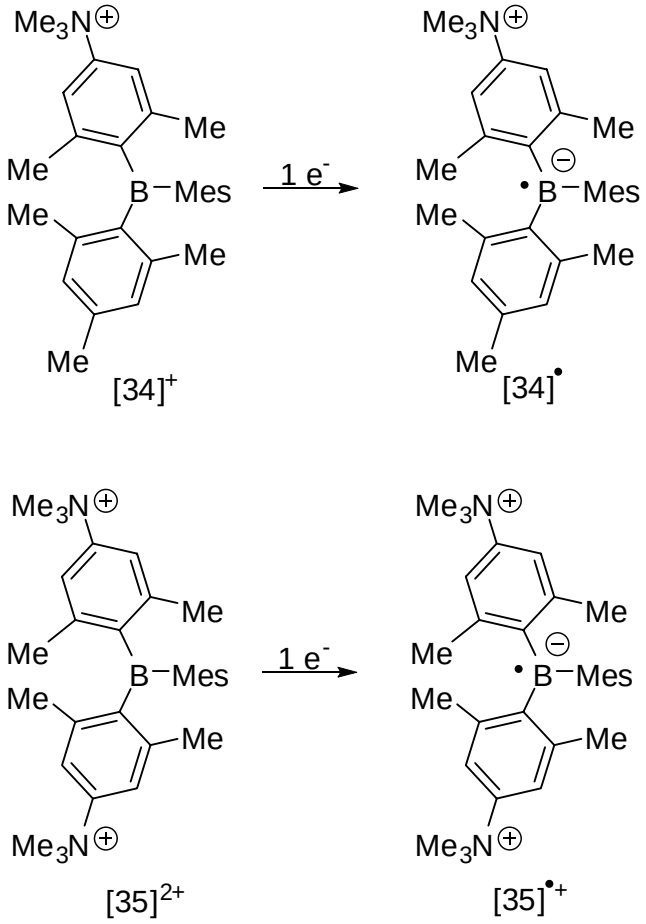

Figure 63: Formation of stable boron centered radicals.

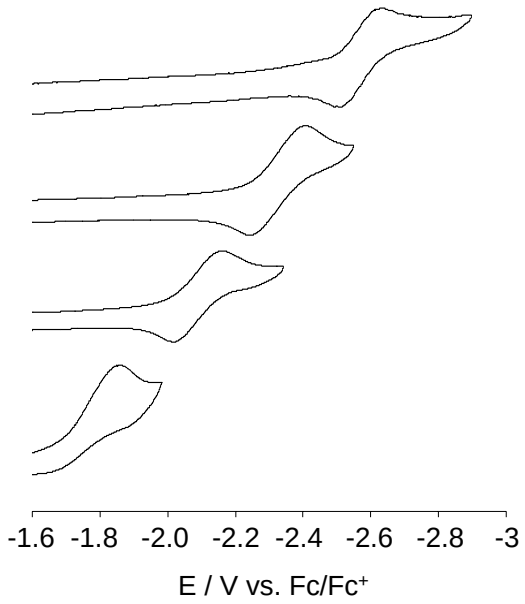

Figure 64: Cyclic voltammograms of **33**, $[\mathbf{34}]^{+}$, $[\mathbf{35}]^{2+}$, and $[\mathbf{36}]^{3+}$ in acetonitrile with a glassy-carbon working electrode in 0.1 M of $n\text{Bu}_4\text{NPF}_6$ solution with scan rate of ν = 300 mV s^{-1}.

A comparison of the peak potential of -2.63 V, -2.41 V, -2.16 V and -1.86 V recorded for **33**, $[\mathbf{34}]^{+}$, $[\mathbf{35}]^{2+}$ and $[\mathbf{36}]^{3+}$, respectively, indicate that $[\mathbf{36}]^{3+}$ is, as expected, the most electron deficient derivative in the series. Remarkably, the reduction peak potential of boranes ($E_{(peak,\ reduction)}$) shows a linear dependence on the number of ammonium substituents (n). A least square fit ($R^2 = 0.995$) of the resulting data affords the following equation:

$$E_{(peak,\ reduction)} = 0.26 \times n - 2.65$$

In other words, substitution of a mesityl group by an Ar^{N+} group leads to an increase of the reduction potential by 260 mV.

In it is interesting to compare these results with those obtained by Norton and Jäkle who investigated the effect caused by the introduction of pentafluorophenyl groups.[78] In these investigations, they found that the reduction potential of Mes_3B, $Mes_2B(C_6F_5)$, and $MesB(C_6F_5)_2$ measured in THF appear at -2.73 V, -2.10 V and -1.72 V (vs. Fc/Fc^+), respectively. Analysis of their data using the least square methods affords:

$$E_{(peak,\ reduction)} = \quad = 0.50 \times n - 2.69$$

$$R^2 = 0.98$$

Thus indicating that substitution of a mesityl group by an C_6F_5 group leads to an increase of the reduction potential by 500 mV. In turn, it can be concluded that the C_6F_5 group is more electron-withdrawing than the Ar^{N+} group (Figure 65).

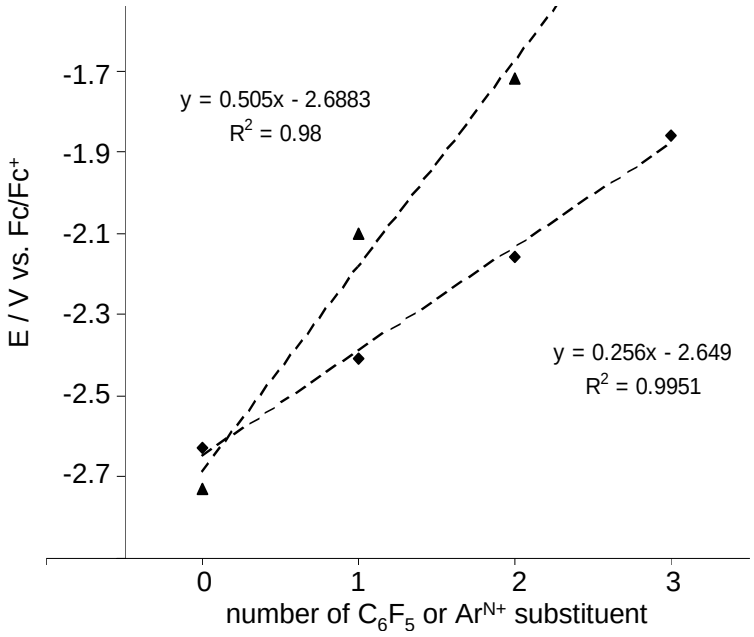

Figure 65: Reduction potential vs. number of C_6F_5 or Ar^{N+} substituent on boranes.

5.4 Conclusion

Three novel cationic boranes that feature similar steric bulk around boron atom but different numbers of positively charged Ar^{N+} substituents have been synthesized and investigated by cyclic voltammetry. The CV data of these compounds shows that the reduction potential of triarylborane is linearly proportional to the number of the pendant positively charged substituents. Because of this linear relationship, the reduction potential can be accurately tuned over a 1 V window. Finally, comparison with the work of Norton and Jäkle shows that effect caused by the introduction of pentafluorophenyl groups is two times stronger than that caused by introduction of Ar^{N+} substituents.

5.5 Experimental section

Synthesis of $Ar^{N}_{2}BF$ (Ar^{N} = 4-(Me_2N)-2,6-Me_2-C_6H_2): 4-Bromo-*N*,*N*,3,5-tetramethyl aniline (10g, 0.04 mol) was allowed to react with excess Mg powder in THF (30 ml) under reflux for 5 hours. Once the reaction mixture was cooled to the room temperature, the THF solution was filtered and then slowly added into an Et_2O solution of $BF_3 \cdot OEt_2$ (2.7 ml, 0.02 mol) at -78 ℃. The reaction mixture was allowed to warm up to room temperature and stirred overnight. The solvents were then removed under reduced pressure and the solid residue was extracted with hexane (3 × 50 ml). The combined hexane fractions were dried under vacuum to afford a yellow solid. This solid was washed with hexane (5 ml) to afford $Ar^{N}_{2}BF$ in moderate yield (3.8 g, yield = 53%). ^{1}H NMR ($CDCl_3$, 399.59 MHz): δ 2.39 (d, 12H, *ortho*-Me), 3.06 (s, 12H,

Ar^N-NMe_2), 6.46(s, 4H, Ar^N-CH). ^{13}C NMR ($CDCl_3$, 100.5 MHz): δ 23.2 (*ortho*-Me), 40.0 (Ar^N-NMe_2), 111.3, 125.6, 144.4, 151.6. ^{19}F NMR ($CDCl_3$, 375.95 MHz): δ -23.4. ^{11}B NMR ($CDCl_3$, 128.2 MHz): δ 52.

Synthesis of [34][OTf]: 4-Lithio-*N*,*N*,3,5-tetramethylaniline (0.2g, 1.3 mmol) was allowed to react with 1.8 equivalent of Mes_2BF (0.68g, 2.3 mmol) in ether (5 ml) at room temperature. After stirring for overnight, reaction was quenched with water and extracted with hexane. The combined hexane solution was dried under vacuum to give a yellow solid which was then washed with small amount of hexane (5 ml) to remove byproducts. The obtained solid residual was methylated with methyl triflate in CH_2Cl_2 without further purification. By adding ether into the reaction mixture, [**34**][OTf] precipitates and was isolated as light yellow solid in moderate yield (0.38 g, yield = 52%). ^1H NMR ($CDCl_3$, 399.59 MHz): δ 1.87 (s, 6H), 1.97 (s, 6H), 2.09 (s, 6H), 2.25 (s, 6H), 3.69 (s, 9H, NMe_3^+), 6.73 (s, 2H, Mes), 6.74 (s, 2H, Mes), 7.21 (s, 2H, Ar^{N+}). ^1H NMR (CD_3CN 299.92 MHz): δ 1.94 (s, 6H), 1.97 (s, 6H), 2.01 (s, 6H), 2.28 (s, 6H), 3.51 (s, 9H, NMe_3^+), 6.85 (s, 4H, Mes), 7.35 (s, 2H, Ar^{N+}). ^{13}C NMR (CD_3CN, 75.4 MHz): δ 23.0, 23.1, 23.2, 57.7, 119.3, 129.7, 141.4, 141.5, 143.6, 148.1. ^{11}B NMR (CD_3CN, 128.2 MHz): δ 83.1.

Synthesis of [35][OTf]$_2$: A ether solution of $Ar^N{}_2BF$ (500 mg, 1.5 mmol) was slowly added into a mesityl lithium (400 mg, 3.2 mmol) suspension in ether at -78 ºC and stirred for 30 minutes before warmed up to room temperature. The reaction was allowed to stir for overnight before quenching with water. After hexane extraction of the quenched mixture, the bright yellow organic layer was washed with brine and dried

over $MgSO_4$. After removing solvent, the crude product was methylated with MeOTf in CH_2Cl_2 without further purification. The white solids of [**35**][OTf]$_2$ were obtained by adding ether into the CH_2Cl_2 solution (885 mg, yield = 77%). ^{1}H NMR (CD_3CN 299.92 MHz): δ 1.97 (s, 6H), 2.08 (s, 6H), 2.13 (s, 6H), 2.28 (s, 3H), 3.52 (s, 18H, NMe_3^+), 6.89 (s, 2H, Mes), 7.40 (s, 4H, Ar^{N+}). ^{13}C NMR (CD_3CN, 100.5 MHz): δ 21.3, 23.2, 23.3, 57.7, 119.1, 119.7, 130.1, 142.1, 142.6, 143.6, 144.1, 148.7. ^{11}B NMR (CD_3CN, 128.2 MHz): δ 83.4.

Synthesis of [36][OTf]$_3$: 4-Lithio-*N*,*N*,3,5-tetramethylaniline (0.31g, 2 mmol) was allowed to react with $Ar^N{}_2BF$ (0.32g, 1 mmol) in ether (10 ml) at room temperature. After stirring for 1 day, the reaction was quenched with water and extracted with hexane. The combined hexane solution was dried under vacuum to give a yellow solid which was methylated with methyl triflate without further purification in a 1:1 CH_2Cl_2/pyridine solution. After vigorous stirring for 3 days, addition of ether into the solution results in precipitation of [**36**][OTf]$_3$ which was further purified by washing with CH_2Cl_2 (100 mL) and obtained as white triflate salts in moderate yield (0.54g, yield = 57%). ^{1}H NMR (CD_3CN 299.92 MHz): δ 2.11 (s, 18H), 3.52 (s, 27H, NMe_3^+), 7.44 (s, 6H, Ar^{N+}). ^{13}C NMR (CD_3CN, 75.4 MHz): δ 23.3, 57.7, 120.2, 144.2, 149.2. ^{11}B NMR (CD_3CN, 128.2 MHz): δ 89.1.

CHAPTER VI

DIARYLBORENIUM CATIONS – SYNTHESIS, STRUCTURE AND ELECTROCHEMISTRY

6.1 Introduction

Although the tri-coordinate neutral boranes have been extensively explored, the reports of the stable borenium remain limited, especially the solid state structural data. Diphenylborenium cations provide a good example for such species which has long been proposed but whose definitive characterization in solution has only recently been achieved. Despite these recent successes, diphenylborenium cations have not been structurally characterized. These difficulties can be correlated to the unsaturation of the boron center and the week p-donating ability of the phenyl groups. In an effort to overcome these limitations, we have decided to probe the use of more sterically protecting aryl substituents featuring *ortho*-methyl groups. We have also probed the stabilizing effects that can be provided by remote amino-substituents appended to the aryl groups of diarylborenium cations.

6.2 Synthesis and characterization of diarylborenium cations

The reaction of Mes_2BF with trimethylsilyltriflate (TMSOTf) and p-dimethylamino-pyridine (DMAP) in refluxing chlorobenzene affords after 24 hours $[Mes_2B\text{-}DMAP]^+OTf^-$ ([**40**][OTf]) (Figure 66).[156]

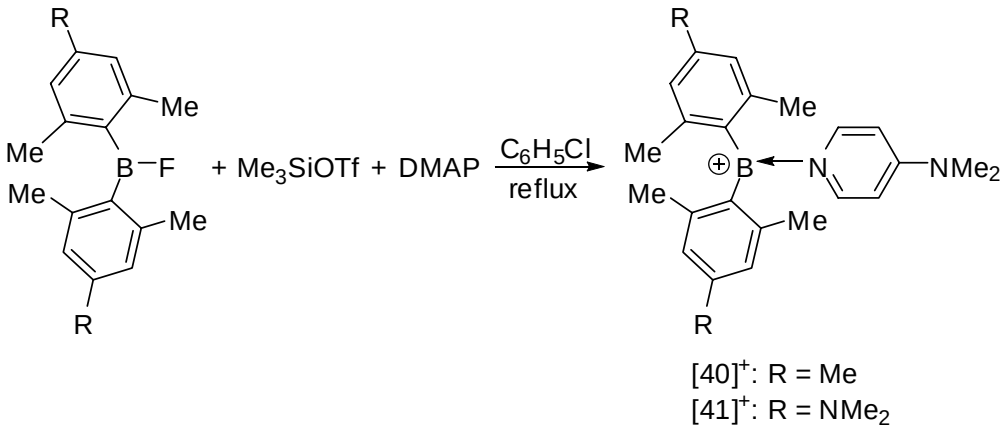

Figure 66: Synthesis of borenium cations.

In an effort to determine the effect of remote amino-substituents on the stability of such borenium ions, we also synthesized $Ar^N{}_2BF$ (Ar^N = 4-(Me_2N)-2,6-Me_2-C_6H_2) and converted it into [$Ar^N{}_2$B-DMAP][OTf] ([**41**][OTf]) by following the method used for [**40**][OTf]. The formation of [**40**][OTf] and [**41**][OTf] was confirmed by ^{1}H NMR which showed the presence of one DMAP ligand bound to the boron center. The ^{1}H NMR spectra of [**40**][OTf] and [**41**][OTf] are also different from those of [Mes_2BF-DMAP] and [$Ar^N{}_2$BF-DMAP], respectively, which could be generated in situ by simple mixing of the diarylboron fluoride with DMAP. Of special note, the ^{1}H-NMR resonance of the Me_2N group of DMAP is shifted downfield by 0.36 ppm on going from [Mes_2BF-DMAP] to [**40**][OTf] and 0.31 ppm on going from [$Ar^N{}_2$BF -DMAP] to [**41**][OTf]. These observation are in agreement with an ionic formulation for [**40**][OTf] and [**41**][OTf]. This was confirmed by the detection of a ^{11}B NMR signal at 64 ppm for [**40**][OTf] and 62 ppm for [**41**][OTf]. These chemical shift are

comparable to the value reported for $[(C_6H_5)_2B(Py)]^+$ (58.2 ppm) which also feature a tricoordinate boron atom.[157] While [**40**][OTf] is isolated as colorless crystals, we note that [**41**][OTf] is an orange solid.

Bearing in mind that only one diarylborenium salt has been previously structurally characterized,[158] we undertook the characterization of [**40**][OTf] and [**41**][OTf] by X-ray analysis. Both salts crystallize in the *P*-1 space group with two molecules in the unit cell (Table 16 and Table 17). Both structures are very similar (Figure 67 and Figure 68). The boron center of [**40**][OTf] and [**41**][OTf] is trigonal planar as indicated by the sum of the bond angles which is equal to 360º in both cases. The B(1)-C(8) (1.560(3)Å in $[\mathbf{40}]^+$, 1.550(4) Å in $[\mathbf{41}]^+$) and B(1)-C(18) bonds (1.570(3)Å in $[\mathbf{40}]^+$, 1.532(4) Å in $[\mathbf{41}]^+$) connecting the aryl ligand to the boron centers are significantly shorter than the C_{Mes}-B bonds measured in Mes_2BPh (1.579(2) Å)[114] suggesting increased π-donation to the electron deficient boron center. The average dihedral angle θ formed between the boron trigonal plane and the plane containing the Mes ligand in $[\mathbf{40}]^+$ and the Ar^N ligand in $[\mathbf{41}]^+$ are respectively equal to 58. 1 º and 48.3 º. The slight shortening of the B(1)-C(8) and B(1)-C(18) bonds as well as the smaller θ angle observed for $[\mathbf{41}]^+$ may be correlated to the stronger π-donating ability of the Ar^N ligand, a conclusion supported by the planarity of the N(3) and N(4) atoms ($\Sigma_{(C\text{-}N\text{-}C)}$ = 359.8º (N(3)) and 358.2º (N(4))). The B(1)-N(1) bonds connecting the DMAP ligand to the boron centers (1.480(3)Å in $[\mathbf{40}]^+$, 1.501(4) Å in $[\mathbf{41}]^+$) in both structures are shorter that the value computed for $[(C_6H_5)_2B(Py)]^+$ (1.552 Å)[157]. They are also shorter than the B-N_{DMAP} bond observed in Ar*P=B(DMAP)Tmp (Ar* = C_6H_3-2,6-(C_6H_2-2,4,6-iPr_3)$_2$; Tmp =

2,2,6,6-tetramethylpiperidino) and are in fact comparable to traditional B-N single bonds.[159, 160] The electron deficiency of the cationic boron center as well as the strong σ-donor character of the DMAP ligand is most certainly responsible for this feature.

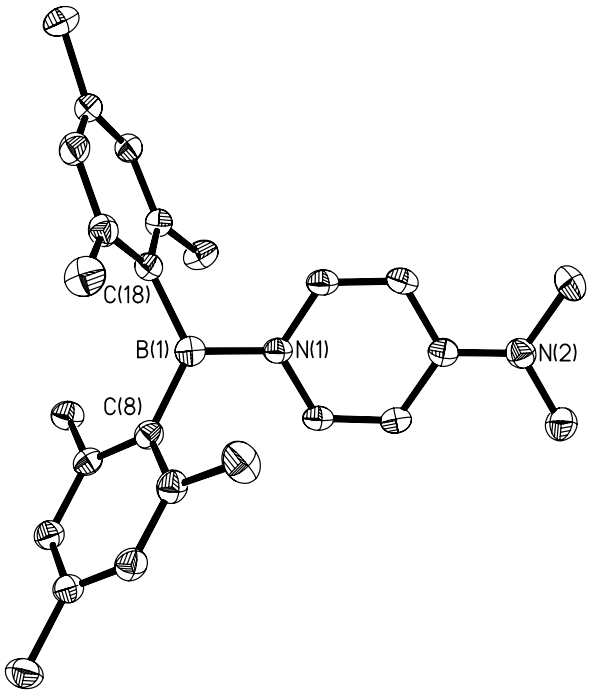

Figure 67: Crystal structure of [**40**]$^+$ with thermal ellipsoids set at the 50% probability level. Hydrogen atoms are omitted for clarity. Selected bond lengths [Å] and bond angles [º]: B(1)-N(1) 1.480(3), B(1)-C(8) 1.560(3), B(1)-C(17) 1.570(3), N(1)-C(1) 1.381(3), N(1)-C(5) 1.374(3), N(2)-C(3) 1.326(3), N(2)-C(6) 1.466(3), N(2)-C(7) 1.466(3), C(1)-C(2) 1.344(3), C(2)-C(3) 1.428(3), C(3)-C(4) 1.428(3), C(4)-C(5) 1.345(3), N(1)-B(1)-C(8) 117.38(19), N(1)-B(1)-C(17) 115.53(19), C(8)-B(1)-C(17) 127.06(19), C(3)-N(2)-C(6) 121.60(19), C(3)-N(2)-C(7) 120.68(19), C(6)-N(2)-C(7) 117.55(19).

Table 16: Crystal data and structure refinement for [**40**][OTf]

Crystal data	**[40][OTf]**
Formula	$C_{26}H_{32}BF_3N_2O_3S$
M_r	520.41
Crystal size (mm^3)	0.51, 0.33, 0.22
Crystal system	Triclinic
Space group	P-1
a (Å)	8.2944(8)
b (Å)	10.4347(10)
c (Å)	16.1597(15)
α (º)	104.6880(10)
β (º)	96.8560(10)
γ (º)	100.4320(10)
V ($Å^3$)	1310.3(2)
Z	2
ρ_{calc} (gcm^{-3})	1.319
μ(Mo K_α) (mm^{-1})	0.175
F(000) (e)	548
Data collection	
T/K	140
Scan mode	ω
hkl range	-10→11, -13→13, -20→21
Measured refl.	15106
Unique refl., [R_{int}]	6033, [0.0306]
Refl. Used for refinement	6033
Refinement	
Refined parameters	325
R_1, wR_2 [all data]	0.0575, 0.1185
ρ_{fin} (max/min) (e $Å^{-3}$)	0.529/-0.568

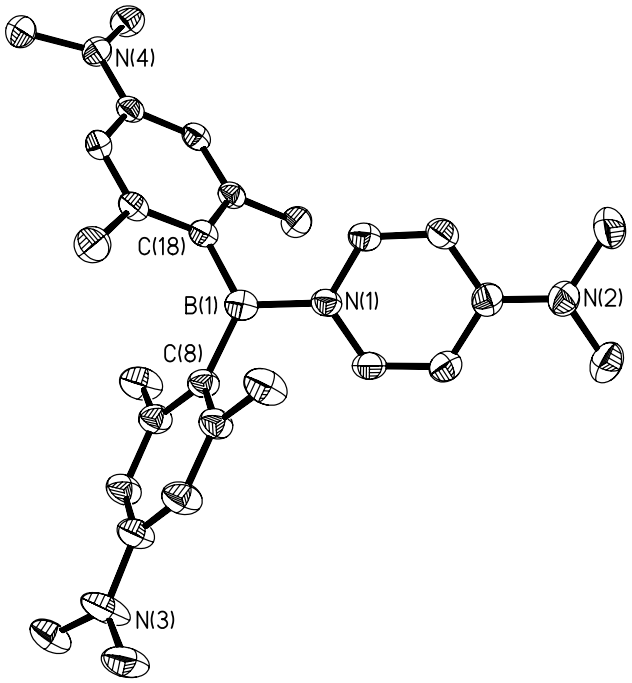

Figure 68: Crystal structure of [**41**]$^+$ with thermal ellipsoids set at the 50% probability level. Hydrogen atoms are omitted for clarity. Selected bond lengths [Å] and bond angles [º]: B(1)-N(1) 1.501(4), B(1)-C(8) 1.550(4), B(1)-C(18) 1.532(4), N(1)-C(1) 1.367(4), N(1)-C(5) 1.358(4), C(1)-C(2) 1.345(4), C(2)-C(3) 1.415(4), C(3)-C(4) 1.417(4), C(4)-C(5) 1.341(4), N(3)-C(11) 1.366(4), N(4)-C(21) 1.363(4), N(1)-B(1)-C(8) 114.7(3), N(1)-B(1)-C(18) 117.5(3), C(8)-B(1)-C(18) 127.8(3), C(3)-N(2)-C(7) 121.7(3), C(3)-N(2)-C(6) 122.2(3), C(7)-N(2)-C(6) 115.2(3), C(11)-N(3)-C(16) 120.5(3), C(11)-N(3)-C(17) 120.5(3), C(16)-N(3)-C(17) 118.8(3), C(21)-N(4)-C(26) 121.3(3), C(21)-N(4)-C(27) 120.9(3), C(26)-N(4)-C(27) 116.0(3).

Table 17: Crystal data and structure refinement for [**41**][OTf]$(OEt_2)_{0.5}$

Crystal data	**[41][OTf]$(OEt_2)_{0.5}$**
Formula	$C_{30}H_{43}BF_3N_4O_{3.5}S$
M_r	615.55
Crystal size (mm^3)	0.22, 0.11, 0.06
Crystal system	Triclinic
Space group	P-1
a (Å)	8.110(3)
b (Å)	13.043(4)
c (Å)	15.489(5)
α (º)	85.454(3)
β (º)	78.149(3)
γ (º)	83.434(4)
V ($Å^3$)	1590.4(9)
Z	2
ρ_{calc} (gcm^{-3})	1.285
μ(Mo K_α) (mm^{-1})	0.158
F(000) (e)	654
Data collection	
T/K	140
Scan mode	ω
hkl range	-9→9, -13→15, -18→18
Measured refl.	11305
Unique refl., [R_{int}]	5861, [0.0295]
Refl. Used for refinement	5861
Refinement	
Refined parameters	380
R_1, wR_2 [all data]	0.0841, 0.1276
ρ_{fin} (max/min) (e $Å^{-3}$)	0.901/-0.748

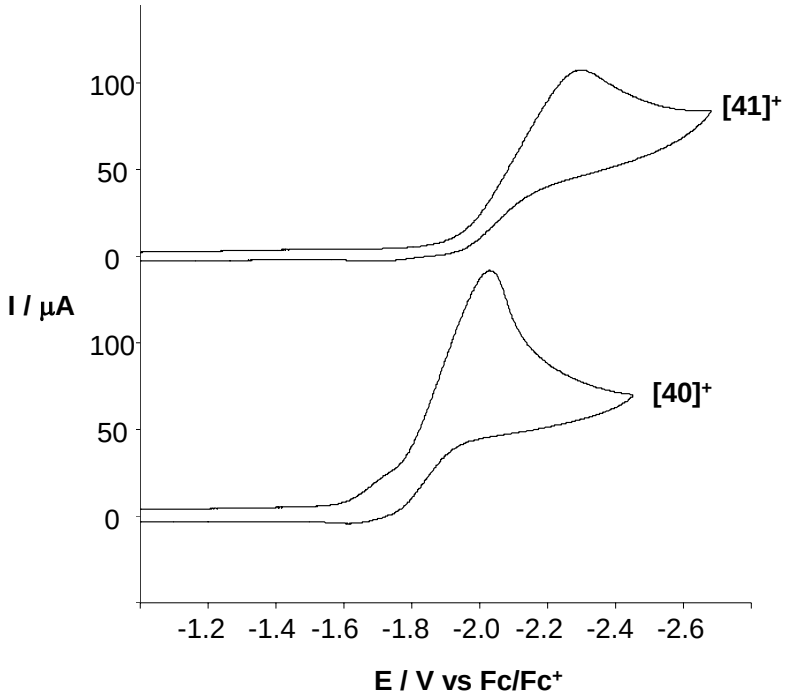

Figure 69: Cyclic voltammograms of [**40**]$^+$ and [**41**]$^+$ in CH_2Cl_2 (7.7 mM for [**40**]$^+$, 7.3 mM for [**41**]$^+$) with a glassy-carbon working electrode (0.1 M nBu$_4$NPF$_6$) at scan rate of 300 mVs^{-1}.

In an attempt to better understand the properties of [**40**]$^+$ and [**41**]$^+$, we have studied their electrochemistry. As indicated by cyclic voltammetry, both [**40**]$^+$ and [**41**]$^+$ undergo an irreversible reduction at E_{peak} -2.03 V and -2.30 V (vs. Fc/Fc$^+$), respectively (Figure 69). Because of their increased electron deficiency, the reduction potential of [**40**]$^+$ and [**41**]$^+$ is more positive than that of neutral boranes, such as Mes$_3$B which is reduced at -2.73 V (vs. Fc/Fc$^+$). It is also important to note that the reduction potential of [**40**]$^+$ is substantially more positive than that of [**41**]$^+$ once again indicating the greater donating ability of the Ar^N ligand. The redox behavior of these derivatives is

different from that of neutral boranes which typically display a reversible one electron reduction wave corresponding to the formation of stable radical anion.[78] Hence, these results indicate that the radical $[Mes_2B\text{-}DMAP]^{\bullet}$ are $[Ar^{N}{}_2B\text{-}DMAP]^{\bullet}$ are not stable. It also suggests that radicals such as $[Mes_2B\text{-pyridine}]^{\bullet}$ whose generation has been attempted[161] might be too unstable to actually observe in solution.[73]

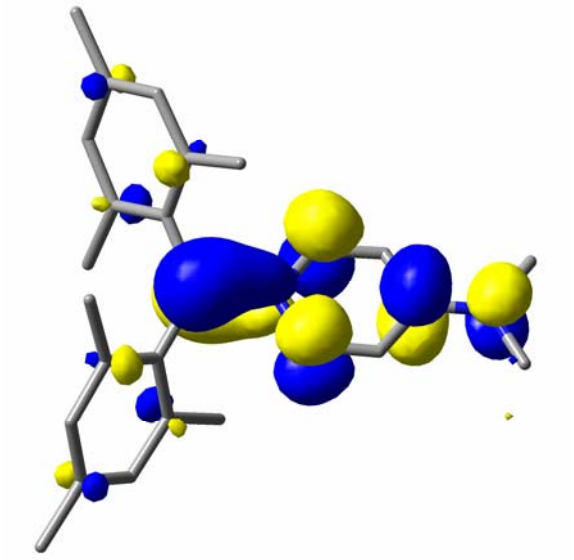

Figure 70: DFT optimized geometry of $[\mathbf{40}]^{+}$ with an overlay of the LUMO (isovalue = 0.03, H-atoms omitted).

A geometry optimization of $[\mathbf{40}]^{+}$ and $[\mathbf{41}]^{+}$ using DFT methods (B3LYP, 6-31G*) affords structures that closely match those observed experimentally. In both cases, the LUMO is localized on the boron atom and DMAP ligand (Figure 70). An evaluation of the orbital energies using the PCM solvation model[162, 163] (solvent = CH_2Cl_2) indicates

that the LUMO of [**40**]$^+$ is 0.37 eV lower than that of [**41**]$^+$. This energy difference is close to the results of our electrochemical measurements (ΔE_{peak}(red) = 0.27 V).

6.3 Conclusion

Two novel diarylborenium cations were prepared in a straightforward synthetic approach and their solid state structures were also determined experimentally. The structural data and electrochemistry results of [**40**]$^+$ and [**41**]$^+$ suggest a stronger π donating ability of Ar^N ligand than mesityl group.

6.4 Experimental section

Electrochemistry: CV measurement of [**40**]$^+$ and [**41**]$^+$ were carried out in a CH_2Cl_2 solution (5 mL) containing (*n*-Bu)$_4$NPF$_6$ (0.1 M) as a support electrolyte and the analyte (7.7 mM for [**40**][OTf], 7.3 mM for [**41**][OTf]). The electrolyte was dried under vacuum prior to use. In all cases, ferrocene was used as an internal standard, and all reduction potentials are reported with respect to the $E_{1/2}$ of the Fc/Fc$^+$ redox couple.

Synthesis of [40][OTf]: Dimesitylboron fluoride (0.60 g, 2.2 mmol), DMAP (0.23 g, 1.9 mmol) and Me_3SiOTf (0.34 mL, 1.9 mmol) were dissolved in 5 mL of chlorobenzene and heated at reflux overnight to give a colorless solution. Upon cooling, compound [**40**][OTf] precipitated and was isolated as a white solid by filtration. It was washed with Et_2O (10 mL) and dried under reduced pressure (0.78 g, yield = 80%). Single crystals were obtained by slow cooling a hot chlorobenzene solution of [**40**][OTf] to -40°C. ^{1}H NMR ($CDCl_3$, 299.91 MHz): δ 2.01 (s, 12H, *ortho*-Me), 2.30

(s, 6H, *para*-Me), 3.43 (s, 6H, DMAP-NMe_2), 6.87 (s, 4H, Mes-CH), 7.00 (d, 2H, $^3J_{H-H}$ = 7.8 Hz, DMAP-CH), 7.87 (d, 2H, $^3J_{H-H}$ = 7.8 Hz, DMAP-CH). ^{13}C NMR ($CDCl_3$, 100.5 MHz): δ 21.3 (*ortho*-Me), 22.5 (*para*-Me), 41.3 (DMAP-NMe_2), 109.2, 122.3, 129.3, 133.2, 142.2, 143.9, 158.1. ^{11}B NMR ($CDCl_3$, 128.2 MHz): δ 64. Anal Calcd for $C_{26}H_{32}BF_3N_2O_3S$: C, 60.01; H, 6.20. Found: C, 59.36; H, 6.16. The sample could be further purified by an additional recrystallization from hot chlorobenzene. Anal Calcd for $C_{26}H_{32}BF_3N_2O_3S$: C, 60.01; H, 6.20. Found: C, 60.16 H, 6.19.

Synthesis of [41][OTf]: $Ar^N{}_2BF$ (0.28 g, 0.85 mmol), DMAP (0.08 g, 0.65 mmol) and Me_3SiOTf (0.11 mL, 0.61 mmol) were dissolved in 5 mL of chlorobenzene and heated at reflux overnight to give an orange solution. After cooling to room temperature, addition of Et_2O (20 mL) resulted in the precipitation of [**41**][OTf] as an orange solid which was isolated by filtration. It was washed with Et_2O (10 mL) and dried under reduced pressure (0.24 g, yield = 69%). Single crystals were obtained by vapor diffusion of Et_2O into a $CHCl_3$ solution of the [**41**][OTf]. ^1H NMR ($CDCl_3$, 399.59 MHz): δ 1.94 (s, 12H, *ortho*-Me), 2.98 (s, 12H, Ar^N-NMe_2), 3.36 (s, 6H, DMAP-NMe_2), 6.32 (s, 4H, Ar^N-CH), 6.91 (d, 2H, $^3J_{H-H}$ = 8.0 Hz, DMAP-CH), 7.89 (d, 2H, $^3J_{H-H}$ = 8.0 Hz, DMAP-CH). ^{13}C NMR ($CDCl_3$, 100.5 MHz): δ 23.4 (*ortho*-Me), 39.8 (Ar^N-NMe_2), 40.9 (DMAP-NMe_2), 108.5, 111.7, 144.3, 152.4, 157.9. ^{11}B NMR ($CDCl_3$, 128.2 MHz): δ 62. Anal Calcd for $C_{28}H_{38}BF_3N_4O_3S$: C, 58.13; H, 6.62. Found: C, 57.60; H, 6.56.

CHAPTER VII

CHARACTERIZATION AND REACTIONS OF A α-SILYLATED CARBOCATION

7.1 Introduction

Carbocations can be efficiently stabilized by β-silyl groups. This stabilization results from a hyperconjugative effect involving the β C-Si bonding electron pair and the empty p-orbital of the carbocationic center (Figure 71). A different situation arises when the silyl group is positioned α from the carbocation. In this case, it has been argued that the effect is destabilizing. This conclusion is based on the observed the low reactivity of the α-silylmethyl halide in SN_1 reactions.[164-166] Moreover, α-silyl carbocation show a tendency to undergo 1,2–alkyl or hydrogen migration to generate β-silyl carbocation,[167, 168] once again reinforcing their inherent instability. On the other hand, theoretical investigation shows that the α-silyl groups may be able to stabilize carbocations through inductive effect.[169]

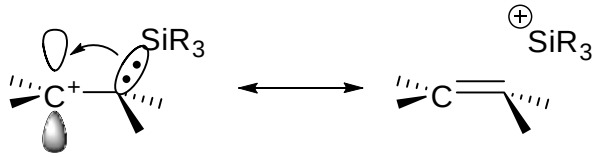

Figure 71: Hyperconjugation in β-silyl carbocation.

Hoping to clarify this apparent paradox, a number of groups have investigated the syntheses of α-silyl carbocations. Olah and co-workers showed that the α-silyl carbocation [**42**]$^+$ can be generated under super acidic conditions by de-hydroxylation of the corresponding alcohols.[170] Unfortunately, this α-silyl carbocation is not stable at ambient temperature. When the temperature is higher than 0ºC, the counter anion attacks the silicon center and triggers a concerted methyl migration from the silicon to the carbocationic center (Figure 72).

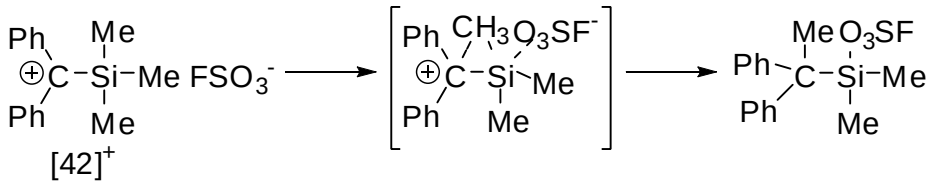

Figure 72: Methyl migration of [**42**]$^+$.

The first structurally characterized α-silylated carbocation ion is a silyl substituted aromatic cation ([**43**]$^+$, Figure 73), in which the trimethylsilyl group is attached to a cyclopropenylium.[171, 172] Theoretical calculation of the molecule shows that the center ring is no longer positive because the silyl group acts as a σ-donor which stabilizes the carbocation..[172]

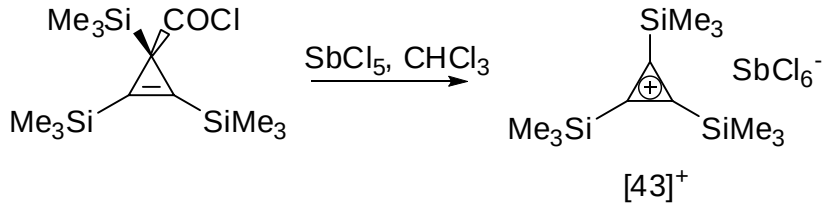

Figure 73: Synthesis of [**43**]$^{+}$.

Another recent example of a structurally characterized α-silylated carbocation [**44**]$^{+}$ was reported by Niecke and co-workers.[173] In this case, the carbocation was synthesized by protonation of the corresponding 1,3-diphosphacyclobutane-2,4-diyl at the 4 position as shown in Figure 74. DFT calculation of the molecule reveals that the stabilizing interaction between the phosphorus lone-pairs and the empty p-orbital of the carbocation plays an important stabilizing role.

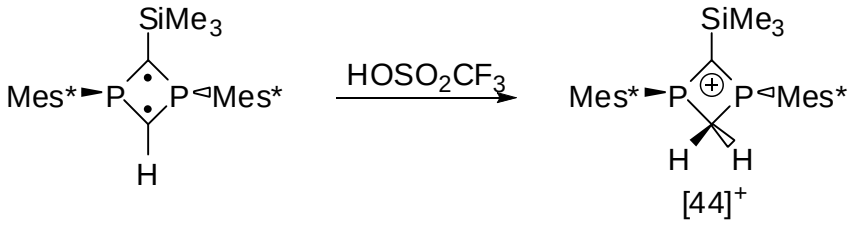

Figure 74: Synthesis of [**44**]$^{+}$.

As part of our contribution to the chemistry of α-silylated carbocation, we decided to synthesize the 9-silyl-*N*-methylacridinium ion and study its properties.

7.2 Synthesis of 9-trimethylsilyl *N*-methylacridinium

Examination of the literature indicates that 9-trimethylsilyl-*N*-methylacridinium was reported in 2004 as an intermediate for the synthesis of *N*-methyl acridone.[174] In the reported procedure, 9,10-dihydroacridine was treated with LDA followed by Me_3SiCl to afford 9-TMS-acridan which was then oxidized with DDQ to give 9-TMS-acridine, the precursor of 9-TMS-acridinium. Since this approach is complicated, we decided to use an alternative method developed by our group.[175] The reaction between 9-lithoacridine and Me_3SiCl followed by methylation with methyl triflate leads to the formation of [**45**][OTf] in good yield (Figure 75).

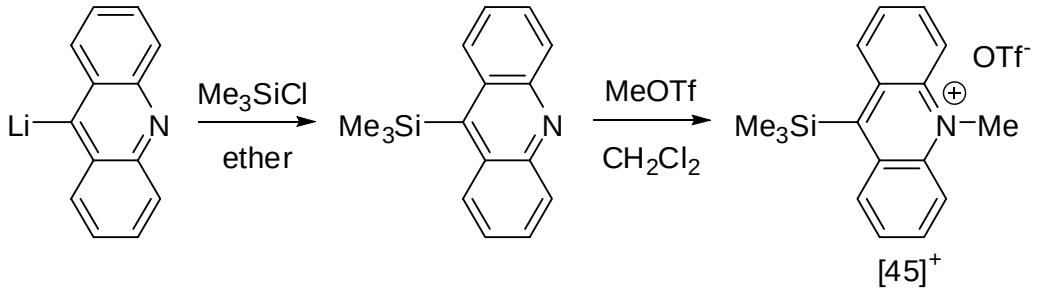

Figure 75: Synthesis of [**45**]$^+$.

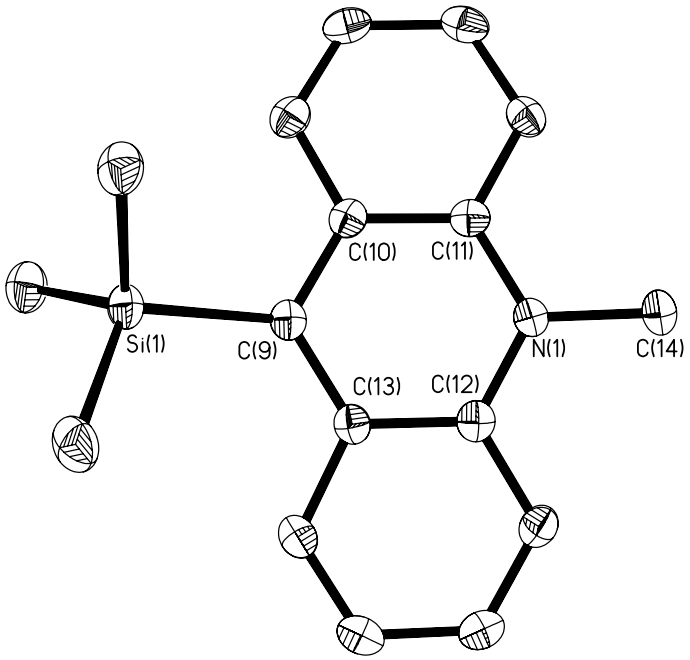

Figure 76: Crystal structure of [**45**]$^+$ with thermal ellipsoids set at the 50% probability level. Hydrogen atoms are omitted for clarity. Selected bond lengths [Å] and bond angles [º]: Si(1)-C(9) 1.937(2), Si(1)-C(15) 1.864(2), Si(1)-C(16) 1.869(2), Si(1)-C(17) 1.860(2), C(9)-C(10) 1.415(3), C(9)-C(13) 1.402(3), N(1)-C(11) 1.368(3), N(1)-C(12) 1.360(3), N(1)-C(14) 1.473(3), Si(1)-C(9)-C(13) 123.62(15), Si(1)-C(9)-C(10)118.66(15), C(10)-C(9)-C(13) 117.09(18), C(11)-N(1)-C(12) 121.08(18), C(11)-N(1)-C(14) 118.96(17), C(12)-N(1)-C(14) 119.95(17).

Table 18: Crystal data and structure refinement for [**45**]$^{+}$[OTf]$^{-}$

Crystal data	[**45**]$^{+}$[OTf]$^{-}$
Formula	$C_{18}H_{20}F_3NO_3SSi$
M_r	415.50
Crystal size (mm^3)	0.47 x 0.12 x 0.08
Crystal system	monoclinic
Space group	P2(1)/n
a (Å)	8.4651(13)
b (Å)	16.248(3)
c (Å)	13.513(2)
α (º)	90.00
β (º)	90.711(2)
γ (º)	90.00
V ($Å^3$)	1858.4(5)
Z	4
ρ_{calc} (gcm^{-3})	1.485
μ(Mo K_α) (mm-1)	0.287
F(000) (e)	864
Data collection	
T/K	140
Scan mode	ω
hkl range	-10→10, -21→20, -17→17
Measured refl.	15791
Unique refl., [R_{int}]	4393, [0.0615]
Refl. Used for refinement	4393
Refinement	
Refined parameters	244
R_1, wR_2 [all data]	0.0629, 0.1519
ρ_{fin} (max/min) (e $Å^{-3}$)	0.504/-0.419

The ^{13}C NMR resonance of the methylium center appears at 173 ppm, a chemical shift which is very close to that of $(Me_2NC_6H_4)_3C^+$ (178 ppm). The ^{29}Si NMR signal appears at -3.2 ppm and is comparable to that reported for [**44**]$^+$ (-3.6 ppm)[173]. Both of the ^{13}C and ^{29}Si NMR measurements support formulation of [**45**]$^+$ as an α-silylated carbocation.

Single crystals of [**45**]$^+$ were obtained by vapor diffusion of ether into a CH_2Cl_2 solution of the salt (Figure 76, Table 18). These yellow crystals belong to the monoclinic P2(1)/n space group. According to the single crystal X-ray diffraction analysis, the closest cation anion distance is equal to 3.3 Å. It involves an oxygen atom of the triflate anion and a *N*-Methyl carbon atom and is much too long to correspond to a C-H···O hydrogen bond. Although the C(9) and N(1) atoms adopt a trigonal planar geometry ($\Sigma_{(C\text{-}C\text{-}C)}C(9) = 359.8°$; $\Sigma_{(C\text{-}N\text{-}C)}N(1) = 360.0°$), the central ring of the acridinyl moiety is distorted. In particular, the C(9) and N(1) atoms depart from the plane defined by C(10)-C(11)-C(12)-C(13) by 0.15 Å and 0.11 Å, respectively. As a result of this deformation, the central ring of acridinyl moiety adopts a bent conformation with a dihedral angle of 15.5˚ between the two phenyl rings.

It is also worth noting that the Si(1)-C(9) bond distance of 1.937 Å is longer than that observed in tris-9-anthrylsilane derivatives (1.88 ~ 1.91Å).[176] Elongation of this bond may result from the electrostatic repulsions occurring between the electropositive silicon atom and the cationic carbon atom. It could also be argued that this molecule is better described as a silylium ion stabilized by a remote *N*-heterocyclic carbene ligand (*r*NHC) (Figure 77), in this case an *N*-methylacridin-9-ylidene ligand. [149, 150]

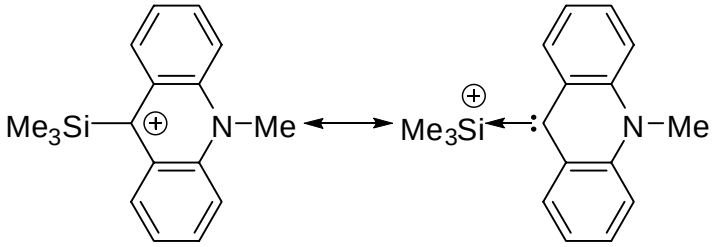

Figure 77: Two resonance structures of [**45**]$^{+}$.

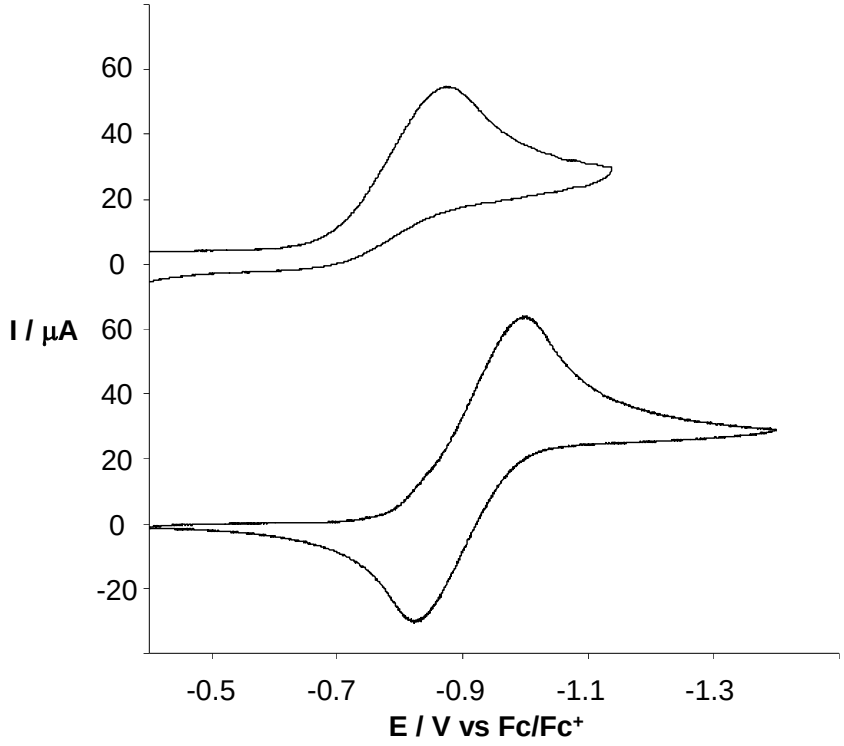

Figure 78: Cyclic voltammogram of [**45**]OTf and [**46**]OTf in CH_2Cl_2 with a glassy carbon working electrode: scan rate 100 mV/sec, 0.1 M NBu_4PF_6.

Since the Me_3Si group is isolobal to a hydrogen atom, we decided to investigate whether $[\mathbf{45}]^+$ would behave like 10-methylacridinium triflate, $[\mathbf{46}]^+$, in reduction reactions. As shown by cyclic voltammetry carried out under identical conditions, both $[\mathbf{45}]^+$ and $[\mathbf{46}]^+$ are reduced at similar potential; -0.91 V and -0.89 V for $[\mathbf{45}]^+$ and $[\mathbf{46}]^+$, respectively (Figure 78). This observation suggests that the Me_3Si group does not have a significant effect on the stability of the acridinium moiety. This can be explained by the fact that the electronegativity of a Me_3Si group (2.25)[177] is close to that of a hydrogen atom (2.2). However, only the reduction of $[\mathbf{45}]^+$ is reversible. The

irreversibility of the reduction wave of [**46**]$^+$ results from a homo-coupling reaction involving two acridinyl radicals.[178] These observations suggest that the Me_3Si group stabilizes the acridinyl radical in a kinetic rather than electronic fashion. Encouraged by the reversible reduction behavior of [**45**]$^+$, we decided to isolate the neutral radical.

The chemical reduction of [**45**]$^+$ is carried out in acetonitrile with Mg as the reducing agent (Figure 79). This neutral radical **45**$^\bullet$ formed in the reaction can be extracted with hexane.

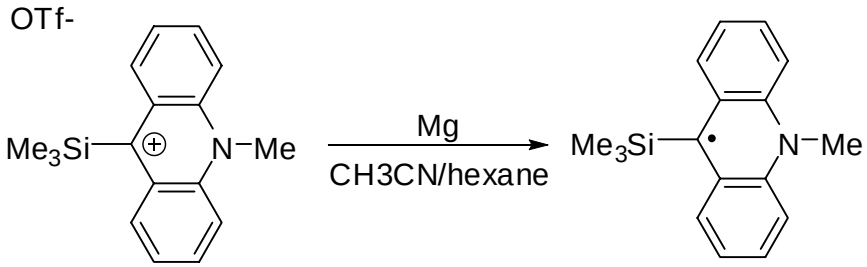

Figure 79: Formation of **45**$^\bullet$.

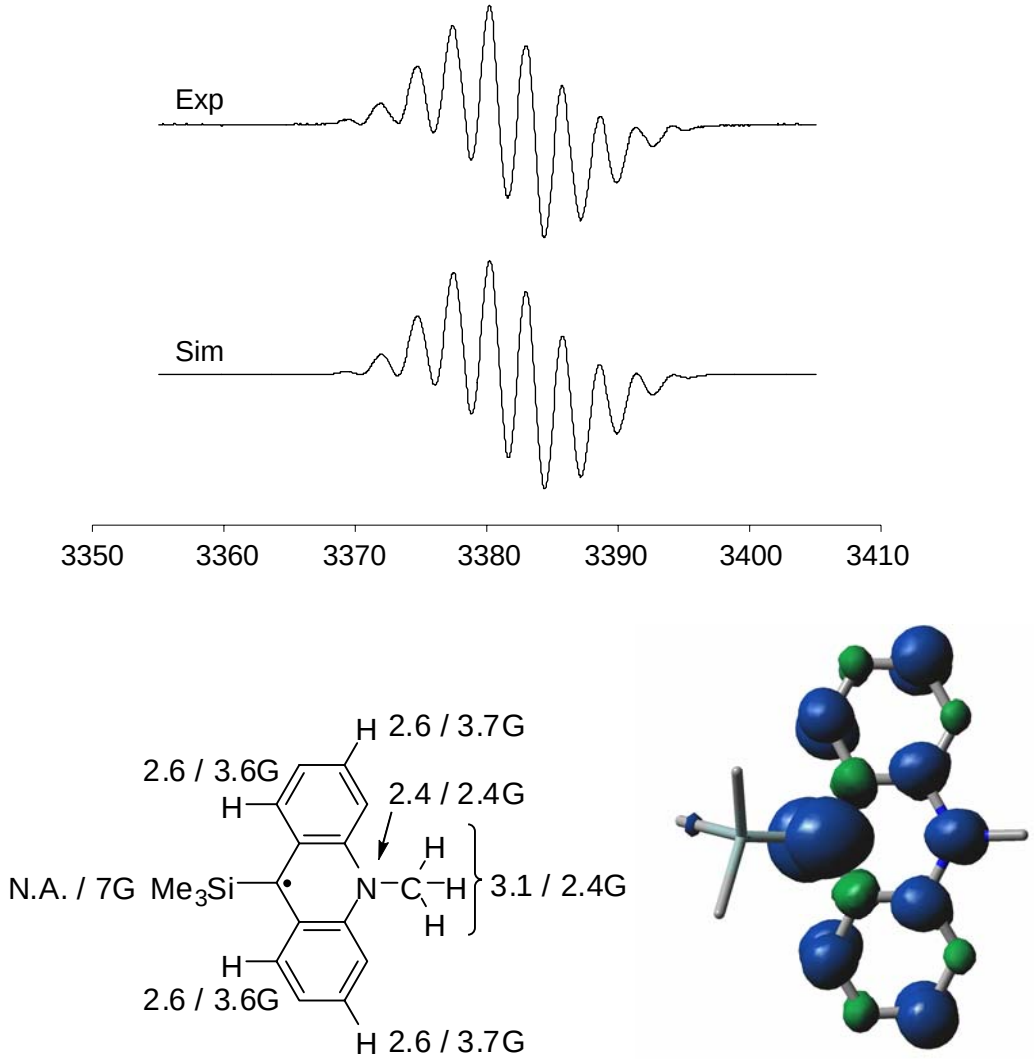

Figure 80: Top: the EPR spectrum of **45**$^{\bullet}$ in hexane at room temperature and the simulated EPR spectrum. Bottom Left: the hyperfine coupling constant used for simulation and the Fermi contact coupling constant calculated using DFT method. Bottom Right: optimized geometry of **45**$^{\bullet}$ with an overlay of the computed spin density (isovalue = 0.0025).

The room temperature EPR spectrum of the radical exhibits a g value of 2.0014 as expected for a free radical. The EPR spectrum can be simulated based on the hyperfine coupling constant listed in Figure 80. Although the DFT computation of the isotropic Fermi contact coupling shows that the unpaired electron is coupled to Si with 7 Gauss, the low abundance of ^{29}Si isotope precludes the observation of the ^{29}Si hyperfine coupling experimentally. Furthermore, the computed spin density of **45**$^{\bullet}$ also shows a low spin density over the silicon atom, re-emphasizing that the Me_3Si group does not participate in stabilizing the radical via electronic effects.

7.3 Reactivity

Since the methylium center is the most electrophilic site in [**45**]$^+$, nucleophilic attacks are expected to occur at the C(9) atom. Upon treatment of [**45**]OTf with $NaBH_4$ in acetonitrile, [**45**]$^+$ is reduced to afford the acridan molecule **47** in almost quantitative yield. The overall upfield shift of the resonances observed in the ^{1}H NMR spectrum of **47** when compared to [**45**]$^+$ is consistent with the formation of a neutral molecule. The ^{1}H NMR resonance of the triarylmethyl hydrogen is detected at 3.36 ppm as a sharp singlet. In addition to the hydride reduction, [**45**]$^+$ can be hydrolyzed under basic condition to give the corresponding alcohol molecule **48** (Figure 81). These two reactions indicate the C(9) atom of the acridinium moiety in [**45**]$^+$ possesses carbocationic character, thus supporting the formulation of [**45**]$^+$ as an α-silylated carbocation.

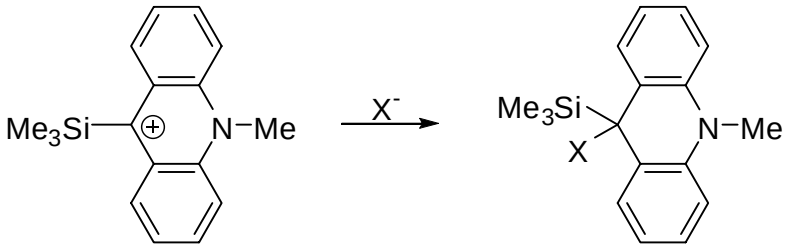

Figure 81: Hydride reduction and hydrolysis reaction of [**45**]$^+$.

Since the silicon is known to be fluorophilic, several silyl-containing derivatives have been investigated for fluoride complexation.[35, 179-181] Encouraged by these precedents, we decided to test the reactivity of [**45**]$^+$ with fluoride anions. Although [**45**]$^+$ hydrolyzed in water overnight, the reaction between [**45**]OTf and KF in aqueous solution at pH 7 is relatively fast. Indeed, in the presence of an excess of KF, solutions of [**45**]$^+$ lose their characteristic yellow color to afford a white cloudy solution within minutes. Isolation of the product of this reaction and analysis by multinuclear NMR indicated formation of the fluorosilane **49**. The overall upfield shift of the resonances observed in the ^{1}H NMR spectrum of **49** when compared to [**45**]$^+$ is consistent with the formation of a neutral molecule. The ^{1}H resonance of the methyl group on the former methylium carbon is observed at 1.84 ppm. The methyl group on the silicon appeared as a doublet at -0.06 ppm with $^3J_{H-F}$ = 7.4 Hz. Accordingly, the ^{19}F resonance of **49** is detected as a septuplet at -167.7 ppm indicating coupling to six methyl hydrogen atoms. The ^{29}Si NMR signal, which appears as a doublet at 21.3 ppm ($^1J_{Si-F}$ = 298.7 Hz), is comparable to that of other $ArMe_2SiF$ derivatives.[182, 183] A similar methyl migration

has been observed by Olah in the case of [**42**]$^{+}$.[170] Mechanistically, we propose that fluoride attack at the silicon atom induces a concerted methyl migration from the silicon to adjacent electrophilic methylium center (Figure 82).

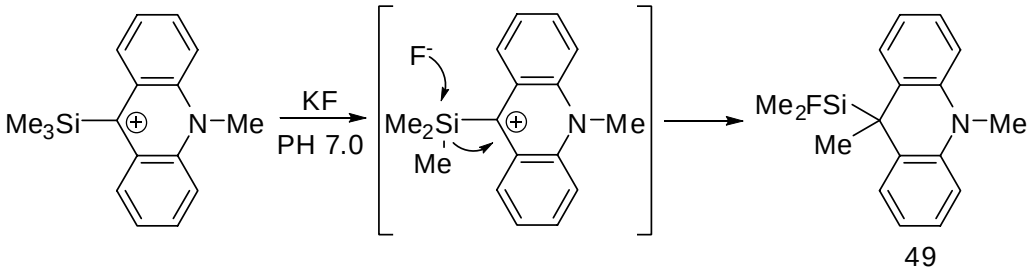

Figure 82: Fluoride induced methyl migration reaction.

Since the fluoride induced methyl migration leads to a loss of aromaticity in the central ring of acridinyl moiety, this reaction is accompanied by a major perturbation of the photophysical properties of the molecule As a result, the absorption band of [**45**]$^{+}$ observed at 435 nm progressively disappears upon addition of fluoride. Thus [**45**]$^{+}$ can be considered as a colorimetric fluoride probe. Unfortunately, the stability of [**45**]$^{+}$ in water at neutral pH is not sufficient to allow for practical applications.

7.4 Conclusion

According to NMR spectroscopy, electrochemistry, and reactivity studies, [**45**]$^{+}$ is indeed an α-silylated carbocation, in which the Me_3Si group plays an important role in kinetically stabilizing the cation. The structural analysis of [**45**]$^{+}$ reveals an alternative description of [**45**]$^{+}$ as a remote *N*-heterocyclic carbene stabilized silylium ion. By

placing the fluorophilic silyl group adjacent to an electrophilic carbocation, a novel fluoride sensor is obtained. Sensing occurs via a fluoride induced methyl migration which is unprecedented. Another attractive feature is the fact that this reaction occurs in water at pH 7. As a result of its strong fluoride affinity, [**45**]$^{+}$ is able to react with KF at pH 7.0 in aqueous media.

7.4 Experimental section

Synthesis of [**45**][OTf]**:** The 9-bromoacridine (1g, 4 mmol) was suspended in 50 ml of ether and cooled to -78°C, followed with the slow addition of 2.85 M of n-BuLi (1.4 ml, 4 mmol). After stirring at -78ºC for 30 minutes, the trimethylchlorosilane (0.8 ml, 6 mmol) was added. The reaction mixture was allowed to warm up to room temperature and stir for overnight. The opaque beige solution was quenched with water, and extracted with ether. The combined organic solution was washed with brine and dried over $MgSO_4$. The solvent were removed under reduced pressure and trimethylsilylacridine was obtained as brown oil, which was converted into the acridinium salt without further purification. The large excess of methyl triflate was added into the CH_2Cl_2 solution of trimethylsilylacridine in glove box and allowed to stir for 1 hour. Addition of ether into the reaction mixture results in the precipitation of [**45**][OTf] as yellow solids (0.96g, yield = 58%). Single crystals of [**45**][OTf] for X-ray structural analysis were obtained by diffusion of ether into a CH_2Cl_2 solution of the salt. ^{1}H NMR (CD_3CN, 400 MHz): 0.78 (s, 9H, $SiMe_3$), 4.75 (s, 3H, NMe), 7.93 (ddd, 2H, $^{3}J_{H\text{-}H}$ = 8.8 Hz, $^{3}J_{H\text{-}H}$ = 6.7 Hz, $^{4}J_{H\text{-}H}$ = 1.1 Hz), 8.32(ddd, 2H, $3J_{H\text{-}H}$ = 9.3 Hz, $^{3}J_{H\text{-}H}$ = 6.7

Hz, $^4J_{H-H}$ = 1.4 Hz), 8.53 (dd, $^3J_{H-H}$ = 9.3 Hz, $^4J_{H-H}$ = 1.1 Hz), 8.79 (dd, $^3J_{H-H}$ = 8.8 Hz, $^4J_{H-H}$ = 1.4 Hz). ^{13}C NMR (CD_3CN, 125.7 MHz): δ 3.6 ($SiMe_3$), 40.3 (NMe), 119.7, 127.8, 132.3, 133.0, 139.0, 140.2, 172.8. ^{29}Si NMR (CD_3CN, 128.2 MHz): δ -3.2.

Synthesis of 47: [**45**][OTf] was dissolved in 5 ml of CH_3CN and allowed to react with $NaBH_4$ for 10 minutes. After reaction, solvent was removed under vacuum and the solid was extracted with ether. The **47** was isolated as white powder after removing solvent. ^{1}H NMR ($CDCl_3$, 400 MHz): -0.12 (s, 9H, $SiMe_3$), 3.21 (s, 3H, NMe), 3.36 (s, 1H), 6.71 (d, 2H, $^3J_{H-H}$ = 8 Hz), 6.8 ~ 6.9 (m, 4H), 7.06 (m, 2H). ^{13}C NMR ($CDCl_3$, 100.5 MHz): δ -3.1 ($SiMe_3$), 32.8 (NMe), 39.1, 111.6, 120.5, 125.5, 126.6, 127.4, 142.6.

Synthesis of 49: The excess of TBAF was added to the $CHCl_3$ solution of [**45**][OTf] (0.05g, 0.12 mmol), and stirred for 30 minutes. After reaction, solvent was removed under vacuum and the solid was extracted with ether. The **49** was obtained as white powder after removing solvent (0.03g, yield = 87%). ^{1}H NMR ($CDCl_3$, 400 MHz): δ -0.06 (d, 6H, $SiFMe_2$, $^3J_{H-F}$ = 7.5 Hz), 1.84 (s, 3H, $^4J_{H-F}$ = 1.2 Hz), 3.27 (s, NMe), 6.75 (dd, 2H, $^3J_{H-H}$ = 8 Hz, $^4J_{H-H}$ = 1.1 Hz), 6.93 (t, $^3J_{H-H}$ = 8 Hz) 7.11 ~ 7.21 (m, 4H). ^{19}F NMR ($CDCl_3$, 375.95 MHz): δ -167.7 (septets, $^3J_{H-F}$ = 7.4 Hz). ^{29}Si NMR ($CDCl_3$, 128.2 MHz): δ 21.3.

CHAPTER VIII

SYNTHESIS AND CHARACTERIZATION OF A CARBODICATION

8.1 Introduction

Due to their electron deficient nature, carbocations are typically unstable and can only be observed in super acidic media or as a transient species. The isolation of carbocation usually requires the use π-donating and/or sterically protecting substituents. Triarylmethylium cation is the classical example of such stable carbocation derivative which has been used as Lewis acid activator in olefin polymerization.

Recent progress in this area of research have focused on the preparation and study of bifunctional dication.[184-187] Owing to the rich coordination chemistry of bi-dentate Lewis acid synthesized on the *peri*-position of naphthalene, chemists have devoted a great deal of efforts to the preparation of 1,8-(bismethylium)naphthalenediyl dications.[188-190] These 1,8-bis(methylium)naphthalenediyl dications undergo a two electron reduction to form a C-C σ-bond between the former methylium centers. The reduced product can be re-oxidized back to the corresponding dication chemically or electrochemically. The anion binding properties of these dications has also been studied.[43, 49, 104] For example, the dication $[\mathbf{50}]^{2+}$ reacts with fluoride to afford $[\mathbf{50\text{-}F}]^{+}$, in which the fluoride oscillates between the two methylium centers (Figure 83).[191] Similar phenomenon was observed in $[\mathbf{51\text{-}H}]^{+}$ that features an unusual $[CHC]^{+}$ three center two electron linkage.[192]

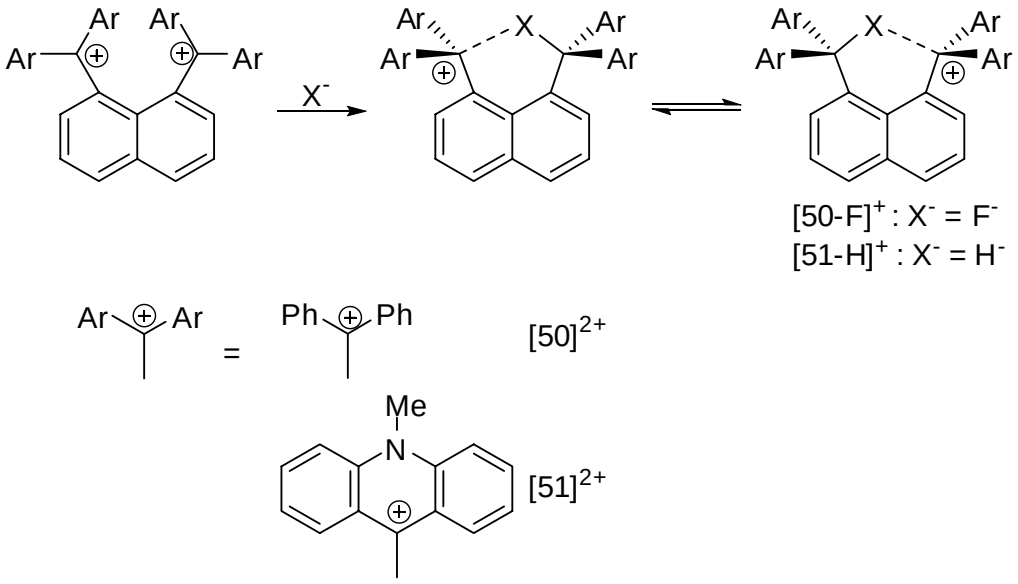

Figure 83: Fluoride and hydride complexation of carbodications.

Encouraged by these results, we decided to synthesize and investigate the electrochemistry of bis-methylium dications that feature a different molecular linker, namely the dimethylsilyl group ($SiMe_2$).

8.2 Synthesis of dication

The synthesis of the target carbodication was straight forward (Figure 84). 9-Lithioacridine was allowed to react with half an equivalent of Me_2SiCl_2 to yield dimethyl-bis(9-acridinyl)silane (**52**), which could be methylated with MeOTf to afford the corresponding dication [**53**]$^{2+}$ as an air- and moisture-stable triflate salt.

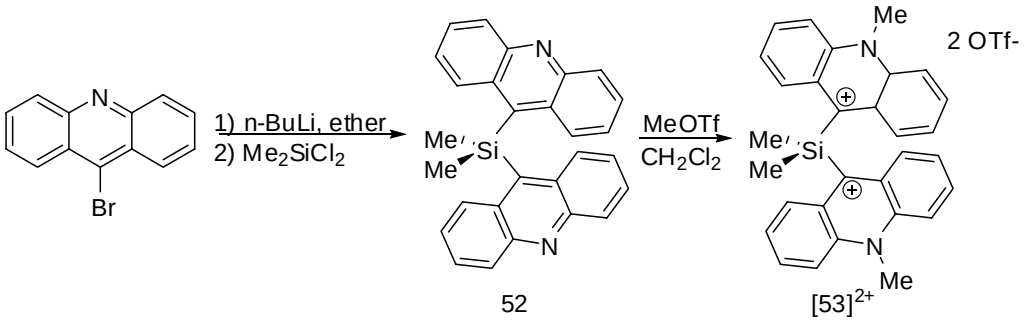

Figure 84: Synthesis of [**53**]$^{2+}$.

Both **52** and [**53**]$^{2+}$ have been fully characterized. The ^{1}H NMR spectra of both compounds exhibit four acridinyl aromatic CH resonances suggesting a free rotation about the Si-C_{ipso} bonds. The ^{1}H resonance of the NMe hydrogen of [**53**]$^{2+}$ observed at 4.8 ppm is typical for *N*-methylacridinium derivatives. The ^{13}C resonance of the methylium carbon atoms in [**53**]$^{2+}$ detected at 167 ppm is comparable to the value observed in [**45**]$^{+}$. In addition, the increased electron deficiency of the silicon atom is reflected by the ^{29}Si NMR resonance of [**53**]$^{2+}$ observed at -0.1 ppm, 12 ppm downfield shifted from that of **52**.

Upon slow cooling of a hexane/ethyl acetate solution of **52**, single crystals of **52** were obtained and analyzed by single crystal X-ray diffractometer. Compound **52** crystallizes in the monoclinic *P*2(1)/c space group with four molecules in the unit cell (Table 19). As shown in Figure 85, both acridinyl rings remain approximately planar, and the bond distances and bond angles within the acridinyl moiety are unremarkable. The Si-C_{ipso} bond distance of 1.904(4) Å and 1.910(4) Å for Si(1)-C(9) and Si(1)-C(23), respectively, are comparable to that in bulky aryl silanes.[176]

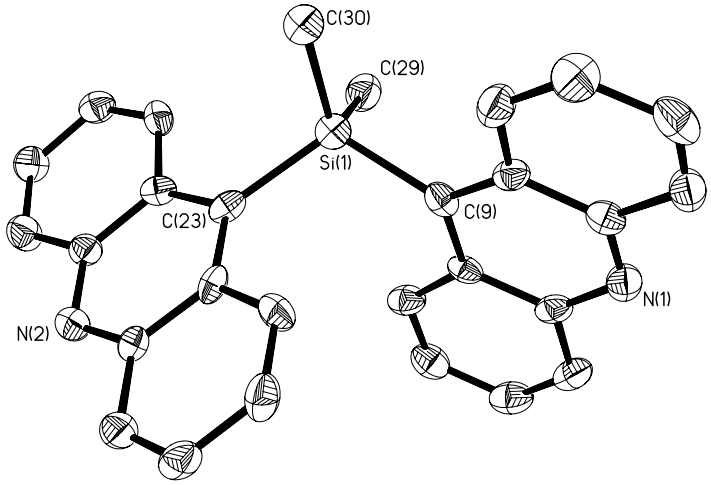

Figure 85: Crystal structure of **52** with thermal ellipsoids set at the 50% probability level. Hydrogen atoms are omitted for clarity. Selected bond lengths [Å] and bond angles [º]: Si(1)-C(9) 1.910(4), Si(1)-C(23) 1.904(4), Si(1)-C(29) 1.865(4), Si(1)-C(30) 1.844(4), C(9)-C(10) 1.417(6), C(9)-C(13) 1.413(6), C(23)-C(24) 1.417(5), C(23)-C(27) 1.417(6), C(9)-Si(1)-C(23) 111.2(2), C(9)-Si(1)-C(29) 101.12(19), C(9)-Si(1)-C(30) 117.7(2), Si(1)-C(9)-C(10) 124.8(4), Si(1)-C(9)-C(13) 118.4(4), C(10)-C(9)-C(13) 116.2(4), Si(1)-C(23)-C(24) 123.0(4), Si(1)-C(23)-C(27) 121.5(4), C(27)-C(23)-C(24) 115.5(4).

Table 19: Crystal data and structure refinement for **52**

Crystal data	**52**
Formula	$C_{28}H_{22}N_2Si$
M_r	414.57
Crystal size (mm^3)	0.12, 0.11 0.1
Crystal system	Monoclinic
Space group	P2(1)/c
a (Å)	7.4462(15)
b (Å)	19.490(4)
c (Å)	14.628(3)
α (º)	90.00
β (º)	97.817(2)
γ (º)	90.00
V ($Å^3$)	2103.1(7)
Z	4
ρ_{calc} (gcm^{-3})	1.309
μ(Mo K_α) (mm-1)	0.130
F(000) (e)	872
Data collection	
T/K	110
Scan mode	ω
hkl range	-6→6,-16→16, -12→12
Measured refl.	9104
Unique refl., [R_{int}]	1382, [0.0455]
Refl. Used for refinement	1382
Refinement	
Refined parameters	280
R_1, wR_2 [all data]	0.0438, 0.1239
ρ_{fin} (max/min) (e $Å^{-3}$)	0.338, -0.326

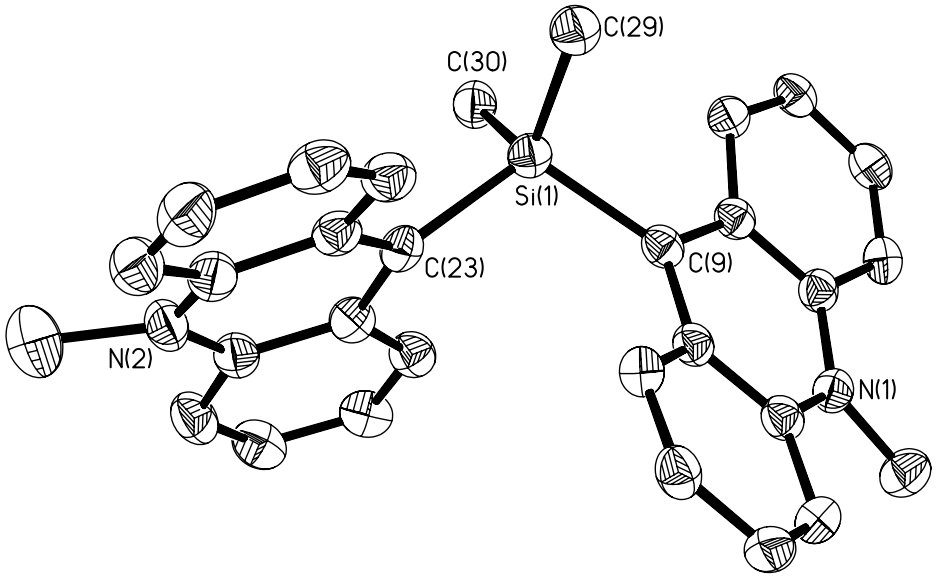

Figure 86: Crystal structure of [**53**]$^{2+}$ with thermal ellipsoids set at the 50% probability level. Hydrogen atoms are omitted for clarity. Selected bond lengths [Å] and bond angles [º]: Si(1)-C(9) 1.924(5), Si(1)-C(23) 1.939(5), Si(1)-C(29) 1.847(5), Si(1)-C(30) 1.872(5), C(9)-C(10) 1.421(6), C(9)-C(13) 1.416(6), C(23)-C(24) 1.418(6), C(23)-C(27) 1.423(7), C(9)-Si(1)-C(23) 111.0(2), C(9)-Si(1)-C(29) 106.2(2), C(9)-Si(1)-C(30) 111.8(2), Si(1)-C(9)-C(10) 122.4(3), Si(1)-C(9)-C(13) 120.8(3), C(10)-C(9)-C(13) 116.7(4), Si(1)-C(23)-C(24) 124.6(3), Si(1)-C(23)-C(27) 117.2(3), C(27)-C(23)-C(24) 117.0(4).

Table 20: Crystal data and structure refinement for [**53**][OTf]$_2$

Crystal data	[**53**][OTf]$_2$
Formula	$C_{32}H_{28}F_6N_2O_6S_2Si$
M_r	742.77
Crystal size (mm^3)	0.35, 0.24, 0.13
Crystal system	Triclinic
Space group	P-1
a (Å)	8.9496(18)
b (Å)	13.630(3)
c (Å)	13.920(3)
α (º)	105.33(3)
β (º)	93.11(3)
γ (º)	106.70(3)
V (Å^3)	1552.9(5)
Z	2
ρ_{calc} (gcm^{-3})	1.589
μ(Mo K$_\alpha$) (mm-1)	0.297
F(000) (e)	764
Data collection	
T/K	110
Scan mode	ω
hkl range	-10→9, -13→15, -15→15
Measured refl.	7100
Unique refl., [R_{int}]	4754, [0.0141]
Refl. Used for refinement	4754
Refinement	
Refined parameters	442
R_1, wR_2 [all data]	0.0917, 0.1653
ρ_{fin} (max/min) (e Å^{-3})	0.776, -0.732

Single crystals of [**53**][OTf]$_2$ were obtained from vapor diffusion of diethyl ether into an acetonitrile solution of the salt and the structure of [**53**][OTf]$_2$ has been determined experimentally as well. The crystal of [**53**][OTf]$_2$ belongs to the triclinic *P*-1 space group with two molecules in the unit cell (Figure 86, Table 20). The two triflate anions in the asymmetric unit show no significant interaction with the silicon atom or the acridinyl moieties. Although the methylium carbon atoms and the nitrogen atoms of the acridinyl ring remain in a trigonal planar geometry, both acridine rings are bent about the central ring with a folding angle of 14.9° and 17.7°. The puckering of the central C_5N ring of acridinyl moieties upon methylation is also observed. This puckering is reflected by the displacement of the methylium carbon atoms and nitrogen atoms above the plane containing C(10)-C(11)-C(12)-C(13) atoms or C(24)-C(25)-C(26)-C(27) atoms (displacement for C(9) : 0.13 Å; for C(23): 0.14 Å; for N(1): 0.13 Å; for N(2): 0.13 Å). Moreover, as the result of the Coulombic repulsion between the positive moieties, the Si(1)-C(9) (Å) and Si(1)-C(23) (Å) bond in [**53**]$^{2+}$ are noticeably longer than that in **52** (Si(1)-C(9) 1.910(4) Å; Si(1)-C(23) 1.904(4) Å), and the distance between two methylium centers are also changed from 3.14 Å in **52** to 3.18 Å in [**53**]$^{2+}$. These metrical parameters indicate that the steric repulsion within [**53**]$^{2+}$ is smaller than that in **52** as the result of longer Si-C bond distance and greater separation between two aromatic groups. Thus, the change of electronic property of the acridinyl moiety upon methylation should be responsible for loss of planarity of the acridinyl groups. Dication [**53**]$^{2+}$ can also be described as a dimethylsilyl dication (Me_2Si^{2+}) stabilized by two *N*-methylacridin-9-ylidene carbene ligands. Such a description has

been adopted for a number of palladium complexes that also feature a *N*-methylacridinium functionality.[149, 150, 193] Therefore, the two extreme bonding descriptions of [**53**]$^{2+}$ depicted in Figure 87 can be considered.

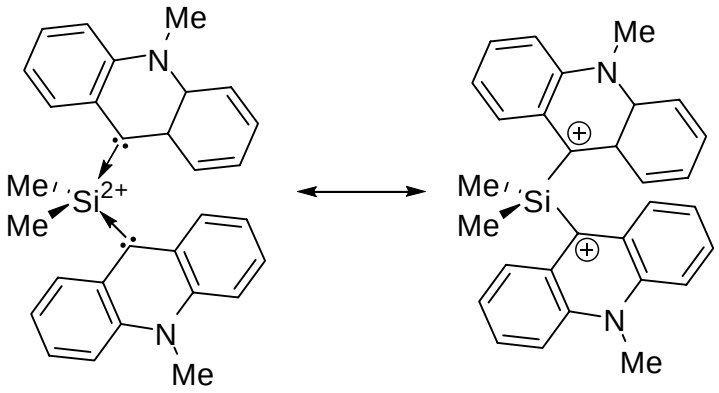

Figure 87: Silylium dication vs. carbodication.

In order to better appreciate the nature of [**53**]$^{2+}$ and the origin of the folding of the acridinium moieties, theoretical computation of **52** and [**53**]$^{2+}$ have been carried out at the B3LYP/6-31g* level of theory. Although the Si-C bond distances of the gas phase optimized geometry slightly deviate from those measured in the crystal, these calculations reproduce the trend observed experimentally. In an attempt to understand the nature of Si-C bond between silicon atom and acridinyl groups, natural population analysis (NPA) was carried out at the optimized geometry of **52** and [**53**]$^{2+}$ at the B3LYP/6-31g* level of theory.[194] The NPA analysis of **52** and [**53**]$^{2+}$ reveals that there is no significant change in the charges on the $SiMe_2$ unit on going from **52** to [**53**]$^{2+}$. Moreover, the charges on the acridinyl groups have increase from -0.5 to 0.5 that is in

consistent with the formation of carbocation. Therefore, $[\mathbf{53}]^{2+}$ should be described as bis-acridinium dication that is linked by a $SiMe_2$ group.

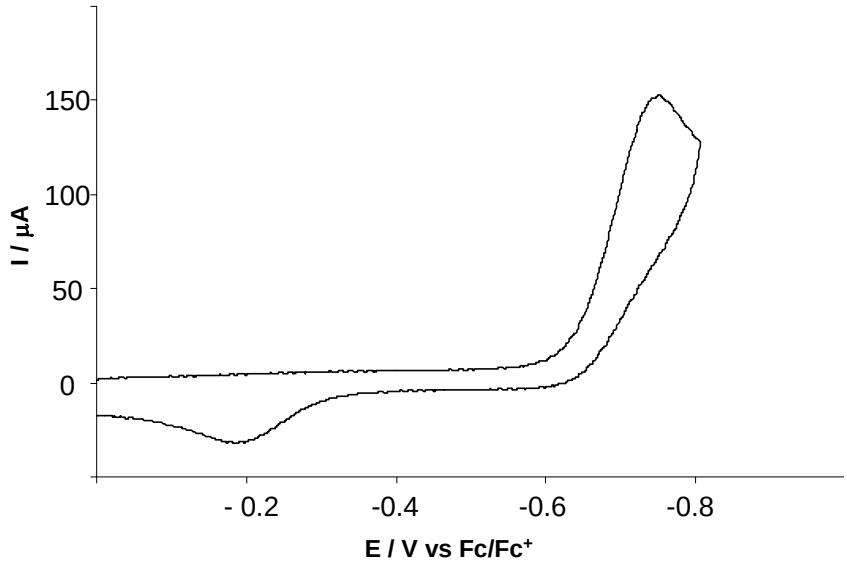

Figure 88: Cyclic voltammogram of $[\mathbf{53}]^{2+}$ in acetonitrile with a glassy carbon electrode (0.1 M nBu$_4$NPF$_6$) at scan rate of 300 mVs^{-1}.

The CV measurement carried out on $[\mathbf{53}]^{2+}$ in acetonitrile reveals an irreversible reduction wave at -0.75 V vs. Fc/Fc^+ (Figure 88). When compared to $[\mathbf{45}]^+$ ($E_{(peak, reduction)}$ = 1.01 V vs. Fc/Fc^+), the peak potential of the reduction wave is 0.26 V more positive which can be assigned to the dicationic and therefore more electrophilic nature of $[\mathbf{53}]^{2+}$. Moreover, reduction of $[\mathbf{53}]^{2+}$ is irreversible while that of $[\mathbf{45}]^+$ is reversible. Bearing in mind that the reduction of $[\mathbf{50}]^{2+}$ and $[\mathbf{51}]^{2+}$ are irreversible because of C-C

bond formation (Figure 89),[188, 189] it is legitimate to question whether [**53**]$^{2+}$ undergoes a similar reductive coupling reaction involving the former methylium centers.

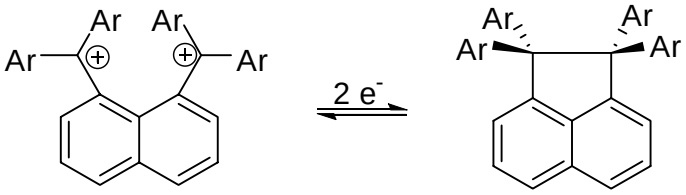

Figure 89: Reduction of 1,8-bismethylium naphthalenediyl dication.

However, a careful examination of the CV spectrum of [**53**]$^{2+}$ does not support this argument because a clear re-oxidation wave is not observable. The inaccessibility of the tetraaryl-silacyclopropane **54** probably results from the steric repulsion that would occur if a silacyclopropane was formed (Figure 90). Therefore, the CV measurement of [**53**]$^{2+}$ suggests that the reduced species is unstable and subject to decomposition.

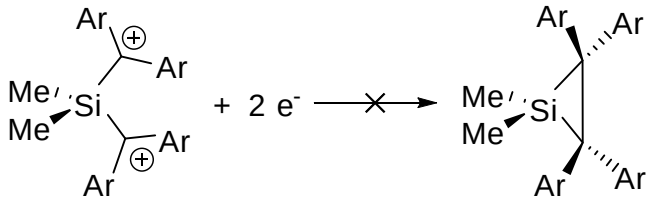

Figure 90: Reduction of [**53**]$^{2+}$.

The complexation of fluoride and hydride anion to $[\mathbf{53}]^{2+}$ has been investigated. Unfortunately, the reaction of $[\mathbf{53}]^{2+}$ with TBAF is not clean and no products could be unambiguously identified. On the other hand, reaction with $NaBH_4$ results in the formation of a neutral species **55** (Figure 91). The ^{1}H and ^{13}C NMR of **55** are in agreement with the formation of bis-acridan derivative. As indicated by ^{1}H NMR spectroscopy, the hydrogen bound to the former methylium center was detected at 3.69 ppm as a sharp singlet. The ^{13}C resonance of the methylium carbon atoms is shifted from 167 ppm in $[\mathbf{53}]^{2+}$ to 36 ppm in **55**. This observation suggests that the C(9) and C(23) atoms are the most electrophilic site in $[\mathbf{53}]^{2+}$, in accordance with the description of $[\mathbf{53}]^{2+}$ as a carbodication.

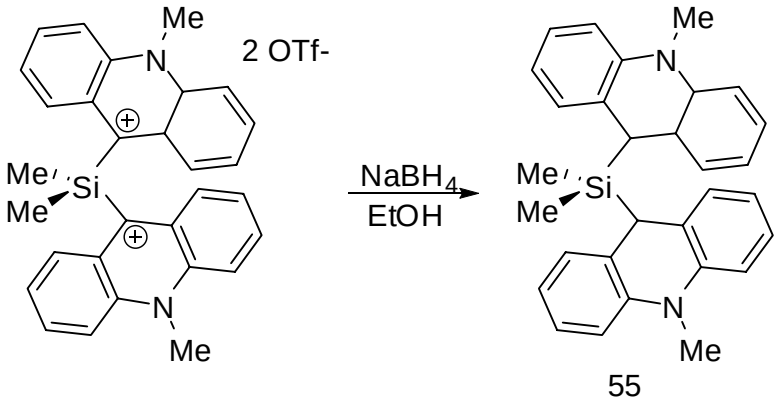

Figure 91: Reaction of $[\mathbf{53}]^{2+}$ with $NaBH_4$.

8.3 Conclusion

A novel carbodication which possesses a dimethylsilyl linker connecting two carbocationic centers has been synthesized and structurally characterized. The

theoretical calculation and reactivity studies carried out on $[\mathbf{53}]^{2+}$ show that this compound is better described as a carbodication rather than a silicon dication. The electron reduction of $[\mathbf{53}]^{2+}$ is irreversible and does not produce the silacyclopropane derivative.

8.4 Experimental section

Synthesis of 52: The 9-bromoacridince (2g, 8 mmol) was suspended in 100 ml of ether and cooled to -78°C, followed with the slow addition of n-BuLi (2.58M, 3.2 ml, 8.3 mmol). After stirring at -78 °C for 30 minutes, the dimethyldichlorosilane was added. The reaction mixture was allowed to warm up to room temperature and stir for overnight. The opaque beige solution was quenched with water, and extracted with ether. The combined organic solution was washed with brine and dried over $MgSO_4$. The solvent were removed under reduced pressure and light brown solid was obtained. Upon washing with hexane for several times, **52** was isolated as light brown solid (0.96g, yield = 58%). Single crystals of **52** for X-ray structural analysis were obtained by layer hexane on over the ethyl acetate solution of compound. ^{1}H NMR ($CDCl_3$, 500 MHz): 1.23 (s, 6H, $SiMe_2$), 7.27 (dd, 4H, $^{3}J_{H-H}$ = 9 Hz, $^{3}J_{H-H}$ = 7.5 Hz), 7.66 (dd, 4H, $^{3}J_{H-H}$ = 9 Hz, $^{3}J_{H-H}$ = 7.5 Hz), 8.23 (d, 4H, $^{3}J_{H-H}$ = 9 Hz), 8.31 (d, 4H, $^{3}J_{H-H}$ = 9 Hz). ^{13}C NMR ($CDCl_3$, 100.5 MHz): δ 6.9 ($SiMe_2$), 125.8, 127.4, 129.4, 130.3, 130.9, 147.6, 148.0. ^{29}Si NMR ($CDCl_3$, MHz): -12 ppm.

Synthesis of [53][OTf]$_2$: **52** (100 mg, 0.24 mmol) was dissolved in 1 mL of dichloromethane/pyridine (5:1) solution with large excess of methyl triflate. After

stirring for 3 days in glove box, ether was added and resulted in the precipitation of the mixture of monocation and dication. After removing the monocation by washing with CH_2Cl_2, the dication was obtained as bright yellow solids (77 mg, yield = 43%). Single crystals of [**53**][OTf]$_2$ were obtained by vapor diffusion of diethyl ether into a solution of CH_3CN of the salt. ^{1}H NMR (CD_3CN, 500 MHz): 1.52 (s, 6H, $SiMe_2$), 4.80 (s, 6H, NMe), 7.67 (ddd, 4H, $^3J_{H-H}$ = 8.8 Hz, $^3J_{H-H}$ = 6.8 Hz, $^4J_{H-H}$ = 1.0 Hz), 8.24 (ddd, 4H, $^3J_{H-H}$ = 9.3 Hz, $^3J_{H-H}$ = 6.8 Hz, $^4J_{H-H}$ = 1.0 Hz), 8.38 (d, $^3J_{H-H}$ = 8.8 Hz), 8.56 (d, $^3J_{H-H}$ = 9.3 Hz). ^{13}C NMR (CD_3CN, 125.6 MHz): δ 6.2 ($SiMe_2$), 40.8 (NMe), 120.4, 129.0, 131.2, 131.8, 139.2, 140.8, 166.9. ^{29}Si NMR (CD_3CN, MHz): δ -0.1. Anal Calcd for. $C_{30}H_{28}SiN_2S_2O_6F_6$: C 51.74; H 3.80. Found: C 51.66; H 3.76.

Synthesis of 55: $NaBH_4$ was added to an ethanol solution (2 mL) of [**53**][OTf]$_2$ (20 mg, 0.03 mmol) and the color of the solution changed from greenish yellow to orange immediately. After reaction, the solvent were removed under reduced pressure and the residual was extracted with hexane (5 mL x 2). The combined hexane solution was dried to give **55** as white powder. ^{1}H NMR ($CDCl_3$, 400 MHz): -0.53 (s, 6H, $SiMe_2$), 3.21 (s, 6H, NMe), 3.69 (s, 2H), 6.69 (dd, 2H, $^3J_{H-H}$ = 7.6 Hz, $^4J_{H-H}$ = 1.4 Hz), 6.73 (d, 2H, $^3J_{H-H}$ = 7.6 Hz), 6.81 (dd, 2H, $^3J_{H-H}$ = 7.6 Hz, $^3J_{H-H}$ = 7.6 Hz), 7.06 (ddd, 2H, $^3J_{H-H}$ = 7.6 Hz, $^3J_{H-H}$ = 7.6 Hz, $^4J_{H-H}$ = 1.4 Hz). ^{13}C NMR ($CDCl_3$, 100.5 MHz): δ -4.5 ($SiMe_2$), 32.9 (NMe), 36.0, 111.7, 120.8, 125.6, 126.6, 127.8, 143.0.

CHAPTER IX

GENERAL CONCLUSION

The work described in this dissertation was dedicated to the synthesis, characterization, fluoride ion affinity and electrochemistry of cationic Lewis acids. These cationic Lewis acids are either boranes or silanes that contain positively charged ligands. The motivation for the present research resides in the fundamental challenge associated with the synthesis and isolation of highly reactive electron deficient cationic derivatives. Another important aspect of this work concerns the formation of stable neutral radicals by reduction of cationic boranes.

9.1 Preparation of cationic Lewis acids for sensing fluoride in aqueous media

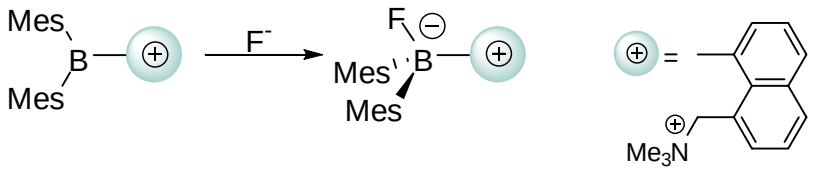

Figure 92: Fluoride complexation of cationic borane [**25**]$^{+}$.

Hoping to prevent the heterolysis of the B-F bond of a triarylfluoroborate complex in water, a cationic borane featuring a pendant ammonium group, [25][OTf], has been synthesized (**Figure 92**). [25]$^{+}$ was found to be well suited for the molecular recognition of fluoride and cyanide ions in water under bi-phasic conditions (Figure 93).

The high fluoride/cyanide affinity of $[25]^+$ is believed to result from favorable Coulombic attraction between the ammonium group and anion which stabilizes the B-F/B-CN bond against heterolysis. The UV-vis titration experiment in THF allows us to establish that $[25]^+$ has a higher affinity for fluoride than cyanide. This selectivity most likely results from steric effects that impede binding of the larger cyanide ion to the sterically congested boron center of $[25]^+$.

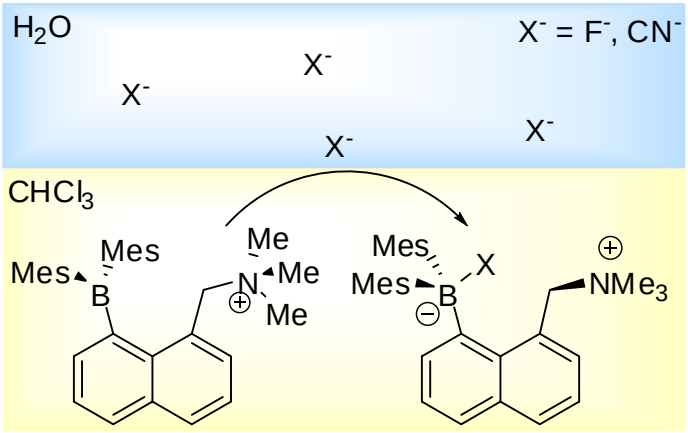

Figure 93: Capture of fluoride/cyanide from water.

In addition to cationic boranes, we also synthesized and investigated the fluoride binding properties of [**45**]$^+$, a molecule that can be described as α-silylated carbocation. By placing the fluorophilic silyl group adjacent to an electrophilic carbocation, a novel fluoride sensor was obtained. Sensing occurs via a fluoride induced methyl migration from the silicon to adjacent electrophilic methylium center (Figure 94) which is

unprecedented. As a result of its strong fluoride affinity, [**45**]$^+$ is able to react with KF in aqueous media at pH 7.0.

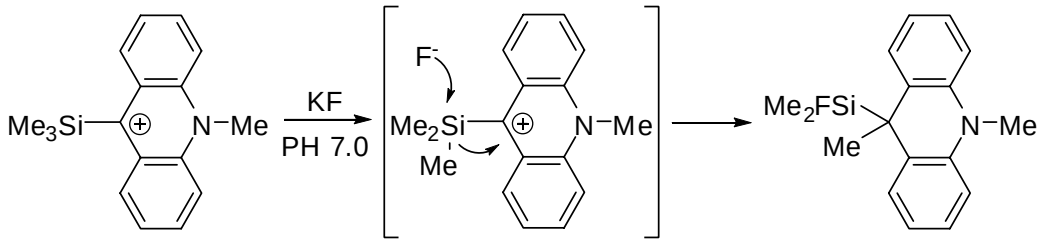

Figure 94: Reaction of [**45**]$^+$ with fluoride.

9.2 Reduction of cationic boranes – formation of radicals and unusual bonding situations

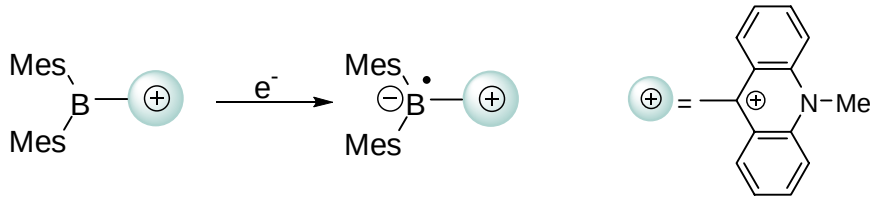

Figure 95: Electro-reduction of cationic borane [**27**]$^+$.

Owing to their highly reducing nature, boron centered radicals are very reactive which complicates their isolation and structural characterization. In order to explore strategies that allow for the stabilization of boron radicals, we have synthesized cationic boranes and investigated their reduction chemistry (Figure 95). The cationic character of these boranes serves to decrease their reduction potential and increase the stability of the resulting radicals. In this part of the research, we have prepared a cationic borane

[**27**]$^{+}$, which features two reversible reduction waves at -0.86 and -1.56 (vs. Fc/Fc^{+}) corresponding to the formation of stable neutral and anionic derivatives (Figure 96).

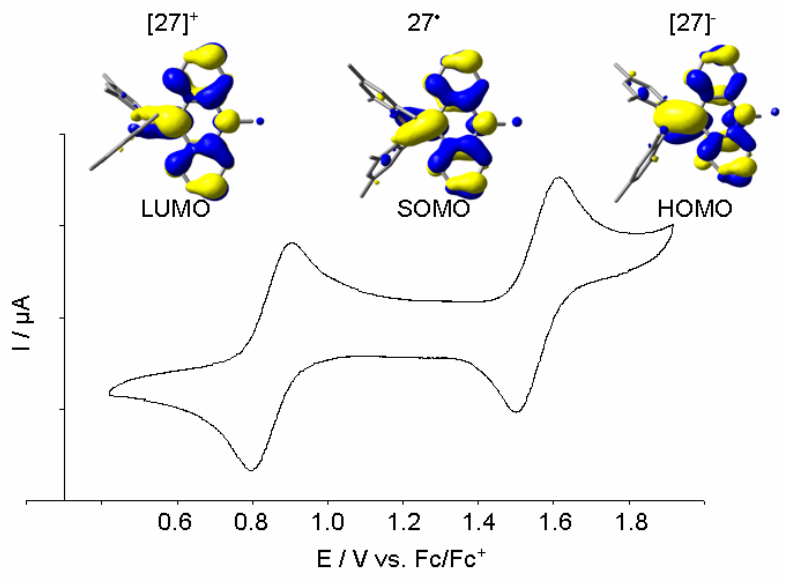

Figure 96: Frontier molecular orbitals of [**27**]$^{+}$, **27**$^{\bullet}$, and [**27**]$^{-}$, and CV of [**27**]$^{+}$.

The one-electron reduction of [**27**]$^{+}$ leads to the formation of a boron containing neutral radical in which the unpaired electron is partly localized in a polarized boron-carbon π bond. Further reduction of **27**$^{\bullet}$ with another electron results in the formation of the borataalkene derivative [**27**]$^{-}$, which features a formal B=C double bond (Figure 97).

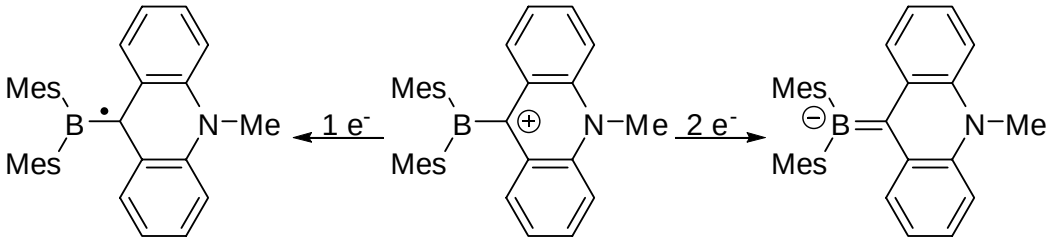

Figure 97: One- and two-electron reduction of [**27**]$^{+}$.

The single crystal X-ray analysis of all three derivatives confirms that the stepwise reduction of [**27**]$^{+}$ leads to the sequential population of the B-C π-bond (Figure 98). Structural changes upon reduction from [**27**]$^{+}$ to **27**$^{\bullet}$ to [**27**]$^{-}$ include: 1) the noticeable shortening of the B(1)-C(9) bond distance from 1.627(5) Å in [**27**]$^{+}$, to 1.559(5) Å in **27**$^{\bullet}$, and to 1.462(8) Å in [**27**]$^{-}$; 2) a steady decrease of the dihedral angle from 62.4° in [**27**]$^{+}$, to 44.8° in **27**$^{\bullet}$, and to 15.3° in [**27**]$^{-}$.

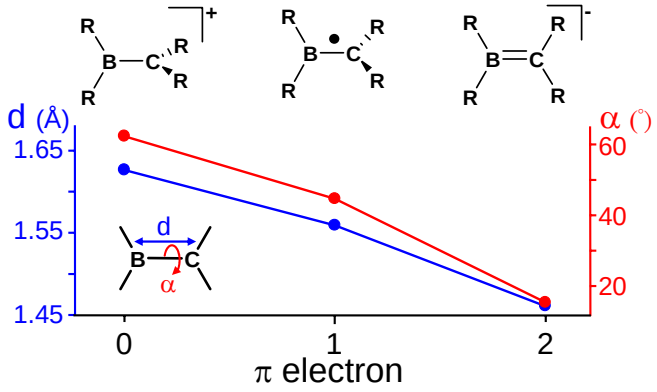

Figure 98: Structural changes vs. number of π electrons in B-C π-bond.

Theoretical computations of the series also support the stepwise population of a B-C π-bond upon reduction of [**27**]$^{+}$. Examination of the frontier molecular orbitals shows that the B(1) and C(9) atomic orbitals contribute 27.5%, 27.6%, and 31.3% to the LUMO of [**27**]$^{+}$, SOMO of **27**$^{\bullet}$, and HOMO of [**27**]$^{-}$, respectively (Figure 96). The NBO analysis of the bonding in [**27**]$^{+}$, **27**$^{\bullet}$ and [**27**]$^{-}$ indicates the combined occupancies of the orbitals connecting B(1) and C(9) in [**27**]$^{+}$, **27**$^{\bullet}$ and [**27**]$^{-}$ are respectively equal to 1.95, 2.77, and 3.62 electrons which is in agreement with an increase of the B-C bond-order upon reduction.

9.3 Synthesis of polycationic boranes as strong organic oxidants

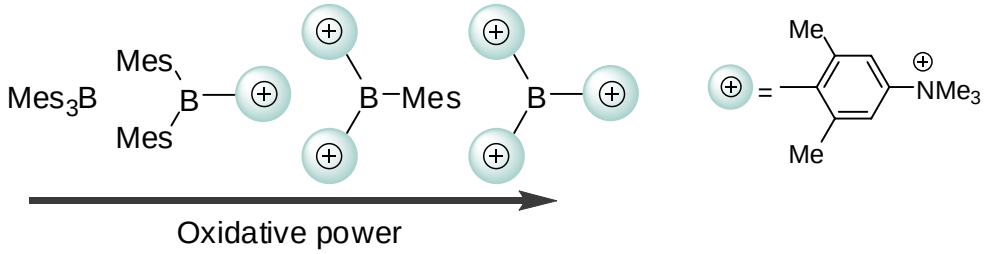

Figure 99: Representation of **33**, [**34**]$^{+}$, [**35**]$^{2+}$, and [**36**]$^{3+}$ placed on an oxidative power scale.

In the last part of this research, we investigated the impact of the cationic nature of these boranes on their oxidative power. In this context, we synthesized three novel cationic boranes ([**34**]$^{+}$, [**35**]$^{2+}$, and [**36**]$^{3+}$) that feature similar steric bulk around the boron atom but different numbers of positively charged Ar^{N+} substituents (Ar^{N+} =

[4-(Me_3N)-2,6-Me_2-C_6H_2]$^+$), and examined their oxidative power via cyclic voltammetry (Figure 99).

As indicated by the CV data of these compounds, the reduction potential of these triarylboranes is linearly proportional to the number of the pendant cationic substituents. Substitution of a mesityl group by an Ar^{N+} group leads to an increase of the reduction potential by 260 mV (Figure 100).

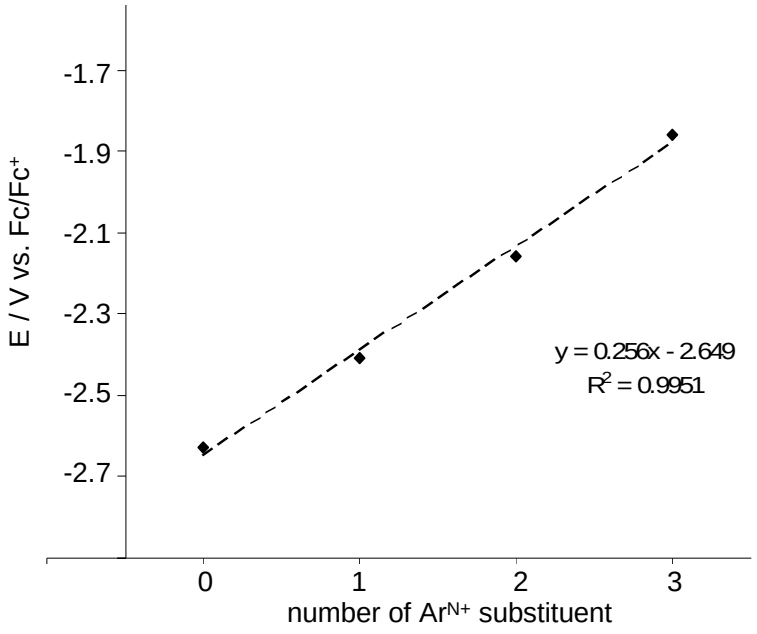

Figure 100: Reduction potential vs. number of C_6F_5 or Ar^{N+} substituents on boranes.

In summary, this dissertation illustrate how the introduction of cationic groups impacts the fluoride ion affinity and reduction potential of triarylboranes. In both cases, this strategy has proven effective in increasing the anion affinity of these derivatives. It

has also proven effective in increasing the reduction potentials of these boranes leading to a stabilization of the resulting radicals.

REFERENCES

1. Public Health Service, Division of Oral Health *Water Fluoridation Reporting System*; Centers of Disease Control: Atlanta, **2002,** December 31.

2. IPCS International Programme on Chemical Safety *Fluorine and fluoride*; World Health Organization: Geneva, **1984,** Environmental Health Criteria 36.

3. IPCS International Programme on Chemical Safety *Fluorides*; World Health Organization: Geneva, **2002,** Environmental Health Criteria 227.

4. Arancibia, J. A.; Rullo, A.; Olivieri, A. C.; Di Nezio, S.; Pistonesi, M.; Lista, A.; Fernandez Band, B. S. *Anal. Chim. Acta* **2004,** *512*, 157-163.

5. Martinez-Manez, R.; Sancenon, F. *Chem. Rev.* **2003,** *103*, 4419-4476.

6. Choi, K.; Hamilton, A. D. *Coord. Chem. Rev.* **2003,** *240*, 101-110.

7. Bondy, C. R.; Loeb, S. J. *Coord. Chem. Rev.* **2003,** *240*, 77-99.

8. Gale, P. A. *Coord. Chem. Rev.* **2003,** *240*, 191-221.

9. Sessler, J. L.; Camiolo, S.; Gale, P. A. *Coord. Chem. Rev.* **2003,** *240*, 17-55.

10. Sessler, J. L.; Davis, J. M. *Acc. Chem. Res.* **2001,** *34*, 989-997.

11. Beer, P. D.; Gale, P. A. *Angew. Chem. Int. Ed.* **2001,** *40*, 486-516.

12. Gale, P. A. *Coord. Chem. Rev.* **2001,** *213*, 79-128.

13. Gale, P. A.; Anzenbacher, P., Jr.; Sessler, J. L. *Coord. Chem. Rev.* **2001,** *222*, 57-102.

14. Gale, P. A. *Coord. Chem. Rev.* **2000,** *199*, 181-233.

15. Beer, P. D.; Cadman, J. *Coord. Chem. Rev.* **2000,** *205*, 131-155.

16. Snowden, T. S.; Anslyn, E. V. *Curr. Opin. Chem. Biol.* **1999,** *3*, 740-746.

17. Beer, P. D. *Acc. Chem. Res.* **1998,** *31*, 71-80.

18. de Silva, A. P.; Gunaratne, H. Q. N.; Gunnlaugsson, T.; Huxley, A. J. M.; McCoy, C. P.; Rademacher, J. T.; Rice, T. E. *Chem. Rev.* **1997,** *97*, 1515-1566.

19. Bianchi, A.; Bowman-James, K.; Garcia-Espana, E. *Supramolecular Chemistry of Anions*; Wiley-VCH: New York, **1997**.

20. Schmidtchen, F. P.; Berger, M. *Chem. Rev.* **1997,** *97*, 1609-1646.

21. Boiocchi, M.; Del Boca, L.; Gomez, D. E.; Fabbrizzi, L.; Licchelli, M.; Monzani, E. *J. Am. Chem. Soc.* **2004,** *126*, 16507-16514.

22. Lin, Z.-H.; Ou, S.-J.; Duan, C.-Y.; Zhang, B.-G.; Bai, Z.-P. *Chem. Commun.* **2006**, 624-626.

23. Bresner, C.; Day, J. K.; Coombs, N. D.; Fallis, I. A.; Aldridge, S.; Coles, S. J.; Hursthouse, M. B. *Dalton Trans.* **2006**, 3660-3667.

24. Bresner, C.; Aldridge, S.; Fallis, I. A.; Jones, C.; Ooi, L.-L. *Angew. Chem. Int. Ed.* **2005,** *44*, 3606-3609.

25. Dusemund, C.; Sandanayake, K. R. A. S.; Shinkai, S. *J. Chem. Soc., Chem. Commun.* **1995**, 333-334.

26. Yamamoto, H.; Ori, A.; Ueda, K.; Dusemund, C.; Shinkai, S. *Chem. Commun.* **1996**, 407-408.

27. Cooper, C. R.; Spencer, N.; James, T. D. *Chem. Commun.* **1998**, 1365-1366.

28. Arimori, S.; Davidson, M. G.; Fyles, T. M.; Hibbert, T. G.; James, T. D.; Kociok-Koehn, G. I. *Chem. Commun.* **2004**, 1640-1641.

29. Badugu, R.; Lakowicz, J. R.; Geddes, C. D. *Curr. Anal. Chem.* **2005,** *1*, 157-170.

30. Badugu, R.; Lakowicz, J. R.; Geddes, C. D. *Sens. Actuator B Chem.* **2005,** *104*, 103-110.

31. DiCesare, N.; Lakowicz, J. R. *Anal. Biochem.* **2002,** *301*, 111-116.

32. Neumann, T.; Dienes, Y.; Baumgartner, T. *Org. Lett.* **2006,** *8*, 495-497.

33. Koskela, S. J. M.; Fyles, T. M.; James, T. D. *Chem. Commun.* **2005**, 945-947.

34. Shiratori, H.; Ohno, T.; Nozaki, K.; Osuka, A. *Chem. Commun.* **1999**, 2181-2182.

35. Yamaguchi, S.; Akiyama, S.; Tamao, K. *J. Organomet. Chem.* **2002,** *652*, 3-9.

36. Entwistle, C. D.; Marder, T. B. *Chem. Mater.* **2004,** *16*, 4574-4585.

37. Entwistle, C. D.; Marder, T. B. *Angew. Chem. Int. Ed.* **2002,** *41*, 2927-2931.

38. Jäkle, F. *Boron: Organoboranes in Encyclopedia of Inorganic Chemistry*; Wiley: Chichester, **2005**.

39. Yamaguchi, S.; Akiyama, S.; Tamao, K. *J. Am. Chem. Soc.* **2000,** *122*, 6335-6336.

40. Yamaguchi, S.; Akiyama, S.; Tamao, K. *J. Am. Chem. Soc.* **2001,** *123*, 11372-11375.

41. Yamaguchi, S.; Shirasaka, T.; Akiyama, S.; Tamao, K. *J. Am. Chem. Soc.* **2002,** *124*, 8816-8817.

42. Kubo, Y.; Yamamoto, M.; Ikeda, M.; Takeuchi, M.; Shinkai, S.; Yamaguchi, S.; Tamao, K. *Angew. Chem. Int. Ed.* **2003,** *42*, 2036-2040.

43. Solé, S.; Gabbaï, F. P. *Chem. Commun.* **2004**, 1284-1285.

44. Parab, K.; Venkatasubbaiah, K.; Jäkle, F. *J. Am. Chem. Soc.* **2006,** *128*, 12879-12885.

45. Miyata, M.; Chujo, Y. *Polym. J.* **2002,** *34*, 967-969.

46. Liu, Z.-Q.; Shi, M.; Li, F.-Y.; Fang, Q.; Chen, Z.-H.; Yi, T.; Huang, C.-H. *Org. Lett.* **2005,** *7*, 5481-5484.

47. Liu, X. Y.; Bai, D. R.; Wang, S. *Angew. Chem. Int. Ed.* **2006,** *45*, 5475-5478.

48. Agou, T.; Kobayashi, J.; Kawashima, T. *Org. Lett.* **2005,** *7*, 4373-4376.

49. Katz, H. E. *J. Org. Chem.* **1985,** *50*, 5027-5032.

50. Williams, V. C.; Piers, W. E.; Clegg, W.; Elsegood, M. R. J.; Collins, S.; Marder, T. B. *J. Am. Chem. Soc.* **1999,** *121*, 3244-3245.

51. Chase, P. A.; Henderson, L. D.; Piers, W. E.; Parvez, M.; Clegg, W.; Elsegood, M. R. J. *Organometallics* **2006,** *25*, 349-357.

52. Melaïmi, M.; Gabbaï, F. P. *J. Am. Chem. Soc.* **2005,** *127*, 9680-9681.

53. Melaïmi, M.; Gabbaï, F. P. *Adv. Organomet. Chem.* **2005,** *53*, 61-99.

54. Katz, H. E. *J. Am. Chem. Soc.* **1985,** *107*, 1420-1421.

55. Katz, H. E. *J. Am. Chem. Soc.* **1986,** *108*, 7640-7645.

56. Katz, H. E. In *Inclusion Compounds*; Atwood, J. L., Davies, J. E. D., MacNicol, D. D., Eds.; Academic Press: New York, **1991,** 4, 391-405.

57. Gabbaï, F. P. *Angew. Chem. Int. Ed.* **2003,** *42*, 2218-2221.

58. Piers, W. E.; Irvine, G. J.; Williams, V. C. *Eur. J. Inorg. Chem.* **2000**, 2131-2142.

59. Amendola, V.; Esteban-Gomez, D.; Fabbrizzi, L.; Licchelli, M.; Monzani, E.; Sancenon, F. *Inorg. Chem.* **2005,** *44*, 8690-8698.

60. Custelcean, R.; Delmau, L. H.; Moyer, B. A.; Sessler, J. L.; Cho, W. S.; Gross, D.; Bates, G. W.; Brooks, S. J.; Light, M. E.; Gale, P. A. *Angew. Chem. Int. Ed.* **2005,** *44*, 2537-2542.

61. Bondy, C. R.; Gale, P. A.; Loeb, S. J. *J. Am. Chem. Soc.* **2004,** *126*, 5030-5031.

62. Padilla-Tosta, M. E.; Lloris, J. M.; Martinez-Manez, R.; Pardo, T.; Sancenon, F.; Soto, J.; Marcos, M. D. *Eur. J. Inorg. Chem.* **2001**, 1221-1226.

63. Beer, P. D.; Dent, S. W. *Chem. Commun.* **1998**, 825-826.

64. Beer, P. D.; Drew, M. G. B.; Knubley, R. J.; Ogden, M. I. *Dalton Trans.* **1995**, 3117-3123.

65. Kinnear, K. I.; Mousley, D. P.; Arafa, E.; Lockhart, J. C. *Dalton Trans.* **1994**, 3637-3643.

66. Arafa, E. A.; Kinnear, K. I.; Lockhart, J. C. *J. Chem. Soc., Chem. Commun.* **1992**, 61-64.

67. Liu, H.; Shao, X. B.; Jia, M.; Jiang, X. K.; Li, Z. T.; Chen, G. J. *Tetrahedron* **2005,** *61*, 8095-8100.

68. Chiu, C.-W.; Gabbaï, F. P. *J. Am. Chem. Soc.* **2006,** *128*, 14248-14249.

69. Agou, T.; Kobayashi, J.; Kawashima, T. *Inorg. Chem.* **2006,** *45*, 9137-9144.

70. Power, P. P. *Chem. Rev.* **2003,** *103*, 789-809.

71. Krause, E.; Polack, H. *Ber. Dtsch. Chem. Ges.* **1926,** *59*, 777-785.

72. Chu, T. L.; Weissmann, T. J. *J. Am. Chem. Soc.* **1956,** *78*, 23-26.

73. Weissman, S. I.; van Willigen, H. *J. Am. Chem. Soc.* **1965,** *87*, 2285-2286.

74. Leffler, J. E.; Watts, G. B.; Tanigaki, T.; Dolan, E.; Miller, D. S. *J. Am. Chem. Soc.* **1970,** *92*, 6825-6830.

75. Olmstead, M. M.; Power, P. P. *J. Am. Chem. Soc.* **1986,** *108*, 4235-4236.

76. Eisch, J. J.; Dluzniewski, T.; Behrooz, M. *Heteroatom Chem.* **1993,** *4*, 235-241.

77. Kwaan, R. J.; Harlan, C. J.; Norton, J. R. *Organometallics* **2001,** *20*, 3818-3820.

78. Cummings, S. A.; Iimura, M.; Harlan, C. J.; Kwaan, R. J.; Trieu, I. V.; Norton, J. R.; Bridgewater, B. M.; Jäkle, F.; Sundararaman, A.; Tilset, M. *Organometallics* **2006,** *25*, 1565-1568.

79. Venkatasubbaiah, K.; Zakharov, L. N.; Kassel, W. S.; Rheingold, A. L.; Jäkle, F. *Angew. Chem. Int. Ed.* **2005,** *44*, 5428-5433.

80. Mueller, P.; Huck, S.; Koeppel, H.; Pritzkow, H.; Siebert, W. *Z. Naturforsch. Teil B* **1995,** *50*, 1476-1484.

81. Brown, H. C.; Dodson, V. H. *J. Am. Chem. Soc.* **1957,** *79*, 2302-2306.

82. Elschenbroich, C.; Kuehlkamp, P.; Behrendt, A.; Harms, K. *Chem. Ber.* **1996,** *129*, 859-869.

83. Klusik, H.; Berndt, A.; Huenig, S. *Angew. Chem. Int. Ed.* **1981,** *20*, 870-871.

84. Grigsby, W. J.; Power, P. P. *Chem. Eur. J.* **1997,** *3*, 368-375.

85. Grigsby, W. J.; Power, P. P. *Chem. Commun.* **1996**, 2235-2236.

86. Moezzi, A.; Olmstead, M. M.; Power, P. P. *J. Am. Chem. Soc.* **1992,** *114*, 2715-2717.

87. Hoefelmeyer, J. D.; Gabbaï, F. P. *J. Am. Chem. Soc.* **2000,** *122*, 9054-9055.

88. Hoefelmeyer, J. D.; Solé, S.; Gabbaï, F. P. *Dalton Trans.* **2004**, 1254-1258.

89. Haddon, R. C. *Nature* **1975,** *256*, 394-396.

90. Oakley, R. T. *Can. J. Chem.* **1993,** *71*, 1775-1784.

91. Mandal, S. K.; Itkis, M. E.; Chi, X.; Samanta, S.; Lidsky, D.; Reed, R. W.; Oakley, R. T.; Tham, F. S.; Haddon, R. C. *J. Am. Chem. Soc.* **2005,** *127*, 8185-8196.

92. Scheschkewitz, D.; Amii, H.; Gornitzka, H.; Schoeller, W. W.; Bourissou, D.; Bertrand, G. *Science* **2002,** 295, 1880-1881.

93. Rodriguez, A.; Prasang, C.; Gandon, V.; Bourg, J.-B.; Bertrand, G. *ACS Symposium Series* **2006,** *917*, 81-93.

94. Rodriguez, A.; Olsen, R. A.; Ghaderi, N.; Scheschkewitz, D.; Tham, F. S.; Mueller, L. J.; Bertrand, G. *Angew. Chem. Int. Ed.* **2004,** *43*, 4880-4883.

95. Rodriguez, A.; Tham, F. S.; Schoeller, W. W.; Bertrand, G. *Angew. Chem. Int. Ed.* **2004,** *43*, 4876-4880.

96. Chen, E. Y.-X.; Marks, T. J. *Chem. Rev.* **2000,** *100*, 1391-1434.

97. Piers, W. E.; Chivers, T. *Chem. Soc. Rev.* **1997,** *26*, 345-354.

98. Piers, W. E. *Adv. Organomet. Chem.* **2005,** *52*, 1-76.

99. Beddows, C. J.; Burrows, A. D.; Connelly, N. G.; Green, M.; Lynam, J. M.; Paget, T. J. *Organometallics* **2001,** *20*, 231-233.

100. Bai, D.-R.; Liu, X.-Y.; Wang, S. *Chem. Eur. J.* **2007,** 13, (20), 5713-5723.

101. Williams, V. C.; Irvine, G. J.; Piers, W. E.; Li, Z.; Collins, S.; Clegg, W.; Elsegood, M. R. J.; Marder, T. B. *Organometallics* **2000,** *19*, 1619-1621.

102. Chai, J.; Lewis, S. P.; Collins, S.; Sciarone, T. J. J.; Henderson, L. D.; Chase, P. A.; Irvine, G. J.; Piers, W. E.; Elsegood, M. R. J.; Clegg, W. *Organometallics* **2007,** *26*, 5667-5679.

103. Lewis, S. P.; Taylor, N. J.; Piers, W. E.; Collins, S. *J. Am. Chem. Soc.* **2003,** *125*, 14686-14687.

104. Melaïmi, M.; Solé, S.; Chiu, C.-W.; Wang, H.; Gabbaï, F. P. *Inorg. Chem.* **2006,** *45*, 8136-8143.

105. Bayer, M. J.; Jalisatgi, S. S.; Smart, B.; Herzog, A.; Knobler, C. B.; Hawthorne, M. F. *Angew. Chem. Int. Ed.* **2004,** *43*, 1854-1857.

106. Viets, D.; Lork, E.; Watson, P. G.; Mews, R. *Angew. Chem. Int. Ed.* **1997,** *36*, 623-624.

107. Haneline, M. R.; Tsunoda, M.; Gabbaï, F. P. *J. Am. Chem. Soc.* **2002,** *124*, 3737-3742.

108. Sun, Y.; Ross, N.; Zhao, S.-B.; Huszarik, K.; Jia, W.-L.; Wang, R.-Y.; Macartney, D.; Wang, S. *J. Am. Chem. Soc.* **2007,** *129*, 7510-7511.

109. Harlan, C. J. H., T.; Fujita, E.; Norton, J. R. *J. Am. Chem. Soc.* **1999,** *121*, 7274-7275.

110. Kaim, W.; Schulz, A. *Angew. Chem. Int. Ed.* **1984,** *23*, 615-616.

111. Schulz, A.; Kaim, W. *Chem. Ber.* **1989,** *122*, 1863-1868.

112. Hudson, R. L.; Williams, F. *J. Am. Chem. Soc.* **1977,** *99*, 7714-7716.

113. Marti, V. P. J.; Roberts, B. P. *J. Chem. Soc., Chem. Commun.* **1984**, 272-274.

114. Fiedler, J.; Zalis, S.; Klein, A.; Hornung, F.; Kaim, W. *Inorg. Chem.* **1996,** *35*, 3039-3043.

115. Wang, H.; Gabbaï, F. P. *Organometallics* **2005,** *24*, 2898-2902.

116. DuPont, T. J. M., J. L. *J. Am. Chem. Soc.* **1975,** *97*, 6375-6382.

117. Hoefelmeyer, J. D.; Gabbaï, F. P. *Organometallics* **2002,** *21*, 982-985.

118. Rathore, R.; Lindeman, S. V.; Kumar, A. S.; Kochi, J. K. *J. Am. Chem. Soc.* **1998,** *120*, 6931-6939.

119. Rajca, A.; Rajca, S.; Desai, S. R. *J. Chem. Soc., Chem. Commun.* **1995**, 1957-1958.

120. Liu, Z.-Q.; Fang, Q.; Cao, D.-X.; Wang, D.; Xu, G.-B. *Org. Lett.* **2004,** *6*, 2933-2936.

121. Chan, M. C. W.; Kui, S. C. F.; Cole, J. M.; McIntyre, G. J.; Matsui, S.; Zhu, N.; Tam, K.-H. *Chem. Eur. J.* **2006,** *12*, 2607-2619.

122. Mountford, A. J.; Hughes, D. L.; Lancaster, S. J. *Chem. Commun.* **2003**, 2148-2149.

123. Collman, J. P.; Christian, P. A.; Current, S.; Denisevich, P.; Halbert, T. R.; Schmittou, E. R.; Hodgson, K. O. *Inorg. Chem.* **1976,** *15*, 223-227.

124. Konig, F. B.; Schonbohm, J.; Bayles, D. *J. Comput. Chem.* **2001,** *22*, 545-559.

125. Kolandaivel, P.; Nirmala, V. *J. Mol. Struct.* **2004,** *694*, 33-38.

126. Bryantsev, V. S.; Hay, B. P. *J. Am. Chem. Soc.* **2005,** *127*, 8282-8283.

127. Kuz'mina, L. G.; Struchkov, Y. T.; Lemenovsky, D. A.; Urazowsky, I. F. *J. Organomet. Chem.* **1984,** *277*, 147-151.

128. Hudnall, T. W.; Gabbai, F. P. *J. Am. Chem. Soc.* **2007,** *129*, 11978-11986.

129. Olmstead, M. M.; Power, P. P.; Weese, K. J.; Doedens, R. J. *J. Am. Chem. Soc.* **1987,** *109*, 2541-2542.

130. Bartlett, R. A.; Power, P. P. *Organometallics* **1986,** *5*, 1916-1917.

131. Pelter, A.; Williams, L.; Wilson, J. W. *Tetrahedron Lett.* **1983,** *24*, 627-630.

132. Pelter, A.; Singaram, B.; Warren, L.; Wilson, J. W. *Tetrahedron* **1993,** *49*, 2965-2978.

133. Pelter, A.; Smith, K.; Elgendy, S. M. A.; Rowlands, M. *Tetrahedron* **1993,** *49*, 7104-18.

134. Cook, K. S.; Piers, W. E.; Woo, T. K.; McDonald, R. *Organometallics* **2001,** *20*, 3927-3937.

135. Cook, K. S.; Piers, W. E.; Hayes, P. G.; Parvez, M. *Organometallics* **2002,** *21*, 2422-2425.

136. Cook, K. S.; Piers, W. E.; McDonald, R. *J. Am. Chem. Soc.* **2002,** *124*, 5411-5418.

137. Power, P. P. *Inorg. Chimi. Acta* **1992,** 443-447.

138. Porter, W. W., III; Vaid, T. P. *J. Org. Chem.* **2005,** *70*, 5028-5035.

139. Klusik, H.; Berndt, A. *J. Organomet. Chem.* **1982,** *232*, C21-C23.

140. Clark, T.; Nelsen, S. F. *J. Am. Chem. Soc.* **1988,** *110*, 868-870.

141. Shida, T.; Egawa, Y.; Kubodera, H.; Kato, T. *J. Chem. Phys.* **1980,** *73*, 5963-5970.

142. Kira, M.; Nakazawa, H.; Sakurai, H. *J. Am. Chem. Soc.* **1983,** *105*, 6983-6987.

143.Kochi, J. K.; Rathore, R.; Zhu, C.; Lindeman, S. V. *Angew. Chem. Int. Ed.* **2000,** *39*, 3671-3674.

144. Chiu, C.-W.; Gabbaï, F. P. *Dalton Trans.* **2008**, in press.

145. Ahlberg, E.; Hammerich, O.; Parker, V. D. *J. Am. Chem. Soc.* **1981,** *103*, 844-849.

146. Piers, W. E.; Bourke, S. C.; Conroy, K. D. *Angew. Chem. Int. Ed.* **2005,** *44*, 5016-5036.

147. Arnett, E. M.; Flowers, R. A., II; Ludwig, R. T.; Meekhof, A. E.; Walek, S. A. *Journal of Physical Organic Chemistry* **1997,** *10*, 499-513.

148. Yuan, Z.; Taylor, N. J.; Ramachandran, R.; Marder, T. B. *Appl. Organomet. Chem.* **1996,** *10*, 305-316.

149. Schneider, S. K. R., Patric; Julius, Gerrit R.; Loschen, Christoph; Raubenheimer, Helgard G.; Frenking, Gernot; Herrmann, Wolfgang A. *Eur. J. Inorg. Chem.* **2005**, 2973-2977.

150. Schneider, S. K. J., Gerrit R.; Loschen, Christoph; Raubenheimer, Helgard G.; Frenking, Gernot; Herrmann, Wolfgang A. *Dalton Trans.* **2006**, 1226-1233.

151. Rebek, J., Jr.; Costello, T.; Marshall, L.; Wattley, R.; Gadwood, R. C.; Onan, K. *J. Am. Chem. Soc.* **1985,** *107*, 7481-7487.

152. Reed, A. E. C., Larry A.; Weinhold, F. *Chem. Rev.* **1988,** *88*, 899-926.

153.Lee, M. H.; Agou, T.; Kobayashi, J.; Kawashima, T.; Gabbaï, F. P. *Chem. Commun.* **2007**, 1133-1135.

154. Cornet, S. M.; Dillon, K. B.; Entwistle, C. D.; Fox, M. A.; Goeta, A. E.; Goodwin, H. P.; Marder, T. B.; Thompson, A. L. *Dalton Trans.* **2003**, 4395-4405.

155. Weese, K. J.; Bartlett, R. A.; Murray, B. D.; Olmstead, M. M.; Power, P. P. *Inorg. Chem.* **1987,** *26*, 2409-2413.

156. Weiss, R.; Puhlhofer, F. G. *J. Am. Chem. Soc.* **2007,** *129*, 547-553.

157. Uddin, M. K.; Nagano, Y.; Fujiyama, R.; Kiyooka, S.; Fujio, M.; Tsuno, Y. *Tetrahedron Lett.* **2005,** *46*, 627-630.

158. Narula, C. K.; Noeth, H. *Inorg. Chem.* **1985,** *24*, 2532-2539.

159. Rivard, E.; Merrill, W. A.; Fettinger, J. C.; Power, P. P. *Chem. Commun.* **2006**, 3800-3802.

160. Rivard, E.; Merrill, W. A.; Fettinger, J. C.; Wolf, R.; Spikes, G. H.; Power, P. P. *Inorg. Chem.* **2007,** *46*, 2971-2978.

161. Leffler, J. E.; Dolan, E.; Tanigaki, T. *J. Am. Chem. Soc.* **1965,** *87*, 927-928.

162. Tomasi, J.; Cammi, R.; Mennucci, B. *Int. J. Quantum Chem.* **1999,** *75*, 783-803.

163. Cossi, M.; Barone, V.; Cammi, R.; Tomasi, J. *Chem. Phys. Lett.* **1996,** *255*, 327-335.

164. Whitmore, F. C.; Sommer, L. H. *J. Am. Chem. Soc.* **1946,** *68*, 481-484.

165. Sommer, L. H.; Dorfman, E.; Goldberg, G. M.; Whitmore, F. C. *J. Am. Chem. Soc.* **1946,** *68*, 488-489.

166. Sommer, L. H.; Whitmore, F. C. *J. Am. Chem. Soc.* **1946,** *68*, 485-487.

167. Drewello, T.; Burgers, P. C.; Zummack, W.; Apeloig, Y.; Schwarz, H. *Organometallics* **1990,** *9*, 1161-1165.

168. Hajdasz, D.; Squires, R. *J. Chem. Soc., Chem. Commun.* **1988**, 1212-1214.

169. Grunenberg, J.; Laschat, S.; Dickner, T. *Eur. J. Org. Chem.* **2003**, 4897-4901.

170. Olah, G. A.; Berrier, A. L.; Field, L. D.; Prakash, G. K. S. *J. Am. Chem. Soc.* **1982,** *104*, 1349-1355.

171. Maier, G.; Volz, D.; Neudert, J. *Synthesis* **1992**, 561-564.

172. de Meijere, A.; Faber, D.; Noltemeyer, M.; Boese, R.; Haumann, T.; Mueller, T.; Bendikov, M.; Matzner, E.; Apeloig, Y. *J. Org. Chem.* **1996,** *61*, 8564-8568.

173. Sebastian, M.; Hoskin, A.; Nieger, M.; Nyulaszi, L.; Niecke, E. *Angew. Chem. Int. Ed.* **2005,** *44*, 1405-1408.

174. Motoyoshiya, J.; Tokutake, K.; Kuroe, M.; Yoshioka, S.; Nishii, Y.; Aoyama, H. *Heterocycles* **2004,** *63*, 1667-1672.

75. Chiu, C.-W.; Gabbaï, F. P. *Angew. Chem. Int. Ed.* **2007,** *46*, 1723-1725.

176. Yamaguchi, S.; Akiyama, S.; Tamao, K. *Organometallics* **1998,** *17*, 4347-4352.

177. Vignollet, Y.; Maire, J. C. *J. Organomet. Chem.* **1969,** *17*, 43-45.

178. Hapiot, P.; Moiroux, J.; Saveant, J. M. *J. Am. Chem. Soc.* **1990,** *112*, 1337-1343.

179. Tamao, K.; Hayashi, T.; Ito, Y. *J. Organomet. Chem.* **1996,** *506*, 85-91.

180. Yamaguchi, S.; Akiyama, S.; Tamao, K. *J. Am. Chem. Soc.* **2000,** *122*, 6793-6794.

181. Kwak, G.; Fujiki, M.; Masuda, T. *Macromolecules* **2004,** *37*, 2422-2426.

182. Hoshi, T.; Nakamura, T.; Suzuki, T.; Ando, M.; Hagiwara, H. *Organometallics* **2000,** *19*, 3170-3178.

183. Kawachi, A.; Tani, A.; Machida, K.; Yamamoto, Y. *Organometallics* **2007,** *26*, 4697-4699.

184. Suzuki, T.; Nishida, J.-I.; Tsuji, T. *Angew. Chem. Int. Ed.* **1997,** *36*, 1329-1331.

185. Suzuki, T.; Nishida, J.-I.; Tsuji, T. *Chem. Commun.* **1998**, 2193-2194.

186. Suzuki, T.; Nishida, J.-I.; Tsuji, T. *Chem. Commun.* **1998**, 1331-1332.

187. Suzuki, T.; Nishida, J.-I.; Ohkita, M.; Tsuji, T. *Angew. Chem. Int. Ed.* **2000**, *39*, 1804-1806.

188. Wang, H.; Gabbaï, F. P. *Angew. Chem. Int. Ed.* **2004**, *43*, 184-187.

189. Kawai, H.; Takeda, T.; Fujiwara, K.; Suzuki, T. *Tetrahedron Lett.* **2004,** *45*, 8289-8293.

190. Wang, H.; Gabbaï, F. P. *Org. Lett.* **2005,** *7*, 283-285.

191. Wang, H.; Webster, C. E.; Perez, L. M.; Hall, M. B.; Gabbaï, F. P. *J. Am. Chem. Soc.* **2004,** *126*, 8189-8196.

192. Kawai, H.; Takeda, T.; Fujiwara, K.; Suzuki, T. *J. Am. Chem. Soc.* **2005,** *127*, 12172-12173.

193. Herrmann, W. A. *Angew. Chem. Int. Ed.* **2002,** *41*, 1290-1309.

194. Berryman, O. B.; Bryantsev, V. S.; Stay, D. P.; Johnson, D. W.; Hay, B. P. *J. Am. Chem. Soc.* **2007,** *129*, 48-58.

VITA

Ching-Wen Chiu

Department of Chemistry
Texas A&M University
College Station 77843-3255

EDUCATION

2003-2008	Texas A&M University, College Station, Texas Ph.D. Chemistry
1999-2001	National Chiao-Tung University, Hsinchu, Taiwan M.S. Applied Chemistry
1995-1999	National Chiao-Tung University, Hsinchu, Taiwan B.S. Applied Chemistry

AWARDS

DIC Young Investigator Award, American Chemical Society, 2008

Martell Travel Award, Chemistry Department, Texas A&M University, 2008

Martell Travel Award, Chemistry Department, Texas A&M University, 2007

Research/Presentation Grant, Texas A&M University, 2006

SELECTED PUBLICATIONS

C.-W. Chiu, F. P. Gabbaï, "Diarylborenium cations - Synthesis, structure and electrochemistry." *Organometallics* **2007**, *in press*

C.-W. Chiu, F. P. Gabbaï, "Cyanide ion complexation by a cationic borane." *Dalton Trans.* **2007**, *in press*

C.-W. Chiu, F. P. Gabbaï, "Structural changes accompanying the stepwise population of a B-C π-bond." *Angew. Chem. Intl. Ed.* **2007**, *46*, 6878-6881

C.-W. Chiu, F. P. Gabbaï, "A 9-borylated acridinyl radical." *Angew. Chem. Intl. Ed.* **2007**, *46,* 1723-1725

C.-W. Chiu, F. P. Gabbaï, "Fluoride ion capture from water with a cationic borane" *J. Am. Chem. Soc.* **2006**, *128*, 14248-14249

M. Melaimi, S. Solé, C.-W. Chiu, H. Wang, F. P. Gabbaï, "A structural and electrochemical investigation in the high fluoride affinity of sterically hindered 1,8-bis(boryl)naphthalenes" *Inorg. Chem.* **2006**, *45,* 8136-8143